Estimating PM2.5 in the Beijing-Tianjin-Hebei Region Using MODIS AOD Products from 2014 to 2015

by

Yuenan Li

A thesis
presented to the University of Waterloo
in fulfillment of the
thesis requirement for the degree of
Master of Science
in
Geography

Waterloo, Ontario, Canada, 2016

AUTHOR'S DECLARATION

I hereby declare that I am the sole author of this thesis. This is a true copy of the thesis, including any required final revisions, as accepted by my examiners.

I understand that my thesis may be made electronically available to the public.

Abstract

Fine particulate matter with a diameter less than 2.5 μm (PM2.5) has harmful impacts on regional climate, economic development and public health. The high PM2.5 concentrations in China's urban areas are mainly caused by combustion of coal and gasoline, industrial pollution and unknown/uncertain sources. The Beijing-Tianjin-Hebei (BTH) region with a land area of 218,000 km^2, which contains 13 cities, is the biggest urbanized region in northern China. The huge population (110 million, 8% of the China's population), local heavy industries and vehicle emissions have resulted in severe air pollution. To monitor ground-level PM2.5 concentration, the Chinese government spent significant expense in building more than 1500 in-situ stations (79 stations in the BTH region). However, most of these stations are situated in urban areas. Besides, each station can only represent a limited area around that station, which leaves the vast rural land out of monitoring. In this situation, geographic information system and remote sensing can be used as complementary tools. Traditional models have used 10 km MODIS Aerosol Optical Depth (AOD) product and proved the statistical relationship between AOD and PM2.5. In 2014, the 3 km MODIS AOD product was released which made PM2.5 estimation with a higher resolution became possible.

This study presents an estimation on PM2.5 distribution in the BTH region from September 2014 to August 2015 by combining the MODIS satellite data, ground measurements of PM2.5, and meteorological documents. Firstly, the 3 km and 10 km MODIS AOD products were validated with AErosol RObotic NETwork (AERONET AOD. Then the MLR and GWR models were employed respectively to estimate PM2.5 concentrations using ground measurements and two MODIS AOD products, meteorological datasets and land use information. Seasonal and regional analyses were also followed to make a comparative study on strengths and weaknesses between the 3 km and 10 km AOD products. Finally, the number of non-accidental deaths attributed to the long-term exposure of PM2.5 in the BTH region was estimated spatially.

The results demonstrated that the 10 km AOD product provided results with a higher accuracy and greater coverage, although the 3 km AOD product could provide more

information about the spatial variations of PM2.5 estimation. Additionally, compared with the global regression, the geographically weighed regression model was able to improve the estimation results. Finally, it was estimated that more than 30,000 people died in the BTH region during the study period attributed to the excessive PM2.5 concentrations.

Acknowledgements

Foremost, sincere thanks and gratitude to my supervisor, Professor Dr. Jonathan Li, for his guidance, advices, patience, and encouragements through my graduate study and thesis work. This work would not have been possible without his continuous support.

It is also with the deepest respect and admiration that I thank my Thesis Examining Committee, including Dr. Rebecca K. Saari, Assistant Professor at the Department of Civil and Environmental Engineering, University of Waterloo, Dr. Lei Liu, Professor at the Department of Civil and Resource Engineering, Dalhousie University, and Dr. Ellsworth LeDrew, Professor at the Department of Geography and Environmental Management, University of Waterloo. Their useful comments and suggestions encouraged me to better improve my thesis work.

I would like to extend a thank you to Dr. Jianjun Wang, Associate Professor, a visiting scholar from the Third Institute of Oceanography, State Oceanic Administration of China for her continuous help, suggestions, feedback and help in the preparation of this work. Also, sincere thanks to my colleagues in Mobile Sensing and Geodata Science Lab for the time we worked together. Special thanks go to Qing Lu, Chen Chen, Dr. Xiaolin Bai, Yifei Chen and Xinqu Chen for our valuable discussions.

I gratefully acknowledge the MODIS Teams for providing AOD products. I would also like to acknowledge the AERONET program for ground-level AOD measurements. At the same time, I must acknowledge ECMWF for ERA-Interim data sets. Also, I appreciate Data Center for Resources and Environmental Sciences, Chinese Academy of Sciences (RESDC) for providing land use datasets.

I am also very thankful to Dr. Kai Liu, Associate Professor at the School of Geography and Planning, Sun Yat-Sen University, who taught me how to study as a researcher and think in critical ways.

At the last, I deeply appreciate my parents for their encouragement, support and love. 最后，感谢父母对我一如既往的鼓励，支持与爱。

Table of Contents

List of Figures

List of Tables

List of Abbreviations

3D	three-dimension
AASTER	Along-Track Scanning Radiometer
ACE	alternating conditional expectation
AERONE	AErosol RObotic NETwork
AF	Attributable fraction
AIC	Akaike Information Criterion
ANN	artificial neural network
AOD	Aerosol optical depth
AVHRR	The Advanced Very High Resolution Radiometer
BAM	Beta Attenuation Monitoring
BHL	boundary layer height
BSRN	Baseline Surface Radiation Network
BTH	Beijing-Tianjin-Hebei
CAAQS	Canadian Ambient Air Quality Standards
CCME	Canadian Council of Ministers of the Environment
CNEMC	China National Environmental Monitoring Center
CR	Contrast Reduction
CRESDA	China Centre for Resources Satellite Data and Application
CRF	Concentration–response function
CV	Cross Validation
DB	Deep Blue
DCCPHS	Data-Center of China Public Health Science
DDV	Dense Dark Vegetation algorithm
DEM	digital elevation model
DT	Dark Target
ECMWF	European Centre for Medium-Range Weather Forecasts
EPA	Environmental Protection Agency
ER	Excess risk
ESA	European Space Agency
ETM+	Enhanced Thematic Mapper Plus
GAM	Generalized Additive Model
GAW-PFR	Global Atmosphere Watch-Precision Filter Radiometer

GDP	Gross Domestic Product
GEOS-Chem	Goddard Earth Observing System Atmospheric Chemistry Transport
GIS	Geographic information system
GRP	Gross Regional Product
GWR	Geographically Weighted Regression
HDF-EOS	Hierarchical Data Format
LABITS	Land Aerosol property and Bidirectional reflectance Inversion by Time Series technique
LSR	Land Surface Reflectance
LUR	Land Use Regression
LUT	Look up table
MAPE	Mean Absolute Percent Error
MECC	Ministry of the Environment and Climate Change
MEPCN	Ministry of Environmental Protection of the People's Republic of China
MERIS	Medium Resolution Imaging Spectrometer
MISR	Multi-angle Imaging SpectroRadiometer
MLR	Multiple Linear Regression
MODIS	moderate-resolution imaging spectroradiometer
MPLNET	Micro-Pulse Lidar Network
NAAQS	National Ambient Air Quality Standard
NASA	National Aeronautics and Space Administration
NCEP	National Centers for Environmental Prediction
NDVI	Normalized difference vegetation index
NOAA	National Oceanic and Atmospheric Administration
OLI	Operational Land Imager
PHOTON	PHOtométrie pour le Traitement Opérationnel de Normalisation Satellitaire
PM	Particulate Matter
PM1	Particulate Matter (diameter <=1 μm)
PM10	Particulate Matter (diameter <=10 μm)
PM2.5	Particulate Matter (diameter <=2.5μm)
POLDER	POLarization and Directionality of the Earth's Reflectances
RESDC	Data Center for Resources and Environmental Sciences, Chinese Academy of Sciences
RH	Relatively humidity
RMSE	Root-Mean-Square Error
RR	Relative risk

RS:	remote sensing
SKYNET:	SkyRadiometer Network
SP	Surface pressure
TEOM	Tapered Element Oscillating Microbalance
TOMS	Total Ozone Mapping Spectrometer
TRIS	Thermal Infrared Sensor
WHO	World Health Organization

Chapter 1. Introduction

1.1 Background

1.1.1 Introduction to PM2.5

Air pollution is a recognized threat to public health and has been globally associated with increasing mortality and morbidity. Recent studies demonstrate that there has been a steadily worldwide increase of the burden of disease attributed to ambient air pollution since 1990 (Forouzanfar et al. 2015). It was reported that 3.7 million people died in 2012 caused by ambient air pollution, and the Southeast Asian and Western Pacific regions bear most of the burden (WHO, 2012).

Currently, the major pollutants include particulates, sulfur oxides, nitrogen oxides, carbon monoxide and ground level ozone. Particulate matter (PM) is a mixture of liquid and solid airborne particles with complex compositions and diameters (Gupta et al., 2006; Lin et al., 2015). PM consist of coarse particles (often defined as particles with a diameter > 2.5 μm), fine particles (PM2.5, particles with a diameter < 2.5 μm) and ultrafine particles (particles with a diameter <0.1 μm) (Wilson et al., 1997; Pope III et al., 2000). Coarse, fine and ultrafine particles differ by size, source, formation mechanism, lifetime and spatial- distribution (Wilson et al., 1997). Compared with coarse-mode particle have an atmospheric half-life of minutes to hours, PM2.5 has a half-life of days to weeks. PM2.5 can travel 100s to 1000s of kilometre, while coarse – mode particle can only travel 1 to 10s of kilometre (Wilson et al., 1997).

The composition of PM2.5 varies due to its source: natural and anthropogenic source. Natural source include sea salt, dust, volcanic eruptions, forest and grassland fires (Emili et al., 2010; Beh et al., 2013), while anthropogenic source include fossil fuel combustion (coal, gasoline and diesel), industrial processes, transportation and uncertain sources (Emili et al., 2010; Wang et al., 2016). Figure 1.1 shows the size range and some of the major components of PM2.5 and PM10. Generally, PM2.5 contains nanoparticles (condensed organic carbon and sulfuric acid vapors), ultrafine particles (fresh high temperature emissions, organic carbon and metal vapors), while PM10 contains the components of PM2.5, and other components such as geological material, pollen and sea salt. (Watson et al., 2002; Cao et al., 2013). In addition, atmospheric chemical reactions also occur among primary particles and result in secondary particles (Franklin et al., 2008).

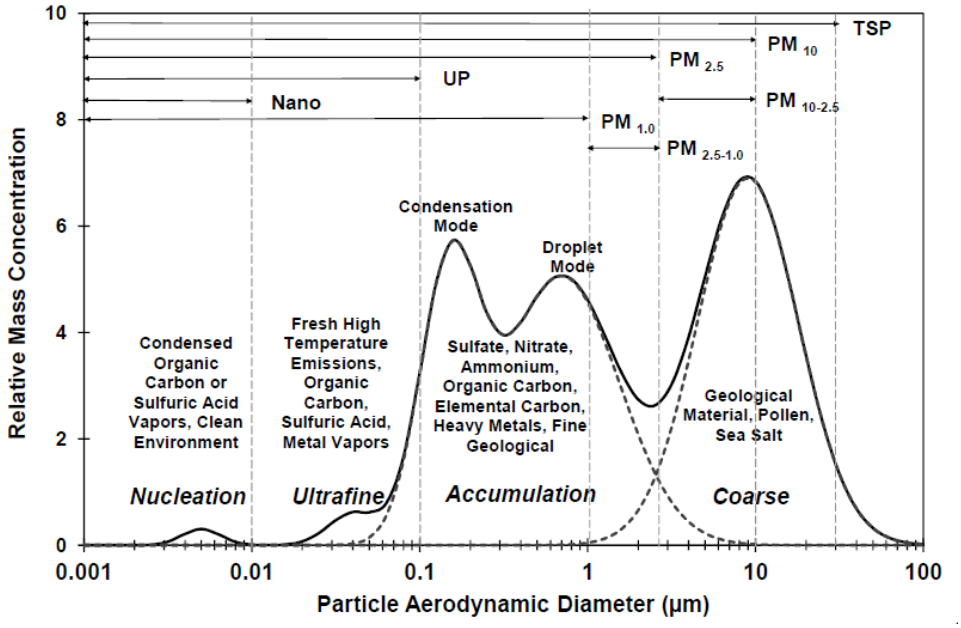

Figure 1.1 Ambient particles' size distribution, patterned after Chow (1995) and Watson (2002).

(Source: Cao et al., 2013)

The increase of PM2.5 has significantly negative effects on weather and climate change, public health and economic development. The PM2.5's effects on climate change can be classified in direct and indirect effects. Direct effects are PM2.5's interactions with radiation, such as scattering and absorbing the solar radiation and terrestrial surface radiation, which influence the radiation budget balance and temperature (Guo et al., 2009; Sokolik et al., 1996). The indirect effect is that PM2.5 may influence the chemical composition and density of the atmosphere which in turn influence the climate. Indirect influences also include altering the characteristics of clouds (even the precipitation) since the formation of clouds depends on atmospheric composition, dynamics and other characteristics (Donner, 2016; Guo et al., 2009; Schwartz et al., 1995). Different components of PM2.5 also play different roles in affecting climate change. For example, sulfate aerosol has cooling effects that may slow down global warming but vary geographically (Change, 2001). Moreover, PM2.5 also contributes to the formation of acid rain (EPA .n.d) and reduces agricultural productivity (Chameides et al., 1999). PM2.5 also causes the reduction of visibility due to the hygroscopic properties of constituent Sulphur (Deng et al., 2011). Usually, with high humidity and low temperature, visibility is easily reduced as SO_2 is converted to sulfate under this circumstance, which also causes the "yellow colour" (The World Bank, 2009; Liu et al., 2014).

Due to its size, PM2.5 can be breathed deeply into the lungs and would never come out (Pope III et al., 2000). Long term and short exposure to PM2.5 has been associated with hospital admissions for

pneumonia, emergency department visits, asthma, bronchitis, cardiovascular problems, respiratory infections, lung cancer, heart disease and premature deaths. (Wellenius et al., 2005; Baccarelli, 2009; Jones et al., 2015; Kioumourtzoglou et al., 2016; Zanobetti et al., 2015). According to a survey in *OECD Environmental Outlook To 2050*, it is estimated that in 2010, 1.4 million people died due to PMs and this number is expected to increase to 2.3 in 2030 and 3.6 in 2050. Most of the premature deaths are elderly with weaker immune systems (EPA. n.d). Children are also at high health risks because their immune and respiratory systems are premature: 40% of asthma cases are children, while the population of children only occupies 25% of the whole world's population (EPA. n.d).Recent research also shows the health risks attributed to PM2.5 differ for men and women: the increase of PM2.5 is associated with a higher increase of heart rhythm disturbance admission to hospital for women than for men (Bell et al., 2015). In addition, PM2.5 can even damage DNA in human cell (Sørensen et al., 2003; Corsini et al., 2013).

In addition to the influence on climate change and human health, PM2.5 also brings economic loss. According to Ontario Ministry of the Environment (MOE) (2005), Ontario was burdened with approximately $9.6 billion CAD economic loss due to the high concentration of ozone and PMs in 2003. $5.28 billion CAD loss was due to U.S. emissions, while the rest, $4.32 billion CAD, is attributed to provincial air pollution. It was also estimated that in the Yangtze River Delta, China, the total economic loss caused by the high concentration of PM2.5 was ¥22.10 billion CNY in 2010 (Wang et al., 2015a). Gao et al (2015) assessed that Beijing's economic loss resulted from the haze in January 2013 was more than $250 million USD.

PM2.5 may also lead to other potential issues, such as international dispute. For example, it is estimated that more than 50% of Ontario's PM2.5 is carried from the U.S. (Ontario MECC, n.d). It was also argued that the dust storms from arid regions of Mongolia and Northern and Western China traveled quickly over Korea and Japan (Chung et al., 2002; Sun et al., 2005; Park et al., 2007). In addition, dust and anthropogenic emissions from Asia traverse the Pacific Ocean and enter North America in a few days during spring when storm and frontal activities are most dynamic (Roberts et al., 2006; Park et al., 2007). These discussions indicate PM2.5 is a global issue and may lead to international disputes.

1.1.2 Global Regulations and Standards towards PM2.5

Complaints on air pollution have been raised since the13th century when coal was first used in London. The most famous event was "the Great Smog of 1952" (or "Big Smoke") in London from December 5 to 9, 1952. It was estimated in the following weeks, over 12,000 residents died due to the PMs and sulfur dioxide in this event (Bell et al., 2004). Along with this smog disaster, the Meuse valley fog of Belgium in 1930, the Los Angeles Photochemical Smog Event in 1940, the Donora Smog in the U.S. in 1948 and the Air Pollution inversion in New York in 1963 and 1966 pushed and urged governments and

public organizations to pay more attention to air pollution and the issue of relevant policies and standards are followed.

Table 1.1 Countries and organization's standards on PM2.5

Country/Region /Organization	Issued Year	Yearly Averaged Standard (μg/m^3)	Daily Averaged Standard(24-hour)/(μg/m^3)	Reference
WHO	2006	10	25	Air Quality Guidelines Global Update 2005
Australia	2005	8	25	National standards for criteria air pollutants 1 in Australia
Canada	2012	10 (Standard for year of 2015)	28 (Standard for year of 2015)	Canadian Ambient Air Quality Standards (CAAQS) for PM2.5 and Ozone
China	2012	15	35	Ambient Air Quality Standards
European Union	2015	25		European Emission Standards- Air Quality Standards
Hong Kong	2014	35	75	Hong Kong's Air Quality Objectives
Taiwan	2012	15	35	Particulate Matters Regulation
United States	2013	12	35	National Ambient Air Quality Standards.

Some countries and organizations' regulations are listed in Table 1.1. In the WHO Air Quality Guidelines (Global Update 2005), PM2.5's yearly and daily (24h) standard was set as 10 μg/m^3 and 25 μg/m^3, respectively. This guideline is widely used as a reference for decision-makers across the world to set air quality management standards and goals (WHO, 2015). However, it is surveyed that, in 1600 cities worldwide, only 12% of the urban population's living environment reached WHO air quality guidelines for PM2.5 (WHO. n.d). Average PM2.5 levels in many developing countries can be 4-12 times higher than the WHO PM2.5 guideline level (WHO. n.d). In Canada, PM standards were firstly set by Canadian Council of Ministers of the Environment (CCME) in 2000 (CCME, 2014). In 2012, Canadian Ambient Air Quality Standards (CAAQS) for Fine Particulate Matter and Ozone set the yearly and daily PM2.5 standards for 2015 at 10 μg/m^3 and 28 μg/m^3, respectively. The standards for 2020 will be reviewed in 2016 (CCME, n.d). In additional to the national standards, provinces may set stricter standards. For instance, in the New Ambient Air Quality Criteria for PM2.5 adopted by the British Columbia (B.C.) government in 2009, the criteria was 25 μg/m^3 daily and 8 μg/m^3 yearly (B.C. Air Quality, n.d.).

For the U.S, PM2.5 was firstly regulated in the National Ambient Air Quality Standards (NAAQS) in 1997 (EPA, 2013). NAAQS are established by the U.S. EPA under the Clean Air Act. Since then, PM2.5 standards have been revised and in the last version revised in 2013, the yearly and daily average PM2.5 are 12 $\mu g/m^3$ and 35 $\mu g/m^3$, respectively (EPA, 2013).

Compared to the above organizations and developed countries, China did not pay adequate attention to implementing policy on PM2.5 before 2012. Although scholars have started field studies on PM2.5 in China since the last century (Yao et al., 2002), PMs seldom came into Chinese horizon, while other countries have already began to revise their regulations. In 1982, the first version of Atmospheric Environmental Quality Standards (GB3095-1982) was released by the Chinese Ministry of Environmental Protection (MEPCN), then revised in 1996 (GB3095-1996), 2000 (GB3095-2000) and 2012 (GB3095-2012). In 2012, PM2.5 was eventually considered a mandatory monitoring index in the 2012 Ambient Air Quality Standards (GB3095-2012). The yearly and daily standards are 15 $\mu g/m^3$ and 35 $\mu g/m^3$, respectively. However, this regulation just came into effect nationally on January 1, 2016. Other countries and regions, such as Australia and the the European Union, also created their own regulations on PM2.5, and their current criterion can be found in Table 1.1.

1.1.3 Monitoring PM2.5 by Ground-level Stations and Remote Sensing Techniques: Pros and Cons

Along with implementing policies and standards, governments and public organizations also built air quality programs or ground-level stations to provide ground-measured PM2.5 information. Such as the AirNow Net of the U.S., the Canadian Air and Precipitation Monitoring Network, and the Chinese National Air Quality Forecasting Information System..

Generally, ground-based monitoring data is regarded as an accurate measurement, but it only represents the concentration in a relatively small region (Tian et al., 2010). Moreover, the number of ground level stations is limited and these stations' distributions are often sparse and unbalanced, which makes continuous spatial monitoring difficult (Hu et al., 2013). Apart from the spatial coverage and resolution, the temporal coverage of ground-level PM monitoring, relying on instrument operation period and functionality, also highly varies (Benas et al., 2013). Moreover, the construction and maintenance of ground-level stations are time-consuming and labor-consuming.

The drawbacks of ground-level monitoring mentioned above have led to an ongoing exploration for PM estimation with remote sensing techniques (Benas et al., 2013), which has the following advantages. Firstly, the image derived from satellite could provide complete and general information air quality anywhere in the world (Hadjimitsis, 2009). Secondly, because satellite provides the opportunity to acquire

global air quality, it also became possible to discover the source of urban air pollutants and even global transportation of air pollutants (Wang et al., 2013).What is more, this method costs less to monitor air quality for developing countries or regions which are in lack of ground-level stations but have severe air pollution. Previous studies have shown the correlation between satellite-derived AOD and ground-level PM2.5 concentration by various models (Chu et al., 2003; Wang, 2003). AOD is a parameter of the extinction of electromagnetic radiation at a given wavelength (Chudnovsky et al., 2014). AOD can describe how much sunlight is blocked by particles in the whole atmosphere(NOAA, n.d.).

However, satellite techniques also have shortcomings. The major issue preventing a robust relationship between AOD and PM2.5 is that AOD presents the whole atmospheric aerosol distribution, while ground-level PM2.5 measurements are measured near the Earth's surface (Benas et al., 2013). Furthermore, due to cloud, snow and ice cover, AOD information cannot always be retrieved from remote sensing instruments, which makes researchers unable to estimate PM2.5 concentrations (Lee et al., 2012).

A few satellite sensors are available for AOD observations such as AVHRR, TOMS, MODIS and MISR. Among these sensors, MODIS, boarded on Terra and Aqua satellite, was the most often used one. In addition, users can use 10km MODIS AOD products provided by NASA instead of retrieving AOD from satellite images themselves. This product has been provided since 2000 and it is based on dark target algorithm and deep blue algorithm. In 2014, a new AOD product, with 3 km spatial resolution was released based on only the dark target algorithm and this product provides a chance to predict PM2.5 concentrations in a high spatial resolution. Various statistical models include the simple linear regression model, the multiple linear regression (MLR) model, the geographically weighted regression (GWR) model and artificial neural network (ANN) algorithms. Van Donkelaar et al (2010) generated a map about global satellite-derived PM2.5 using the averaged AOD from MISR and MODIS during 2001 and 2006. Their results are shown in Figure 1.2.

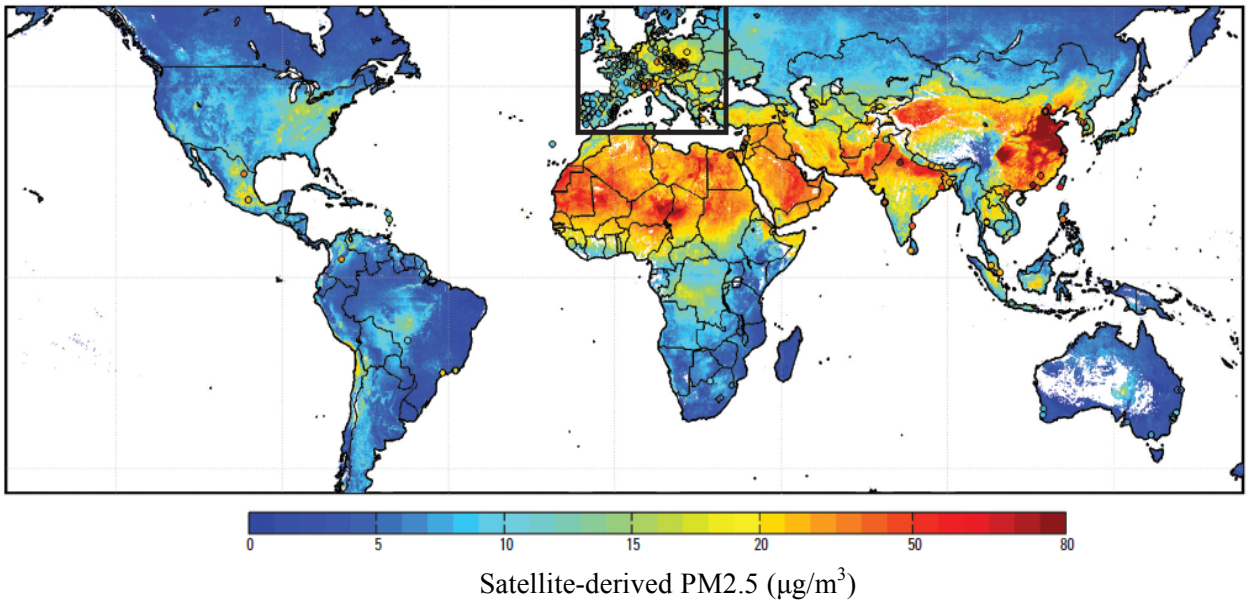

Figure 1.2 Global satellite-derived PM2.5 (µg/m3) averaged from 2001 to 2006.(Source: van Donkelaar et al., 2010)

1.1.4 PM 2.5 in Beijing-Tianjin-Hebei Region of China

Figure 1.2, shows that, the highest value of PM2.5 was distributed in northern China, which was even higher than that in Sahara Desert, where sand storm are prevalent and usually result in high value of PM2.5.. The region of Beijing, Tianjin and Hebei Province, i.e., the BTH region, are all located in the region with the highest PM2.5 concentrations in Figure 1.2. The BTH region consists of 13 cities in total and it is the economic, political and cultural center of China. To a larger extent, to study PM2.5 patterns will provide references for local governments on their economic restructuring. In 2014, the BTH region's population reached 110 million. Moreover, due to the enactment of "Two-Child Policy" and the abolition of "One-Child Policy" in 2015, a new baby boom is happening in the BTH region now. The increasing population will bring more resources consumption and more air pollutants, which in turn means that more people's health will be affected by this severe air pollution. Thus, to monitor and regulate local pollutant emission will be a challenging task in the following years. Additionally, studying PM2.5 concentrations and emissions may help to reduce international disputes. For example, it has been discussed the dust from arid regions of China and Mongolia could quickly travel over Japan and Korean, and could even reach North America (Park et al., 2007).

In conclusion, to explore the use of remote sensing techniques in the estimation of PM2.5 in the BTH region will not only benefit local citizens' health and their quality of life, but also facilitate local

government to take corresponding actions in regulating pollutants emission and protecting its local environment. This study will even contribute to local and global sustainable development.

1.2 Objective of the Study

Overall, the goal of this study is to explore the remote sensing datasets and statistical models for estimating PM2.5 concentrations in the BTH region from September 2014 to August 2015. The specific objectives of this thesis are as following:

- To validate the new MODIS AOD product (the 3 km AOD product) with ground level AOD measurements;
- To compare the difference of performance between the 3 km and 10 km AOD products in PM2.5 estimation at various spatial and temporal scales;
- To explore the MLR and the GWR model in PM 2.5 prediction;
- To apply remote sensing techniques to the public health field for mortality estimation.

1.3 Structure of the Thesis

This thesis consists of six chapters and the remaining chapters are as follows:

Chapter 2 reviews previous studies on PM2.5, AOD, the algorithms and models in PM2.5 estimations, and the application of public health in use of satellite remote sensing technology.

Chapter 3 introduces the study area and describes the datasets used in this study.

Chapter 4 explains the approaches and models, such as MLR and GWR in estimating PM2.5 concentrations.

Chapter 5 presents and compares the major results from different models and products. In addition, it also presents the results in the application of public health.

Chapter 6 draws the conclusion of this study, including the contribution, the uncertainties and limitations of this study, and the potential directions for improvement in the future.

Chapter 2. Literature Review

2.1 Ground-level Measurements of PM2.5

Air quality monitoring networks and programs have been established in many countries and regions to provide pollutant concentrations at variable scales (Tian et al., 2010). Most of them have made their air quality monitoring data freely available online and began to provide PM2.5 monitoring data. Table 2.1 presents some of the air quality programs across the world. For Canada, apart from the national air quality program listed in Table 2.1, Ontario (ON), British Columbia (BC), Newfoundland and Labrador (NL) and Quebec (QC) also have their own air quality program (Air Quality Ontario; British Columbia Air Quality; Department of Environment and Conservation, Newfoundland and Labrador; Province of Québec - Air Quality Index).

Since 2000, China National Environmental Monitoring Center (CNEMC) has started air quality daily report and forecasting work in 47 major cities. However, only sulfur dioxide (SO_2), nitrogen dioxide (NO_2) and PM10 was monitored at that time. In 2012, the number of monitored cites increased to 75 and PM firstly became one of the monitoring items. However, PM2.5 monitoring data was confidential until January 1, 2014. Since then, public can acquire PM2.5 real-time monitoring information in 190 cities. On January 1, 2016, Chinese National Air Quality Forecasting Information System (http://106.37.208.228:8082/) started to provide PM2.5, PM10, SO_2, NO_2, carbon monoxide (CO) and Ozone (O_3) forecasting information in 24 and 48 hours. But only 36 major cities are currently in this forecasting program.

Table 2.1 Main air quality programs around the world

Country		Air Quality Program
America	United State	AirNow Net
	Canada	Air Quality Ontario
	Canada	Canada Air Quality - AQI Maps
	Canada	Canadian Air and Precipitation Monitoring Network (CAPMoN)
	Canada	Environment Canada Air Quality Index
	Mexico	Sistema De Monitoreo Atmosférico de la Ciudad de México
	Brazil	Qualidade do Ar - São Paulo
Asia	China	Current Air Pollution Index (API)
	China	Shanghai Environment Monitoring Center (SEMC)
	India	Air Quality Index
	Taiwan	Current PSI
	Thailand	Regional Air Quality Data
Australia/ Oceania	Australia	Air Quality Index for Western Australia
	Australia	EPA Victoria
	New Zealand	New Zealand Ministry for the Environment - Air Quality
Europe	Europe	Air Quality Levels in Europe - European Environment Agency
	Europe	Air Quality in Europe - CITEAIR
	France	Airparif
	Germany	Umweltbundesamt (UBA) - Current concentrations of air pollutants in Germany
	Italy	SINAnet
	Netherlands	Rijksinstituut (Rural Air Quality Monitoring Network)
	Sweden	Swedish Environmental Research Institute
	Switzerland	Federal Office for the Environment FOEN
	United Kingdom	UK-AIR Daily Air Quality Index

(Source: AirNow Network, 2016)

In terms of the devices for measurement of PM2.5, PM2.5 can be continuously monitored by Tapered Element Oscillating Microbalance (TEOM), Beta Attenuation Monitoring (BAM) and Gravimetric Method, which are not only claimed in Chinese National Ambient Air Quality Standard (NAAQS, GB3905-2012) but also recommended by United States Environmental Protection Agency (U.S. EPA) and Canadian

Council of Ministers of the Environment (CCME) (U.S. EPA, 2006; CCME, 2011). TEOM install filter membranes in a tapered oscillating microbalance. When the sample air is drawn through the filter membrane, PM2.5 accumulates and the oscillation's frequency changes, then the instrument can calculate and output PM2.5 mass concentrations continuously (Queensland Government, 2016). TEOMS have been approved as a measuring method in the Europe (EN12341), U.S. (Designation no. EQPM-1090-079) and etc. (Winkel et al., 2015). Similarly, BAM method is to measure the beta ray's attenuation when beta ray flux through the tape impregnated with PM2.5 (Gobeli, et al., 2008). The National Air Quality Monitoring Network of the Netherlands Gravimetric is currently using this method (Winkel et al., 2015). Gravimetric Method is measured bases on the air volume and the weight difference before and after the sample air goes through filter (MEPCN, HJ 618-2011)

2.2 Aerosol Optical Depth

Aerosol optical depth (AOD) is a dimensionless parameter indicating the extinction of electromagnetic radiation at a given wavelength (Chudnovsky et al., 2014). All types of particles in the atmosphere, including PM2.5, dust and smoke can prevent sunlight by absorbing or scattering (NOAA, n.d.), and AOD can delineate the degree of the attenuation (NOAA, n.d.). AOD values often range from 0 to 2. A value smaller than 0.1 indicates an extremely clear sky with good visibility, while a value larger than1 usually indicates severe hazy conditions (NASA, 2000).

The research on AOD monitoring progressed fast in last 20 years. Two methods are mainly utilized for AOD survey, the ground station-based method and the satellite remote sensing- based method. The ground station-based method mainly adopts the sun spectrophotometer and other instruments: these instruments deployed in stations can acquire the AOD information accurately, but those information can only reflect a limited geographic space. Various ground level monitoring network have been built, such as Aerosol BObotic Network (AEORNET), SkyRadiometer Network (SKYNET), and etc. Remote Sensing technique has advantages, which ground level monitoring site do not have, to monitor AOD, such as the broader coverages. MODIS AOD product is the most widely used remote sensing data in recent years' study.

2.2.1 Ground-level AOD measurement.

Various international and national networks have been established for long-term AOD observation. AEORNET program is established by NASA and PHOTONS (PHOtométrie pour le Traitement Opérationnel de Normalisation Satellitaire; Univ. of Lille 1, CNES, and CNRS-INSU) then extended by other networks, national agencies, institutes, universities, individuals, etc. AERONET is contributed with other networks including (AEROCAN, Baseline Surface Radiation Network (BSRN), Global Atmosphere

Watch-Precision Filter Radiometer (GAW-PFR) network, SKYNET, and etc.) (Levin et al., 2008). National networks are supported by Chinese Sun Hazemeter Network (CASHNET), Australia Bureau of Meteorology (BOM), Finnish Meteorological Institute (FMI), German Weather Service (DWD), Japan Meteorological Agency, U.S. (networks including Atmospheric Radiation Measurement (ARM) Program and Surface Radiation (SURFRAD) (Levin et al., 2008).

AERONET is a network of sun/sky radiometers to provide global, long-term and continuous ground-level AOD information with high temporal resolution (15 min) and low uncertainties (0.01-0.02) (Sayer et al., 2013). The installation of AERONET instruments has started in early 1990s and more than 750 sites have been built until now. The distributions of AERONET sites are shown in Figure 2.1. The instrument deployed in AERONET site is an automatic tracking sun and sky scanning radiometers (CIMEL Electronique CE-318 Sun-sky radiometer) (Hollben et al., 1998; Choi et al., 2016), which is shown in Figure 2.2. Direct radiation is measured by this instrument with a 1.2° full field of view at 340, 380, 440, 500, 675, 870, 940, and 1020 nm (nominal wavelengths) every 15 minutes (Eck et al., 2005; Choi et al., 2016;). Except 940nm, which is used for column water vapor retrieval, all other wavelengths are used for AOD retrieval (Hollben et al., 2001; Eck et al., 2010; Choi et al., 2016). With a high accuracy (0.015 uncertainty) (Slutsker et al. 1999), AERONET AOD is widely used to validate AOD retrievals from satellite sensor systems, including MODIS (Munchak et al., 2014; Tao et al., 2015), TOMS (Torres, 2002), SeaWiFS (Mélin et al., 2010), MISR (Bibi et al., 2015) and AVHRR (Kahn et al., 2005).

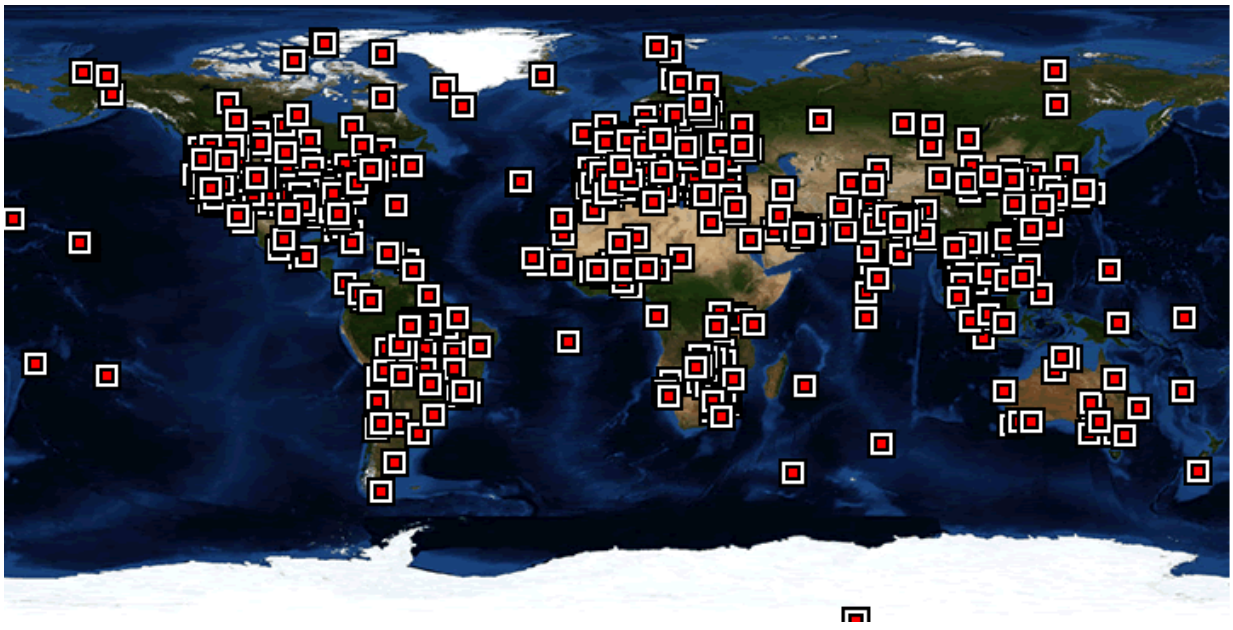

Figure 2.1AERONET sites (Source, AERONET, 2016a)

Figure 2.2 CIMEL Sunphotometer (Source: AERONET, 2016b)

SKYNET is an observation network to study aerosol-cloud-radiation interaction. Until now, more than 25 sites have been built and their locations are shown in Figure 2.3. It can be found most of the sites are deployed in Asia, including Japan, China, India, Mongolia and Europe. All sites are equipped with a sky radiometer and radiation instruments as main instruments. Some selected sites are also equipped with other instruments such as the cloud camera. Sano et al. (2013) showed that the difference between SKYNET and AERONET AOD at a wavelength of 0.67 is less than 0.008, which indicates that they have similar accuracy in AOD monitoring.

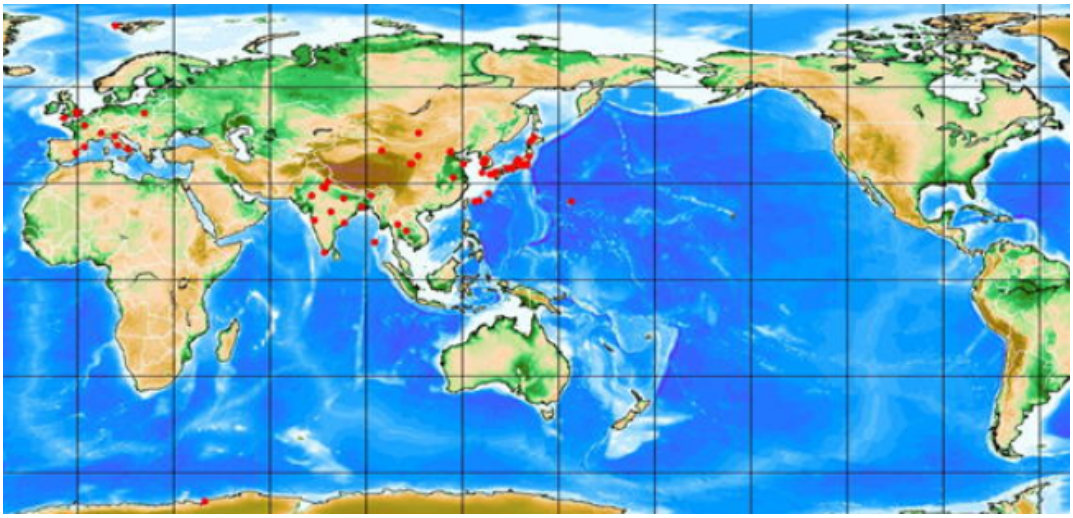

Figure 2.3 SKYNET/skyradiometer sites map. Sites with data available as of July 30, 2013 are shown in red. (Source: SKYNET, 2016)

GAW-PFR network is built with the equipment of a new generation of sunphotometers, PFR (Lavin et al., 2008) by World Meteorological Organization GAW programme. A first comparison in 2000 at Mauna Loa showed an excellent agreement within 0.005 between AERONET AOD and GAW-PER AOD (McArthur et al., 2003).

In addition, Lidar is a useful technology for aerosols' measurement. Several Lidar networks are available for relevant profiles such as the Micro-Pulse Lidar Network of NASA (MPLNET).

2.2.2 Satellite Data and Algorithms for AOD retrieval

The Remote Sensing research on aerosol began from the mid-1970s and nowadays a very rich system by using the satellite remote sensing AOD have been built (Guo et al., 2009). In this subsection, the satellite sensor system for AOD retrieval and most widely used algorithms are reviewed.

2.2.2.1 Satellite Sensor Systems for AOD Retrieval

Since the development of remote sensing techniques from 1980s, satellite images have been explored for AOD retrieval. Most often used sensors for AOD observation are listed in Table 2.2, which is explained in the following content.

The Advanced Very High Resolution Radiometer (AVHRR) was the earliest sensor used in AOD study (Guo et al., 2009). In 1978, the AVHRR was aboard on TIROS-N. Since then, almost 40 years AVHRR datasets have been accumulated which makes it a unique data series for a long-term continuous record of aerosol properties over both ocean and land. However, retrieving AOD from AVHRR images is a challenging work because of the limitation of band-setting: there is only one visible wavelength (Mei et al., 2013). Kaufman et al. (1998) retrieved AOD from AVHRR data from dark dense vegetation. In 2012, Land Aerosol property and Bidirectional reflectance Inversion by Time Series technique (LABITS) was proposed by Li et al. (2012) for aerosol retrieval from NOAA AVHRR data. Although AVHRR AOD can facilitate the aerosol climatology and climate change study after 1980s, snow, ice, and cloud cover still impede AVHRR from retrieving AOD. Additionally, this monitor is too sensitive to detect cloud, systematic and random error range, which has fluctuation (Liu et al. 2004).

Similar with AVHRR, the Total Ozone Mapping Spectrometer (TOMS) has also been able to provide AOD data from 1978 to present. The TOMS aboard on Meteor-3 stopped in December 1994, and it was succeeded by TOMS aboard on Earth Probe launched later in July 1996, but this definitely left a gap in data availability. This dataset consists of daily Ozone data and monthly AOD at 1° resolution. As a backscattered near-ultraviolet radiations satellite, TOMS has strong analysis capabilities to identify aerosol sizes and types for regional studies (Torres et al., 2002).

The POLarization and Directionality of the Earth's Reflectances (POLDER) instrument is the only instrument to offer a global and long-term polarized observations (Wang et al., 2015b). With POLDER monitor, AOD with thin cloud condition can be retrieved due to polarization property of the monitor (Xia et al., 2009). Moreover, because polarization is sensitive to particle's size, aerosol types can be identified by different polarized reflectance (Li et al., 2015). However, this monitor only served from 1996 to 2012. Furthermore, AOD retrieved from POLDER shows low accuracy (Quaas et al., 2005) and the results with dust weather need to be improved because of the complex particles polarization characteristics (Xia et al., 2009).

Compared with other monitors, the Sea-viewing Wide Field-of-view Sensor (SeaWiFS), designed for observing water surface, provides more stable and accurate AOD data especially over ocean. An AOD dataset is provided based on "Deep Blue" algorithm at 550nm (algorithms are reviewed in the next sub subsection). However, SeaWiFS was only in operation during 1997 and 2010.

Moderate Resolution Imaging Spectroradiometer (MODIS) is carried on both Terra and Aqua launched in 1999 and 2002, respectively. The band designation for MODIS can be found in Table 2.3: there are seven well-calibrated channels for spectral information ranging from visible to SWIR wavelength (470, 550, 670, 870, 1240, 1640 and 2100 nm) (Chu et al., 2003). MODIS derives an AOD product (Terra: MOD04_L2; Aqua: MYD04_L2) at 10 km resolution using "Deep Blue" (DB) and "Dark Target" (DT) algorithms. DT is adopted over ocean and dark land, such as vegetated area, while DB is applied over the entire land areas including both dark and bright surfaces in MODIS Collection 6 (C6) product. "Collection" means a MODIS dataset and previous collections include 001, 003, 004, 005 and 051. Data user can choose the parameter when downloading data online, such as "AOD_550_Dark_Target_Deep_Blue_Combined" and "Deep_Blue_Aerosol_Optical_Depth_550_Land". For more detailed product information, please refer to MODIS Website (http://modis.gsfc.nasa.gov/). In 2014, DT algorithm team released 3 km MODIS AOD product in a separate file (Terra: MOD04_3K; Aqua: MYD04_3K) as a part of MODIS C6 production. Xie et al (2015) estimated PM2.5 within urban region in Beijing, China using 3 km MODIS AOD product. In the same year, Retails et al. (2015) identified the correlations between 3 km MODIS AOD product and ground-based PM10 measurements in the area of Athens, Greece. AOD retrieved from MODIS by using visible spectrum and infrared spectrum can reduce errors caused by a single band calibration (Xie et al., 2011). Meanwhile, the high temporal resolution (twice a day provided by Terra and Aqua) is another advantage of MODIS AOD product over others. However, cloud, snow and ice still affect the accuracy of AOD retrieval from MODIS (Gupta et al. 2006).

Table 2.2 Most often used sensors for AOD observation

Sensor	Satellite	Spectral Coverage (μm)	Spatial Resolution (km)	Temporal Resolution (day)	Launched Year	Out of Service Year	Organization	Major Advantages for AOD Retrieval	Major Disadvantages /Challenges for AOD Retrieval
AVHRR	TIORS-N/NOAA	0.55-12.5	1.09	0.5	1978		U.S.: NOAA	Long-term high-resolution observation (38years)	Band-setting (only one visible wavelength) (Mei et al., 2013)
TOMS	Nimbus-7/Meteor 3/Earth Probe	0.31-0.38	1°	1	1978		U.S.: NASA	Long-term observation (36) years	AOD data is provided monthly (George et al., 2013)
POLDER	Adeos/Parasol	0.44-0.91	6.00*7.00	4	1996	2012	France: CNES	AOD with thin cloud condition can be retrieved; Multi-angle observation.	It has been out of service since 2012; Low accuracy(Quaas et al., 2005)
SeaWiFS	OrbView2	0.40-0.89	1.00 /4 .00	1	1997	2010	U.S.: NASA	Stable and accurate AOD data especially over ocean	It has been out of service since 2010
MODIS	Terra/Aqua	0.41-14.39	0.25/0.50/1.00	1	1999		U.S.: NASA	High temporal resolution (twice a day from Terra and Aqua)	Cloud, snow and ice still affects AOD retrieval.
MISR	Terra	0.45-0.87	0.25	2-9 depending on latitude	1999		U.S.: NASA	Observation from multi-angles.	Some areas can only be covered 3-4 time per month.
AATSR	ENVISAT	0.55-12	1.00	35	2002	2012	European: ESA	Better accuracy in desert region than MODIS AOD(Bevan et al. 2012)	Less accuracy in other region on land than MODIS AOD (Bevan et al.. 2012)
MERIS	ENVISAT	0.39-1.04	1.05/0.26	3	2002	2012	European: ESA	Good accuracy in arid area (Benas et al. 2013).	Could not reach an ideal accuracy over water surface (Benas et al., 2013).
CCD	HJ-1	0.45-0.90	0.03	4	2008		China: CRESDA	High spatial-resolution	Band setting (the lack of a shortwave infrared band) makes it different to retrieve AOD (Sun et al., 2010).
OLI/TRIS	Landsat 8	0.44-1.38	0.03	16	2013	2013	U.S.: NASA	High spatial-resolution	Low temporal resolution.

Table 2.3 Band designation for MODIS

Primary Use	Band	Bandwidth (Band1-19:nm; Band20-36:um)	Spectral Radiance (W/m2 -μm-sr)	Spatial Resolution(m)
Land/Cloud/Aerosols Boundaries	1	620 - 670	21.80	250
	2	841 - 876	24.70	
Land/Cloud/Aerosols Boundaries	3	459 - 479	35.30	500
	4	545 - 565	29.00	
	5	1230 - 1250	5.40	
	6	1628 - 1652	7.30	
	7	2105 - 2155	1.00	
Ocean Color/Phytoplankton/Biogeochemistry	8	405 - 420	44.90	1000
	9	438 - 448	41.90	
	10	483 - 493	32.10	
	11	526 - 536	27.90	
	12	546 - 556	21.00	
	13	662 - 672	9.50	
	14	673 - 683	8.70	
	15	743 - 753	10.20	
	16	862 - 877	6.20	
Atmospheric Water Vapor	17	890 - 920	10.00	
	18	931 - 941	3.60	
	19	915 - 965	15.00	
Surface/Cloud Temperature	20	3.70 - 3.84	0.45(300K)	
	21	3.93 - 3.99	2.38(335K)	
	22	3.93 - 3.99	0.67(300K)	
	23	4.02 - 4.08	0.79(300K)	
Atmospheric Temperature	24	4.43 - 4.50	0.17(250K)	
	25	4.48 - 4.55	0.59(275K)	
Cirrus Clouds Water Vapor	26	1.36 - 1.39	6.00	
	27	6.54 - 6.90	1.16(240K)	
	28	7.18 - 7.48	2.18(250K)	
Cloud Properties	29	8.40 - 8.70	9.58(300K)	
Ozone	30	9.58 - 9.88	3.69(250K)	
Surface/Cloud Temperature	31	10.78 - 11.28	9.55(300K)	
	32	11.77 - 12.27	8.94(300K)	
Cloud Top Altitude	33	13.19 - 13.49	4.52(260K)	
	34	13.49 - 13.79	3.76(250K)	
	35	13.79 - 14.09	3.11(240K)	
	36	14.09 - 14.39	2.08(220K)	

(Source: NASA, 2016)

Multi-angle Imaging SpectroRadiometer (MISR), carried only on Terra, collects information from multi- nine angles. Most of the aerosol information comes from the observation taken at scattering angles. Scattering angles are the angles between observation direction and initial sun's direction. These additional information makes it possible to derive aerosol properties (NASA, n.d.b). Another unique property for MISR is its sub-pixels: every standard 17.6 km ×17.6 km pixel containes16 sub-regions (1.1 km × 1.1 km). This property highly increases the ability to avoid cloud disturbance significantly (Martonchik et al. 2004). However, due to the characteristics of MISR orbit, the monitor only passes certain places near the equator 3 or 4 times per month. Long time gap raises difficulties in studying aerosols in those areas where are in lack of ground based monitors (Martonchik et al., 2004).

In addition to MISR, Advanced Along-Track Scanning Radiometer (AATSR) also provides two-angle observation (55° and 90°). Together with AATSR, Medium Resolution Imaging Spectrometer (MERIS) is also launched on Envisat ("Environmental Satellite") in 2002. MISR's nine-angle observation is able to reduce the error caused by atmospheric scattering and absorption of single angle monitors. The AOD derived from AASTR, in the desert region, shows a better accuracy than that derived from MODIS, while in other regions on land, it is less accurate than that derived from MISR (Bevan et al., 2012). Similar with AATSR, MERIS data shows a good accuracy in an arid area. However, AOD retrieved with MERIS data over water surface could not reach an ideal accuracy (Benas et al., 2013). Various algorithms have been developed for retrieving AOD from AATSR and MERIS, such as MERIS/AATSR synergy algorithm (North et al., 2009) and the Multi-Angle Implementation of Atmospheric Correction) (MAIAC) algorithm (Lyapustin et al., 2011). Basing on synergistic MERIS/AATSR aerosol observation, Beloconi et al. (2016) estimated urban PM10 and PM2.5 concentrations in Greater London Area in 2016.

Huan Jing 1 (HJ-1) satellite, carrying a charge-coupled device (HJ-1 CCD) sensors, was launched in 2008 by Chinese Resources Satellite Application Center. The high spatial and temporal resolution (30 m; 4 days) makes HJ-1/CCD a suitable instrument for AOD monitoring. However, due to the absence of shortwave infrared band, it becomes a challenge for HJ-1/CCD to utilize traditional algorithms, such as DDV, to retrieve AOD data. Sun et al. (2010) developed a new algorithm for HJ-1/CCD by combining MODIS surface reflectance as a support. Li et al. (2011) used the similar method to estimate AOD with a resolution of 100 m, but its applicability on different underlying surface was still an issue. Yu et al. (2015) applied DDV algorithm over dark pixels and DB algorithm on light pixels but the results still had high biases with MODIS AOD.

Landsat8 was launched in February 2013 successfully and sensors boarded on it consist the Operational Land Image (OLI) and the Thermal Infrared Sensor (TIRS). Compared to the Enhanced Thematic Mapper Plus (ETM+) on Landsat-7, OLI has two new bands: blue (0.43-0.45μm) and SWIR (1.36-1.39μm). Zhang et al. (2015) applied DT algorithm toOLI data to retrieve AOD over Beijing. Later in the same year, Sun et al. (2015) constructed a Land Surface Reflectance (LSR) database with MODIS surface reflectance product, based on which AOD can be retrieved from OLI data at 500 m spatial resolution. Although the high resolution of OLI data will facilitate scientists to monitor AOD even air quality variables on regional scale, the relatively low temporal resolution (16 days) is the main limitation of this dataset.

2.2.2.2 Algorithm for AOD Retrieval

Until now, more than 10 algorithms have been explored for AOD retrieval from satellite datasets, such as Multi-channel Reflectance, Dense Dark Vegetation algorithm (DDV, also known as dark target (DT) algorithm), Structure Function Algorithm, Contrast Reduction (CR) algorithm and Deep Blue (DB) algorithm. Some of the most often used algorithms are listed in Table 2.4. MODIS Atmosphere Discipline Group adopts DDV and DB to retrieve MODIS AOD product.

Multichannel Reflectance algorithm's principle is, the aerosol characteristics can be identified with different channels by being compared with channels' reflectance ratio, namely color ratio (Guo et al., 2009). Durkee (1986) applied the Multichannel Reflectance algorithm on AVHRR Channels 1 and 2 to retrieve AOD over water bodies.

Kaufman et al (1988) utilized Dark Object algorithm to estimate AOD via the low reflectance of dark vegetation in the visible spectrum. Since then, this method has been widely used to generate satellite retrieved AOD, such as MODIS AOD product. DDV assumes earth as a Lambertian. For the dark object (the pixel covered with vegetation), the reflectance in the red and blue band are negligible. So the satellite received reflectance can be considered the contribution from atmosphere. Dark object can be identified by normalized difference vegetation index (NDVI) (Zhang et al., 2015). The apparent reflectance received by satellite can be described as Eq. (2-1):

$$\rho_{TOA}(\mu_s, \mu_v, \emptyset) = \rho_0(\mu_s, \mu_v, \emptyset) + \frac{T(\mu_s)\cdot T(\mu_v)\rho_s(\mu_s,\mu_v,\emptyset)}{[1-\rho_s(\mu_s,\mu_v,\emptyset)S]} \quad (2\text{-}1)$$

where ρ_{TOA} is the reflectance of top of atmosphere; $\mu s = \cos\theta_s$, $\mu v = \cos\theta_v$, θ_s is solar azimuth; θ_v is satellite azimuth, and $\emptyset$ is relative azimuth; ρ_0, T and S represent atmospheric status; ρ_s is surface reflectance. Assuming different atmospheric parameters and geometric information, lookup table (LUT) can be generated by the Second Simulation of a Satellite Signal in the Solar Spectrum (6S)

model based on the relationship between AOD and, ρ_0, T and S. Then LUT can be used to retrieve AOD. Simulation of the Satellite Signal in the Solar Spectrum (5S) model was developed by Tanre et al. (1986) to simulate the solar radiation. Later, Vermote et al. (1997) developed 5S model to 6S model in 1997. 6S model is available online (http://6s.ltdri.org/#) along with the user manual. However, due to the principles of DDV, this algorithm does not work well in regions where are in lack of surface plants, such as Polar Regions and desert.

Table 2.4 Summary of the most often used AOD retrieval methods

Algorithm	Advantages	Limitation	References
Multichannel Reflectance	Work well with water bodies.		Durkee et al. (1986)
Dense Dark Vegetation	Easy principles. Work well with the surface covered with vegetation.	Does not work well with the surface without vegetation (dark target).	Kaufman et al. (1988)
Structure Function Method	Works well in the desert, urban and other bright area	The choice of reference needs easily increase the accidental error	Tanre et al. (1988)
Polarization and Directionality of the Earth's Reflectance	Helps to retrieve aerosol of mixed pixel with water over land	BRDF is required.	Leroy et al. (1997)
Thermal Infrared Contrast Method	Work well with arid and half-arid region	Does not work well with the areas with less dust.	Tanre et al. (1991)
Deep Blue Method	Can be worked with any satellite monitors with blue band	Inapplicable for historical AOD research.	Hsu et al. (2004)
Simplified Aerosol Retrieval Algorithm(SARA)	Does not require LUT in the computation; Work well with both bright urban and dark rural surfaces (Bilal et al., 2013); Better applicability at different level of air pollution (Li et al., 2015).	Does not work well for high-level AOD (Bilal et al., 2013); Applicable only with MODIS collections.	Bilal et al. (2013)

Structure function method assumes that surface reflectance does not change during the daytime, so AOD information can be derived basing on the difference of surface reflectance with a given

reference atmospheric condition (Tanre et al. 1988). This method works well in the desert, urban and other bright area. However, the choice of reference is easy to increase the accidental error.

Polarization and Directionality algorithm has been applied with POLDER, MODIS data and other monitors' data (Vachon et al. 2004). Polarization is also known as bidirectional reflectance. This algorithm relies on backward scattering polarization characteristics to estimate AOD. This algorithm could help to retrieve aerosol of mixed pixel with water over land (Leroy et al., 1997). However, Polarization and Directionality algorithm requires Bidirectional Reflectance Distribution Function (BRDF).

For thermal infrared contrast method, AOD can be retrieved because infrared channel is sensitive to the dust (Ackerman, 1997). This method is based on a series of continuous contrast of observations. This method works well with arid and half-arid area, but it may not work well for the areas with less dust (Guo et al., 2009).

To increase accuracy in AOD retrieval over bright area like desert or bare land, Hsu et al. (2004) purposed a novel algorithm (deep blue), based on the blue band. Surface reflectance is low at these blue wavelengths so the aerosol's change can be detected with the change of total reflectance and enhanced spectral contrast (Hus et al., 2004; Ginoux et al., 2012). Compared with previous algorithms which mainly used bands longer than 600nm (Red), deep blue algorithm can be implemented with any satellite monitors with blue band (Hsu et al., 2004). However, early monitors, such as AVHRR and TOMS, do not contain blue band. So when doing historical AOD research, deep blue algorithm may be inapplicable.

2.3 PM2.5 Estimation Models

2.3.1 Factors

Meteorological parameters and socio-economic factors have been widely utilized as inputs to perfect models. These factors are listed in Table 2.5.

Table 2.5 Factors used in PM2.5 estimation models

Type	Factors	Principles	Reference
Natural/ Meteorological Parameters	Visibility (m)	Meteorological variables and other natural factors affect the formation and dispersion of PM2.5; PM2.5 also affect some weather conditions, such as visibility.	You et al. (2016)
	Relative Humidity (%)		Kumar et al. (2007)
	Precipitation (mm)		Tai et al. (2010)
	Temperature (K)		Kumar et al. (2007)
	Wind Speed(m/s)/Direction		Lei et al. (2015)
	Boundary Layer Height (m)		Just et al. (2015)
	Elevation (m)		Paciorek et al. (2008a)
	Pressure (hPa)		van Donkelaar et al. (2006)
	Dew Point (K)		Zhang (2013)
Socio-economic Factors	GDP (dollar)	Human activities generate considerable amount of PM2.5	Wang et al. (2016)
	Population		
	Road Density (m/m2)		Paciorek et al. (2008a)
	Land Use Information		Kloog et al. (2012)

Meteorological variables and other natural factors affect the formation and dispersion of PM2.5. At the same time, PM2.5 also affect some weather conditions, such as visibility, so weather conditions' variance can be considered as the reflection of PM2.5' effects. More specifically, as introduced in Section 2.1, components in PM2.5 can severely reduce visibility by absorption and scattering of lights due to their hygroscopic property (Chen et al., 2014). This is because with the content of Sulphur, PM2.5 are hygroscopic. With the higher humidity, the hygroscopic particles absorb more water, then scattering becomes more intensive (Deng et al., 2011). Moreover, RH helps the formation of ammonium nitrate (Tai et al., 2010). However, precipitation has a negative correlation with PM2.5 components due to scavenging effect (Tai et al., 2010). In addition, temperature is positively associated with some components of PM2.5, such as sulfate and organic carbon and. (Tai et al., 2010). At the same time, it has been found there is a negative correlation between temperature and nitrate in some regions (Tai et al., 2010). Additionally, wind speed and wind direction strongly associate with the concentrations of PM 2.5 because PM 2.5 components can be carried by wind from the source region of air pollution to other areas (Tai et al., 2010). Furthermore, Planetary boundary layer (PBL) is the lowest part of the atmosphere and it can affect regional pollutants dispersion (Hu et al., 2014). During the daytime, the height of PBL (HPBL) increased a few kilometres due to the sun radiation, while at

night, HPBL decreases and PBL becomes stable (Miao et al., 2015). It is often assumed that PMs are well mixed in PBL (Gupta et al., 2006; Koelemeijer et al., 2006; Di Nicolantonio et al., 2007; Wu et al., 2012). Therefore HBPL is often used to improve PM2.5-AOD estimation model. Regions with high value of elevations, such as mountain or plateau region, tend to impede pollutant's dispersion. Also, with the increase of elevation, PM2.5 concentration and composition also changes due to the changes of temperature and pressure. Therefore elevation is also utilized as an independent variable in the model. Other meteorological factors, such as dew point, can also contribute to PM2.5-AOD estimation models (Zhang, 2013).

However, the use of only meteorological factors is not sufficient to explain PM2.5 concentrations because human activities also generate a considerable amount of PM2.5. Road traffic, aviation and marine transportation, household activities (cooling and heating), construction, and industry (especially heavy industry) are all emission sources of PM2.5 (Keuken et al., 2013; Lin et al., 2013). Thus, GDP, population, road density, and other land use information are also utilized to perfect models reflecting the impact of human activities on PM2.5 (Paciorek et al., 2008a; Kloog et al., 2012; Wang et al., 2016).

2.3.2 Models

Current PM2.5-AOD estimation models can be classified into two types: observation-based and simulation-based methods (Lin et al., 2015). Simulation-based models are mainly basing on chemical transport models (Drury et al., 2010; Liu et al., 2004; Martin, & Park, 2006; van Donkelaar et al., 2010) while observation-based models mainly rely on statistical regression (Lin et al., 2015). Table 2.6 presents some typical models which are described in the following content.

2.3.2.1 Simulation-based Model

Simulated-based models are always based on 3D chemical transport models (3D CTM) (San José et al., 2008). These models have been developed since 1990s (San José et al., 2008) and always consist of a meteorological driver and a chemical transport module. Liu et al. (2004) introduced Goddard Earth Observing System Atmospheric Chemistry Transport (GEOS-Chem) model into AOD-PM2.5 simulation. GEOS-Chem is driven by meteorological variables from the GEOS of NASA (Chen et al., 2009). Later, van Donkelaar et al. (2006) applied GEOS-Chem model and calculated the PM2.5 concentration with MODIS and MISR data for 2001 to 2005 at a global level. In their research, it is estimated that Northern India and East Asia were exposed to pronounced PM2.5 levels (40-50 $\mu g/m^3$) and more than 30% of the global population were exposed to PM2.5 concentrations higher than 35 $\mu g/m^3$. However, the PM2.5 range they estimated is from 0 to 50 $\mu g/m^3$, which does not indicate the

varied situation when PM2.5 were higher than 50 μg/m^3, which is common in China and India. In 2015, van Donkelaar et al (2015a) continued to utilize GEOS-Chem model and SeaWiFS, MISR and MODIS data to develop a global map of mean PM2.5 concentrations from 2001 to 2010, which is shown in Figure 2.4. The PM2.5 concentration s in China exceeds 80 μg/m^3.

The Weather Research and Forecasting model coupled with Chemistry (WRF-Chem) is a numerical weather prediction system for atmospheric research needs (Tie et al., 2007). WRF-Chem models results present a good association with the correct emission database (San José et al., 2008; Saide et al., 2011). Eta-CMAQ and MM5-CMAQ model have also been applied in estimating PM2.5 (Yu et al., 2004; San Joset al., 2008; Lang et al., 2013). For more examples of meteorological drivers and chemical transport modules, please refer to San José's research (2008).

The main advantage of these models is these models are able to simulate the factors (such as chemical composition and particulate size) affecting the correlation between AOD and PM2.5. However, complex principles and operations are major shortages of these models.

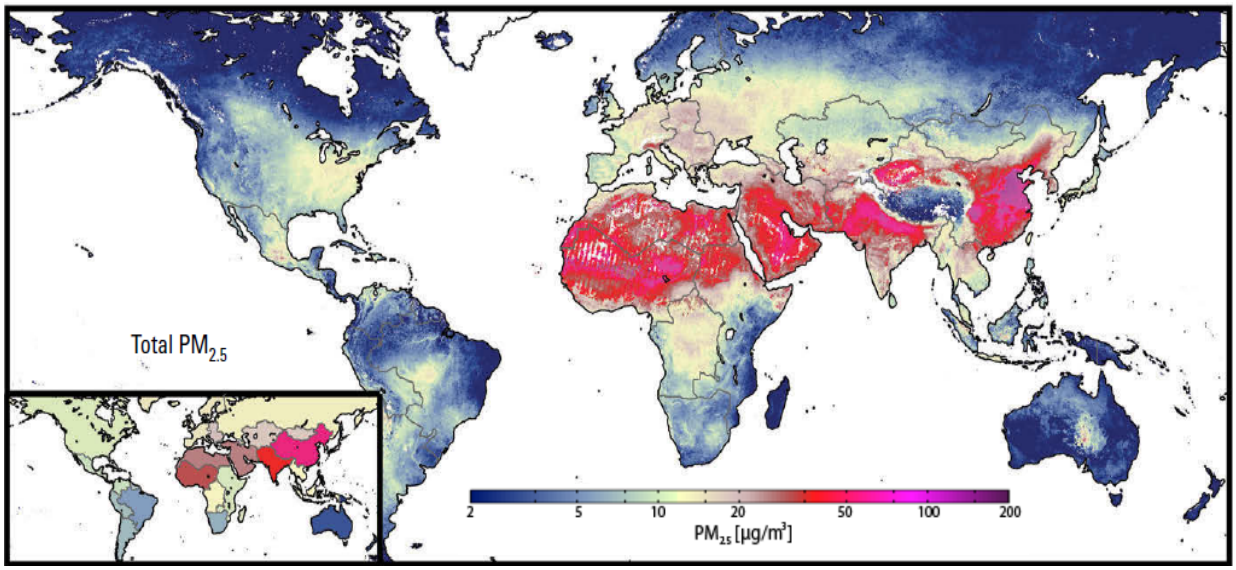

Figure 2.4 Global mean PM2.5 concentrations from 2001 to 2010 (Source: van Donkelaar et al., 2015)

Table 2.6 Most often used PM2.5-AOD models

Type	Model	Strength	Weakness		References
Simulation-Based Model	GEOs-CHEM	Simulate chemical composition and particulate size	Complex principles and operations		Liu et al. (2004)
	Eta-CMAQ				Yu et al. (2004)
	MM5-CMAQ;				San José et al. (2008)
	WRF-CHEM				Saide et al. (2011)
Observation-Based Model	Simple Linear Regression	Simple principles	Aerosol structure, composition and size are not considered; They can hardly predict episodic events; They tend to overestimated the low concentrations and underestimated the high ones	Other factors are not considered	Chu et al. (2003)
	Multiple Linear Regression (MLR)	More factors can be taken into account.		Low spatial resolution of the estimation from the MLR model with only meteorological factors	Li et al. (2011)
	Land Use Regression (LUR)	It is an useful tool to study intra-urban variability of PM2.5 with a high spatial resolution (Meng et al., 2016)		Temporal resolution is limited (Kloog et al., 2012); LUR does not predict for short-term exposure study (Kloog et al., 2012)	Kloog et al. (2012)
	Non-linear Model	This model describes non-linear relationship between dependent and independent variables and computing intensity is not added (Li et al., 2011)		This model only works for certain areas or seasons (Li et al., 2011).	Engel-Cox et al. (2004)
	Generalized Additive Model (GAM)	Non-linear relationship between dependent and independent variables can be considered		Local variables are not considered	Li et al. (2011)
	Geographically Weighted Regression (GWR)	The consideration of local variables.		Computing intensity is increased.	Hu et al. (2013)
	Artificial Neural Network algorithms	This model is helpful to reduce uncertainties and improve the accuracy when estimating high and low PM mass (Gupta et al., 2009b)		Computing intensity is increased. Some sites with high concentrations were still underestimated (Wu et al., et al., 2012)	Gupta. (2009b)

2.3.2.2 Observation-based Model

The general form of simple linear regression model can be described as Eq. (2-2):

$$PM2.5 = C + M * AOD \quad (2\text{-}2)$$

where C is the intercept and M is the slope (Gupta et al., 2009a).

Chu et al. (2003) applied this simple linear regression model to estimate PM10 concentration with daily averaged AERONET AOD measurements in Italy and the coefficient of determination (R^2) was 0.67. At the same time, Wang & Christopher (2003) adopted MODIS AOD product (Level 2, Version 4) and 7 stations' PM2.5 concentrations in Alabama, U.S. and built a simple linear regression with a R^2 of 0.49. Li et al. (2005) also demonstrated a good correlations between PM10 and AOD in Hong Kong with simple linear regression. Although their researches present AOD as a useful tool for PM estimation, most researchers agree that AOD alone cannot retrieve surface distribution of PM2.5 with satisfied accuracies because the inconsideration of other factors may affect AOD-PM2.5 relationship (Paciorek et al., 2008b; Gupta et al., 2009a).

To incorporate more parameters, the MLR model was developed (Gupta & Christopher, 2009a; Li et al., 2011). The general form of multiple regression models can be described as Eq. (2-3):

$$PM2.5 = C_1 + C_2 * AOD + C_{3\ldots n} * V_{3\ldots n} \quad (2\text{-}3)$$

where C_1 is the intercept of this model and C_2 is the regression coefficient for AOD. C_3-C_n are regression coefficients for the corresponding predictor variables, while V_3-V_n are predictor variables (Gupta, 2009a). These variables could be temperature, relative humidity, height of the planetary boundary layer and wind speed. Gupta et al. (2009a) developed MLR equations with AOD and meteorological factors over the southern U.S. Their results indicated there were up to threefold increases from simple linear regression's correlation coefficients to the MLR model's correlation coefficients. Li et al. (2011) applied MODIS AOD and NCEP (National Centers for Environmental Prediction) in regression models and the R square is improved from 0.24 in simple linear regression model to 0.44 in the MLR model. Though showing a better capacity due to the consideration of more relevant variables, most previous MLR models with meteorological factors are based on a global, national or regional level, the variability within a city can hardly be derived due to the spatial resolutions.

In this situation, it is more accurate to estimate the intra-urban variability of PM levels with land-use regression models (Meng et al., 2016). Land use regression (LUR) is one of the multivariate regression models and it incorporates land use variables at a monitored level, such as elevation, traffic density and account, PM2.5 point emissions, road density and road type, the distance to main road and the percentage

of urban area (Ryan et al., 2007; Kloog et al., 2012). Though the LUR model could help to study PM2.5 distribution with a high resolution, the temporal resolution is often limited because land use terms do not generally vary in a short time (Kloog et al., 2012; Meng et al., 2016).

Although aforementioned studies proved linear regression as a strong tool to predict PM2.5, PM2.5-AOD relationship could be non-linear (Engel-Cox et al., 2004; Liu et al., 2005). A general format of non-linear model can be described as Eq (2-4) (Li et al., 2011):

$$\log(PM_{2.5}) = a_0 + a_{AOD} \cdot \log(AOD) + + a_{RH} \cdot RH + a_T \cdot \log(T) \ldots + a_V \cdot f(V) \quad (2\text{-}4)$$

where a_0 is the intercept, a_{AOD}, a_{RH}, a_T and a_V are regression coefficients of $\log(AOD)$, RH (relatively humidity), $\log(T)$ (T: Temperature) and function of other variables. Li et al. (2011) showed non-linear regression model shows a better performance (R^2=0.49) than simple and multiple linear regression (R^2= 0.24; 0.44). You et al. (2016) also improve the coefficient of determination from 0.08 when using linear regression to 0.61 when using non-linear regression in a semi-arid area in northern China. Similar to non-linear regression model, a more complex model, generalized additive model (GAM) also allows non-linear function of variables. This model is developed for each scaling method at each site (Liu et al., 2011). By allowing some of all variables to be non-linear related to dependent variable, GAM improves the capacity of traditional linear regression (Liu et al., 2009; Liu et al., 2011; Liu et al., 2012). Though non-linear model is able to improve the accuracy in these studies, it only works for certain areas and or seasons (Li et al., 2011). Moreover, similar to linear regression, this model does not consider local variables: this is because the correlations between AOD and PM2.5 are non-stationary, so the dependent and independent variables are not spatially constant (Engel-Cox et al., 2004; Hu et al., 2009; Hu et al., 2013).

To solve this problem, spatial regression model, such as the GWR model is also applied to build a local relationship between AOD and PM2.5 (Hu et al., 2013). Instead of assuming global geographic uniformity, GWR estimates PM2.5 in consideration of local variability. The GWR model can be expressed as Eq. (2-5):

$$PM_{2.5\,sd} = a_{0,sd} + a_{1,sd}AOD_{sd} + a_{2,sd}V_{2,sd} + a_{3,sd}V_{3,sd} \ldots\ldots a_{n,sd}V_{n,sd} \quad (2\text{-}5)$$

where $PM_{2.5\,sd}$ is PM2.5 concentration at location *s* on day *d*; $a_{0,sd}$ is the intercept at location *s* on day *d;* $V_{2,sd}$ to $V_{n,sd}$ are values of variables 2 to n at location s on day d; $a_{2,sd}$ to $a_{n,sd}$ are slopes of corresponding variables. Hu et al. (2013) adopted both Ordinary Least Squares and the GWR model to estimate PM2.5 in U.S., and R squre was slightly improved when using the GWR model. Van Donkelaar et al. (2015) also built the GWR model over North America to estimate PM2.5 and their research shows compared with the linear regression, the GWR model yields significant improvement of accuracy (R^2 = 0.62 versus R^2 = 0.62) compared with the linear regression. The GWR model has also been applied in China at a national level in

previous studies (Ma et al., 2014). You et al. (2016) used the GWR model with the 3 km AOD product to estimate PM2.5 concentrations at a national-scale. Their model could explained 81% of the dairy PM2.5 variations. However, they did not validate the 3 km AOD product before using. Moreover, they did not compare the performances between the 3 km and 10 km AOD products.

In most statistics models, the regression equations show better capacity in predicting mean concentration rather than episodic events, besides, they tend to overestimate the low concentrations while underestimated the high ones (Dye et al., 1998; Hubbard & Cobourn, 1998; Ryan, 1995; Gupta et al, 2009a). To solve these problems along with reducing the uncertainties in the estimation, neural network approach is developed. Roughly, neural network is a set of computer algorithms designed to simulate biological neural network in learning and pattern recognition (Gupta et al, 2009b). Gupta et al. (2009b) compared the simple correlation (R^2= 0.36), multiple regression (R^2=0.46) and neural network (R^2=0.55) models in southeast U.S and neural network model had the highest accuracy. However there was no unified and integrated instruction for neural network(Gupta et al., 2009b; Liu et al., 2005). Wu et al. (2012) and Guo et al. (2013) also applied back-propagation artificial neural network (BP ANN) over China. However, some sites with high PM mass were underestimated.

Other models may include mixed effect model (Lee et al., 2012), alternating conditional expectation (ACE) model (Benas et al., 2013) and semi-empirical observation-based models (Chu et al., 2013; Tao et al., 2013).

Though various observation- based models works well to estimate PM2.5 in most regions, a major issue for these models is the lack of vertical information of AOD since AOD present the entire aerosol's property while PM2.5 is only measured close to surface (Gupta et al., 2009b). Meanwhile, most observation-based models work well in predicting averaged PM2.5 concentration in daily or monthly scales but can hardly predict episodic event. Also, high concentrations are usually underestimated.

2.4 PM2.5-Mortality

Mortality includes non-accidental mortality and accidental mortality. This study only discuss the non-accidental mortality. The published evidence has proved the relationship between PM2.5 exposure and non-accidental mortality (Gamble et al., 1998; Franklin et al., 2007; Shi et al., 2016). As mentioned in Section 2.1, concentration–response function (CRF) is often used to quantitatively describe the mortality and PM2.5. In addition, relative risk, excess risk and odds ratio, are also used in quantitative studies in public health field (Lu et al., 2015). Relative risk (RR) is the risk or bad outcome of a group exposed to a treatment (such as PM2.5) compared with another group without this treatment (Irwig et al., 2008). A RR greater than 1 indicates the risk is increased when people are exposed to the treatment, while a RR less than 1 indicates a

safer circumstance (the risk is decreased) (Irwig et al., 2008). Excess risk (ER) is also known as excess relative risk (Fry et al., 2013). The relationship between ER and RR are ca be described as Eq. (2-6) (Fry et al., 2013; Lu et al., 2015):

$$ER(\%) = (RR - 1) * 100\% \quad (2\text{-}6)$$

Though numerous studies have been conducted in developing countries, ER and RR cannot be simply transferred to Chinese context (Lu et al., 2014). This is because ER and RR vary in different regions due to the difference in air pollution level, the vulnerability of people to PM2.5, the composition of PM2.5 and the population structure. The ERs of total non-accidental mortality due to exposure to PM2.5 in previous studies are shown in Table 2.7: ER (%) denotes the percent increase of total non-accidental mortality with per 10 μg/m^{3}increment of PM2.5.

Usually, long-term exposure (Pope III et al., 2002; Zeger et al., 2008; Cao et al., 2011; Shi et al., 2016; Zhang et al., 2016) brings higher ER than short-term does (Huang et al., 2012; Lu et al., 2015; Shi et al., 2016). ER for low concentrations is higher than ER in the whole study cohort (WHO, 2015; Shi et al., 2016). Women experience higher ER than men do (Huang et al., 2012). The ER may be different due to PM2.5 composition: Laden et al (2000) found the ER of PM2.5 from mobile sources (3.4% increase in daily mortality with 10 μg/m^3) was higher than that from coal combustion (1.1% increase) while PM2.5 from crustal particles had no association with daily mortality. Cao et al. (2011) indicate that ER in China may be lower than the type found in developed countries. The ER or RR study in China were mainly focus on short-term (usually 1 day) or long-term (1 or more years), and there are seldom study based on seasonal exposure.

Attributable fraction (AF) can assess the proportion of the disease (or mortality) attributed to a certain risk (such as PM2.5) in a population (Steenland et al., 2006). AF can be derived from RR or ER. The relationship between AF and RR can be described by Eq. (2-7) (Steenland et al., 2006; Anenberg et al., 2009):

$$AF = (RR - 1)/RR \quad (2\text{-}7)$$

Based on the definition of AF, the distributed total non-accidental mortality rate can be determined by Eq. (2-8) (Nawahda et al., 2012):

$$Total\ non - accidental\ Mortality_{pm2.5} = pop * Total\ non - accidental\ Mortality\ Baseline * AF_{PM2.5} * \Delta PM_{2.5} \quad (2\text{-}8)$$

where $Total\ non - accidental\ Mortality_{pm2.5}$ is the mortality attributed to $\Delta PM_{2.5}$ exposure; pop is the exposed population.

Traditional numerical analysis can only provide a statistical description of PM2.5-mortality relationship. Nowadays, remote sensing techniques provide a opportunity to examine the spatial pattern of mortality attributed to PM2.5.

Table 2.7 ER (95%CI) of total non-accidental mortality due to the exposure to PM2.5 in previous studies

Author	Study Time	Study Area	ER (%) of Total non-accidental Mortality (95%CI)
Shi et al. (2016)	2003-2008	U.S.: New England Region	2.14 (short-term (2 days) exposure) 9.28 (long-term (1 year) exposure)
Zeger et al. (2008)	2000-2005	U.S.: metropolis	6.8-13.2 (long-term (6 years) exposure)
Pope III et al. (2002)	1979-1983; 1999-2000	U.S.: 50 States in U.S.	4 (long-term (1-4 year) exposure)
Zhang et al. (2016)	2013	China: Shenzhen	0.69 (long-term (1 year) exposure)
Lu et al. (2015)	1999-2013	China: mainland, Hong Kong and Taiwan	0.4 (short-term (daily)exposure)
Lee et al. (2015)	2001-2008	11 East Asian cities (Korea. Japan, Taiwan and China)	0.38 (short term(daily) exposure)
Cao et al. (2012)	2004-2008	China: Xi'an	0.18 (short term(daily) exposure)
Huang et al. (2012)	2004-2008	China: Xi'an	0.25 (Female, short-term (daily) exposure) 0.17 (Male, short-term(daily) exposure)
Cao et al. (2011)	1991-2000	30 Provinces in China	0.9 (long-term (1 year) exposure)

ER: Excess Risk for mortality are presented as % (95%CI) per 10μg/m^3 increment of PM2.5

CI: Confidence interval

2.5 Chapter Summary

PM2.5 can be acquired from air quality monitoring networks and programs established in many countries and regions. However, ground-level PM2.5 can only present a limited area around the monitoring sites. In this situation, satellite measurements can be adopted to acquire PM2.5 with greater spatial coverage. The strong relationship between satellite AOD and PM2.5 has been found in previous research. Numerous satellites and algorithms have been employed for AOD retrieval. In previous studies, MODIS is the most often used satellite and MODIS also provides AOD product derived with deep blue and dark target vegetation algorithms to users directly so that users do not have to retrieve AOD from RS data by themselves. In 2014, NASA released MODIS Collection 6 product containing an AOD product with 3 km resolution. Usually, ground-level AOD measurements, such as AOD provided by AERONET, can be adopted to calibrate satellite AOD. Current models for AOD-PM2.5 can be classified into simulation-based and observation-based methods. In observation models, linear regression are most often used and spatial regression can consider the spatial autocorrelation. To improve the PM2.5-AOD estimation model, other factors, such as meteorological and socio-economic factors, are also taken into consideration in more complex models. At last, the PM2.5 distribution estimated from satellite data can contribute to epidemiology study as an application, such as mortality rate estimation.

Chapter 3. Study Area and Data

3.1 Study Area

The Beijing-Tianjin-Hebei (BTH) region, also known as the Jing-Jin-Ji region, is the capital region of China. As the core area of the Bohai Economic Rim, the BTH region consists of two municipalities (Beijing and Tianjin) and eleven prefecture-level cities in Hebei Province (Shijiazhuang, Baoding, Langfang, Tangshan, Zhangjiakou, Chengde, Qinhuangdao, Cangzhou, Hengshui, Xingtai and Handan).

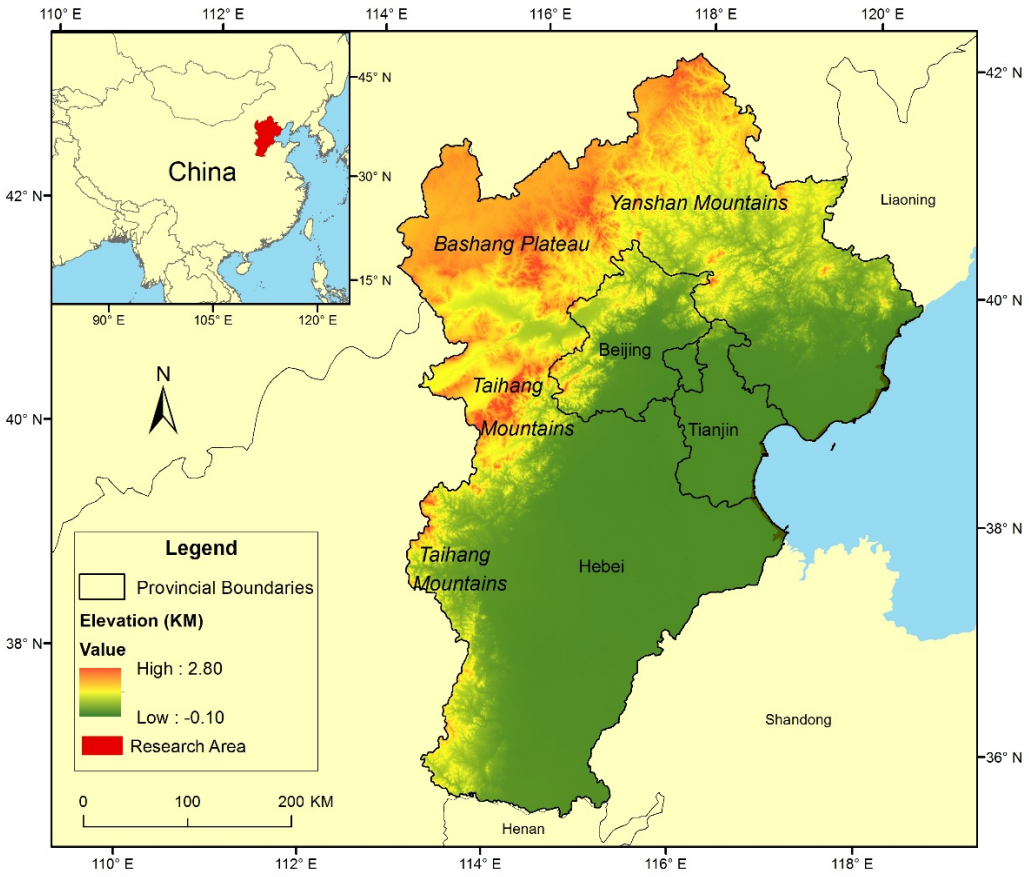

Figure 3.1 Study area

Presented in Figure 3.1, the BTH region, with an area of 217,127 km^2 (The Central People's Government of the People's Republic of China, 2016), is located northeastern mainland China between the longitude of 113°27′-119°50′ East and the latitudes of 36°05′～42°40′ North. It is bounded on the southeast and south by Shandong and Henan Province. Northern BTH region is neighbour to Inner Mongolia and Liaoning Province, and western BTH region is adjacent to Shanxi Province, which is rich in coal resources. Eastwardly, the BTH region faces Korea and Japan across the Bohai Sea. With a temperate continental

monsoon climate, the BTH region has humid and hot summers, and dry and cold winters. The 2014 annual average temperature in the BTH region was from 3.8 ℃ to 15.5℃ while annual average precipitation was around 400 mm (China Meteorological Administration, 2015).

As the center of the Bohai Economic Rim, the BTH region has always been the China's economic development leader since Chinese Reform and Opening up Policy in 1978. The 2014 BTH Gross Regional Product (GRP) is RMB 66478.91 million yuan, which is 10.45% of 2014 Gross Domestic Product (GDP, RMB 634043.4 million yuan) (China Statistical Yearbook, 2015). According to the World Bank's data, in 2014, the BTH region's GRP is only lower than 15 countries' GDP in the world and higher than that of the rest, such as Indonesia, Netherlands, Turkey and Saudi Arabia. As the capital of China and the core area of the BTH region, Beijing has an integrated industrial system and is in the advanced industrialization stage because of its political, cultural and information strength. Tianjin, the biggest harbor city in northern China, has strength in logistics, shipping and aviation. Tianjin Port is not only an important node in the BTH region's modern transportation system but also a vital port for international trade. Shijiazhuang is the capital city of Hebei province and it is called "A City on the Railway" because it is an important railway hub. Owing to its transportation and natural resources, heavy industries and manufacturing are the mainstay industries in Shijiazhuang. Tangshan is famous for its heavy industries such as coal-mining, metallurgic and ceramic industry.

Economic development always comes with employment opportunities and attracts migrants. At the same time, with China's urbanization, the BTH region has become one of the most populated regions in China. In 2014, the BTH region's population reached 110.53 million, which accounts for 8.1% of nation's population (United Nations, 2015). As all know, "One-Child Policy", issued in 1980, is an important policy for China to slow down its population explosion. However, in 2015, Chinese government issued the "Two-Child Policy" and repealed the old "One-Child Policy", and a new increase of population in the near future is expected.

The dense population, high-speed economic development and urbanization, industrial process, congested local traffic and coal consumption for winter heating all make the BHT region the most concentrated region of PM2.5 in China. During the study period, as shown in Figure 3.4 , none of the eleven cities reached the national annual standard (15 $\mu g/m^3$) and some of their averaged PM2.5 were 500% higher than national standard and 800% higher than WHO guideline (10 $\mu g/m^3$). Trapped by surrounding mountains and plateau, air pollutant in the BTH region accumulate easily. Specifically, the BTH region has a complex topography with three geographic units: North China Plain, Yan Mountains and Taihang Mountains, and Bashang Plateau. As shown in Figure 3.1, most of southeastern and central BTH region lies on the North China Plain. Taihang Mountains run through the western BTH region while Yan Mountains

range surround the BTH region from north. Bashan Plateau, located in the northern part of Zhangjiakou and Chengde, is the southeastern edge of the Mongolian Plateau. Therefore, only the northwest wind could dissipate air pollutant while the southeast wind helps to accumulate air pollutant in the BTH region.

3.2 Data

3.2.1 MODIS 10 km and 3 km Data

Similar to other geographic features, aerosols also vary on different research scales. Thus, the choice of spatial scale becomes important to fulfill specific research need. The traditional 10 km MODIS AOD product works well in climate related application but it is insufficient in fine scale's study (Leigh et al., 2014). Therefore, 3 km MODIS AOD was released in 2014 as a part of MODIS Collection 6 product (MYD04_3K and MOD04_3K). As shown in Figure 3.2, with a higher spatial resolution, MODIS 3km AOD products can help to display more variation than the 10 km AOD product does. The grids with invalid data are mainly due to the cloud, ice and snow cover or other reasons related with algorithms. MODIS AOD product files are stored in Hierarchical Data Format (HDF-EOS).

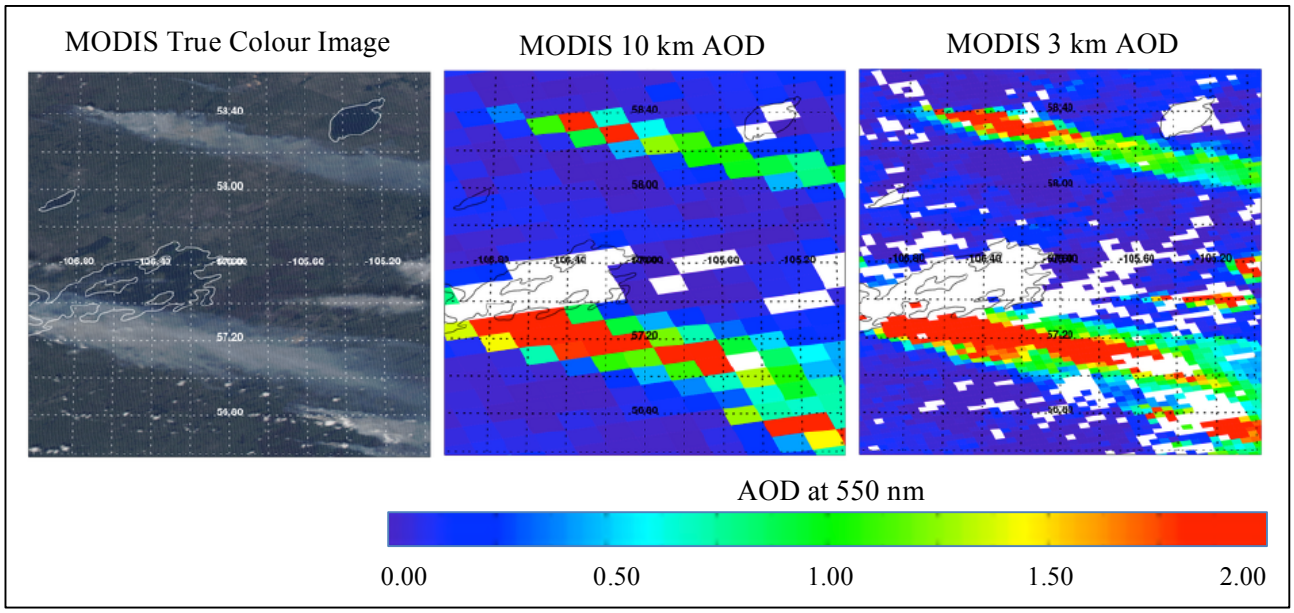

Figure 3.2 A comparison of the MODIS True Colour Image, MODIS10 km AOD and 3 km AOD Products (Source: Leigh et al., 2014)

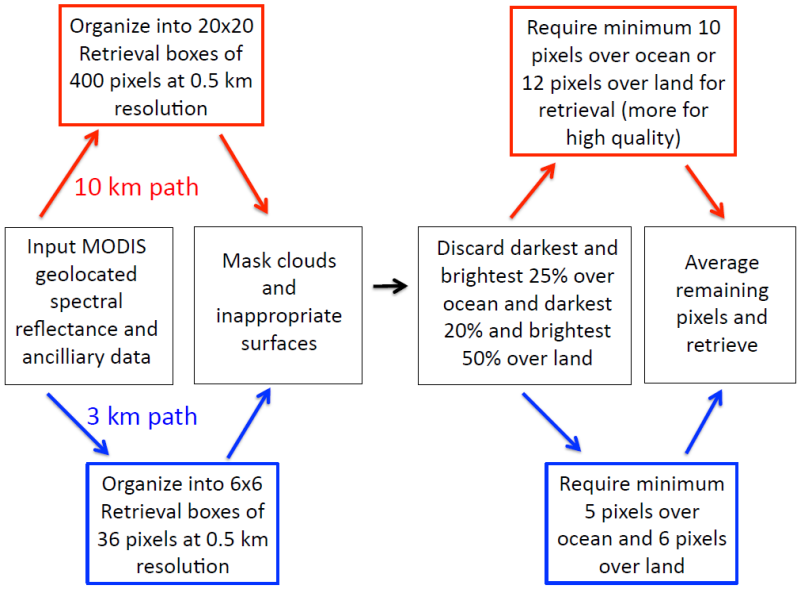

Figure 3.3 Retrieval algorithms for the 10 km and 3 km AOD products (Source: Leigh et al., 2014)

Based on the 10 km Dark Target AOD product, the 3 km AOD product is generated with dark target (DT) algorithm by using three waveband (0.47, 0.66 and 2.12 μm) , using similar inversion methods and LUT (Xie et al., 2015; Leigh et al., 2014). As shown in Figure 3.3, the processes flow for 10 km and 3 km DT AOD product are similar: the input data is retrieved in a box with 20 × 20 and 6×6 pixels for 10 km and 3 km data, respectively. Clouds, ice and snow cover will impede dark target algorithm, so after last step, clouds and inappropriate surfaces are masked, followed by a process to discard darkest and brightest reflectivity range to reduce uncertainties (Xie et al., 2015; Leigh et al., 2014). In addition to the size of retrieval boxes, another difference is, the retrieval algorithm for 10 km AOD requires at least 12 valid pixels, while the 3 km AOD requires 6 valid pixels in a box. If the number of valid pixels in a box cannot reach this requirement, this box would be dropped in retrieved result. This indicates 3 km algorithm attempts a "better quality" retrieval by increasing the minimum percentage of "good" pixels in 3 km algorithm compared to that in 10 km algorithm. The other procedures in generating the 3 km product remains unchanged as that of 10 km dark target product. In addition to DT algorithm applied in both products, 10 km product also adopts Deep Blue algorithm. As introduced in Chapter.2, DB algorithm is helpful to increase AOD retrieval's accuracy over bright area, such as desert or bright area within urban area. At the same time, AOD can be retrieved with a greater coverage with both DT and DB algorithms than with only DT method.

Compared with 10 km product, 3 km product is able to better retrieve smoke plume through cloud. Also, 3 km product provides information closer to islands and coastlines. However, higher resolution comes

with more noise. According to Leigh et al. (2014)' s validation, although products with 3 km and 10 km are both correlated well with AERONET AOD measurement, higher biases and uncertainties can be observed in 3 km product.

Quality (QA) flag is an indicator of the assessment on AOD data's quality from algorithm team and the QA flag values range from 0-3. QA3 is the recommended quality level for land products (NASA, n.d.c). Each pixel has its QA flag. In this study, only these pixels with QA3 was used.

In this thesis, in order to match MODIS AOD retrievals with the acquision time of meteorological data (Acquired time: 14:00), only Aqua satellite, operated on sun-synchronized orbit with a period of approximately 100 minutes, was employed in this study. Aqua's overpass time at equator is at local time 13:30 in ascending order, which suggests that the satellite normally flies over the study area during 13:30 pm to 14:00 pm.

To evaluate 3 km and 10 km products' performance in AOD estimation, AOD measurement from AERONET was used for MODIS AOD validation. The temporal resolution of ground-level AERONET AOD is 15 minutes on average (Zhou et al., 2009). Five sites have been built in the BTH region, which are presented in Table 3.1. However, only Beijing and Xianghe sites were well operated during the research period. Therefore, Xianghe and Beijing sites' AOD were calibrated with satellite-derived AOD in this study.

Table 3.1 AERONET Stations in the BTH region

Station Name	Latitude	Longitude	Operation Time
Beijing	39.98° N	116.38° E	7-March-2001-Present
Xianghe	39.75° N	116.96° E	20-March-2001-Present
Beijing-CAMS	The data in research period cannot be retrieved		
PKU_PEK	Station was out of operation in research period.		
Yufa_PEK	Station was out of operation in research period.		

AERONET AOD inversion product has three data quality levels: Level 1.0 (unscreened data but may not have final calibration applied), Level 1.5 (cloud-screened data but may not have final calibration applied. These data are not quality assured.), and Level 2.0 (pre- and post-field calibration applied, cloud-screened, and quality-assured data) (NASA, n.d.a). In this project, only the data at level 2 was adopted. .

3.2.2 Ground-level PM2.5 Measurements

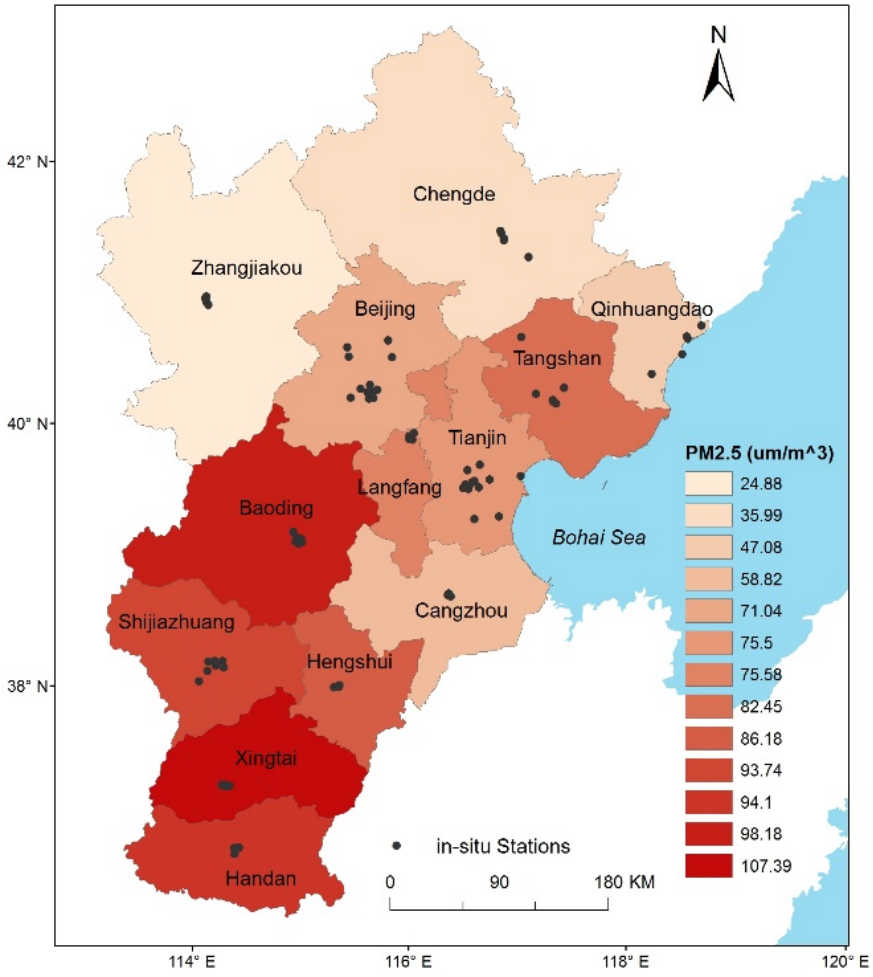

Figure 3.4 Ground monitoring stations' locations and the averaged PM2.5 of every city' all stations during the study period

Hourly PM concentrations measured at 14:00 in 79 ground stations in the BTH region were acquired from MEPCN (http://www.zhb.gov.cn/). The locations of these 79 stations are shown in Figure 3.4 and most of them are located in the urban area. Please refer to Appendix I for more specific information about these stations (City, Station Name, Station Code, Longitude and Latitude). Ground-level PM2.5 concentrations were mainly measured by the TEOM and BAM instruments as introduced in Chapter 2. On the basis of the Environmental Protection Standard of China (HJ 618-2011), all the measurements had been processed with calibration and quality control (MEPCN, 2011). Averaged PM2.5 of every city' all stations during the study period is shown in Figure 3.4. It can be found the averaged PM2.5 of all cites were ranged from 24 μg/m^{3}to 108 μg/m^{3}and none of them reached the national standard (15 μg/m^3). It should also be noted that this "averaged PM2.5" is roughly determined by limited number of stations so biases are existing.

3.2.3 Supplementary Data

Supplementary data include meteorological data, social-economic data, land use data and mortality information.

3.2.3.1 Meteorological Data

In this project, meteorological data was obtained from the European Centre for Medium-Range Weather Forecasts (ECMWF) reanalysis datasets (ERA-Interim). ECMWF uses its data assimilation systems and forecast models to re-analyze observation datasets. As one of the ECMWF's reanalysis datasets, ERA-Interim is a global atmosphere reanalysis from 1979. In this study, the meteorological data from September 2014 to August 2015 was used. The meteorological data included surface temperature (temperature at 2 m) (K), surface pressure (Pa), wind speed (m/s), relative humidity (%) and boundary layer height (BLH) (m). The acquired time, spatial resolution and step's information of every factor have been listed in Table 3.2.

Table 3.2 Meteorological data used in this study

<table>
<tr><th>Meteorological Data</th><th>Beijing Time</th><th>Spatial Resolution</th><th>Step</th></tr>
<tr><td>Temperature (K)</td><td rowspan="4">14:00</td><td rowspan="5">0.125°</td><td rowspan="3">0</td></tr>
<tr><td>Surface Pressure (Pa)</td></tr>
<tr><td>U Wind/V Wind Speed (m/s)</td></tr>
<tr><td>Relative humidity (%)</td><td rowspan="2">3</td></tr>
<tr><td>Boundary Layer Height (m)</td><td>8:00; 20:00</td></tr>
</table>

U wind: wind from the west

V wind: wind from the south.

Step= 3: this factor is re-analyzed on a 3 hours-averaged time level.

In Table 3.2, wind speeds consist of wind speeds from two directions: Uwind is the wind from west to east while Vwind is the wind from south to north. The temporal resolutions of temperature, wind speed and RH are four times per day (2:00, 8:00, 14:00, and 20:00 Beijing Time). Thus for these three factors, the data acquired at 14:00 was adopted to be matched with the remote sensing AOD time. For BLH, the temporal resolution is twice a day (8:00 and 20:00 Beijing time). Thus BLH at 8:00 and 20:00 were both used in model building because the time variation of BLH is complex during the day time and the BLH at 14:00 cannot be simply determined by BLH at 8:00 and 12:00. The spatial resolutions of these four factors are all of 0.125°. The step indicates whether the data is re-analyzed based on an averaged-time or not. Step 0 means this data is not on an averaged-time level while 3 means this factor is re-analyzed at a 3 hours –

averaged level. The spatially averaged values of these seven factors during research period are shown in Figure 3.5.

The values of annual averaged BLH at 8:00 ranged from 536 m to 1490 m (Figure 3.5 (a)) while those of BLH at 20:00 ranged from 114 m to 394 m (Figure 3.5 (b)): the high values for both factors were mainly distributed on mountain areas. The Uwind and Vwind speed ranged from -0.72 to 3.78 m/s and -1.46 to 0.63 m/s, respectively. The negative value means the wind was from the inverse direction. From the Figures 3.5 (c) and (d), it can be seen that the plain area of the BTH region, such as Handan, Hengshui and Tianjin, were often experienced the wind from the south while for the mountainous region, such as Chengde and Zhangjiakou, winds were often from the northwest. For the annual averaged RH, though distribution was complex, the coastal regions, such as some areas of Tangshan and Tianjin, had the highest value of RH. The temperature and surface pressure had similar distributions: the low values were located in the plain area while high values were located in mountainous regions.

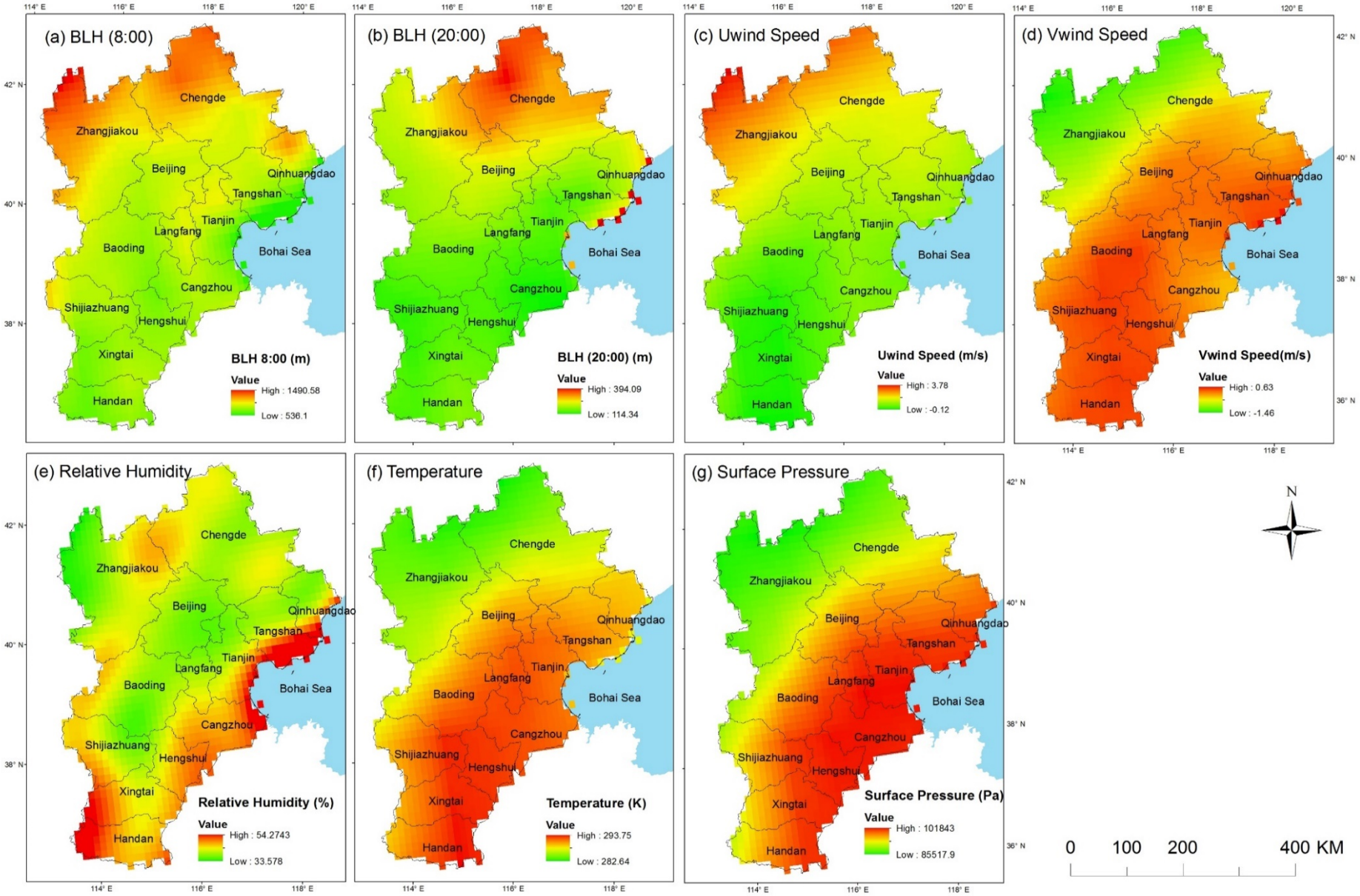

Figure 3.5 Annual averaged meteorological factors during the study period

3.2.3.2 Socio-economic and Land Use Data

In this thesis, spatial socio-economic and land used data involves GDP, population, the percent of urban area, and elevation data.

The GDP, population, and land use data were provided by the Data Center for Resources and Environmental Sciences, Chinese Academy of Sciences (RESDC) (http://www.resdc.cn). Based on 2010 national census data, these two data sets were all generated at 1 km spatial resolution. GDP and population' spatial distribution are shown in Figures 3.6(a) and (b).

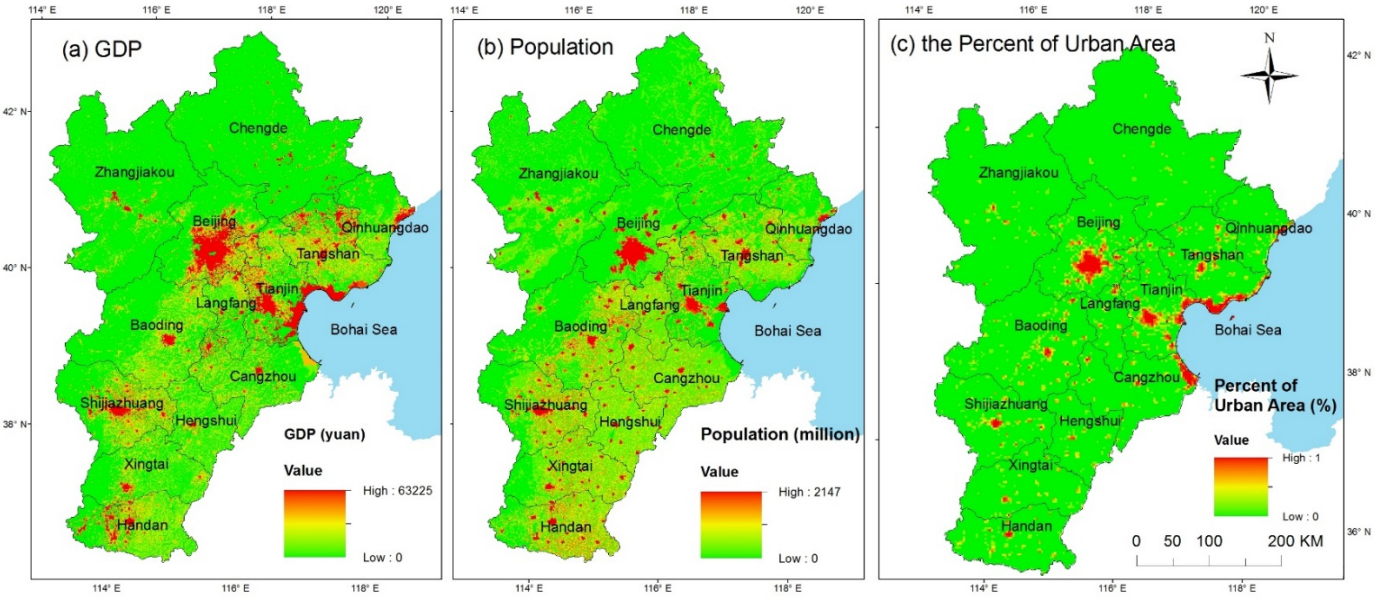

Figure 3.6 GDP and land use data in 2010

RESDC also provided 2010 land use data at 1 km through remote sensing data and other techniques. Basing on the land use data, urban area (Code number: 51) could be extracted and the percent of the urban area was then aggregated on 3 km and 10 km resolutions by ArcGIS 10.3.1 in this study for later analysis. The percent of urban area with 3 km resolution is shown in Figure 3.6 (c). Beijing was the most concentrated city for all three factors.

Elevation data was obtained from the digital elevation model (DEM) of the Shuttle Radar Topography Mission (SRTM) with a resolution of 30m. The elevation data of the BTH region is presented in Figure 3.1.

3.2.3.3 Health Data

To provide an example on how to apply remote sensing techniques in other fields, such as epidemiology study, this study also estimated the spatial mortality rate attributed by PM2.5 exceeding Chinese annual

averaged standard (15 μg/m^3) in the BTH region. Thus health data was also employed in this thesis. Health data involved in this study included an ER and a total non-accidental mortality baseline data. Cao et al. (2011) examined the association between air pollutants and mortality from 1991 to 2000 based on the annual average air pollution exposure in 30 provinces in China. In their research, it is estimated that 10 μg/m^3 increase of PM2.5 was corresponded with 0.90% increment in total non-accidental mortality, which was adopted as the ER in this study.

The all-cause mortality of China can be required from China Statistical Yearbook and 2014 is the most recent year with available data. So in this paper, the mortality data of 2014 was used instead of the study period (between September 2014 and Auguest 2015). In 2014, the mortality of China was 0.716% (China Statistical Yearbook, 2015). All-cause mortality consists of non-accidental mortality and accidental mortality. Non-accidental mortality can be categorized by the International Classification of Diseases 10th Revision (ICD-10: A00-R99) (Ma et al., 2015). The detailed causes of death information was provided by the Data-Center of China Public Health Science (DCCPHS) and the most recent version was 2008 National Disease and Cause Death Database. Basing on this database, non-accidental death accounted for 90.44% of all-cause mortality. Due to the lack of more recent data, it was assumed that this proportion kept stable from 2008 to 2014 and 90.44% is then used to determine the 2014 non-accidental mortality from all-cause mortality. Therefore, 2014 non-accidental mortality was estimated to be 0.647%, which was used as the non-accidental mortality baseline in this research.

3.3 Chapter Summary

Overall, the BTH region has always been the economic leader in China. Both heavy industries and the coal combustion for winter heating in northern China produced considerable amount of air pollutant. Moreover, the dense population and transportation also aggravated the severe pollution. However, because BTH is surrounded by mountains and plateau in northern and western sides, air pollutants are easy to be accumulated due to the wind from west and from south. In this study MODIS AOD at the 3 km and 10 km AOD from September 2014 to August 2015 were used to build models with the ground-level PM2.5 acquired from MEPCN. Along with finer resolution, 3 km product also brings more noise. Other supplementary data were also involved including GDP, population and land used data from RESDC, and meteorological data from ECMWF. For a further application of remote sensing results, ER from Lu et al (2015), and the non-accidental mortality information from local organization were also utilized.

Chapter 4. Methodology

This chapter describes the methodology. Section 4.1 presents an overview of workflow. Section 4.2 explains AOD validation method. Section4.3 describes the data preprocessing and Section 4.4 explains the MLR and GWR models' construction. Section 4.5 explains how mortality distribution was determined and a summary of this chapter is followed.

4.1 Overview of Workflow

The methodology contains four modules, which are AOD validation, data preprocessing, model construction, and application (see Figure 4.1). The first module is AOD validation. The 10 km and 3 km MODIS AOD were calibrated with ground-level AOD acquired from AERONET. In the second module, along with the in-situ PM2.5 after data cleaning, MODIS AOD and meteorological data were conducted with outlier identification and removal steps. Then PM2.5 concentrations were matched with all the variables, including AOD, meteorological data, social-economic factors and land-use information from September 2014 to August 2015 in the BTH region. Then this result was inputted into the MLR and GWR models in the third module. After the validation for each model, a seasonal analysis and a regional analysis were followed. Then based on the population's spatial distribution data, the population exposed to a long-term harmful level of PM2.5 was derived. At the same time, the spatial mortality rate attributed from PM2.5's seasonal change was generated based on ER and total non-accidental mortality documents.

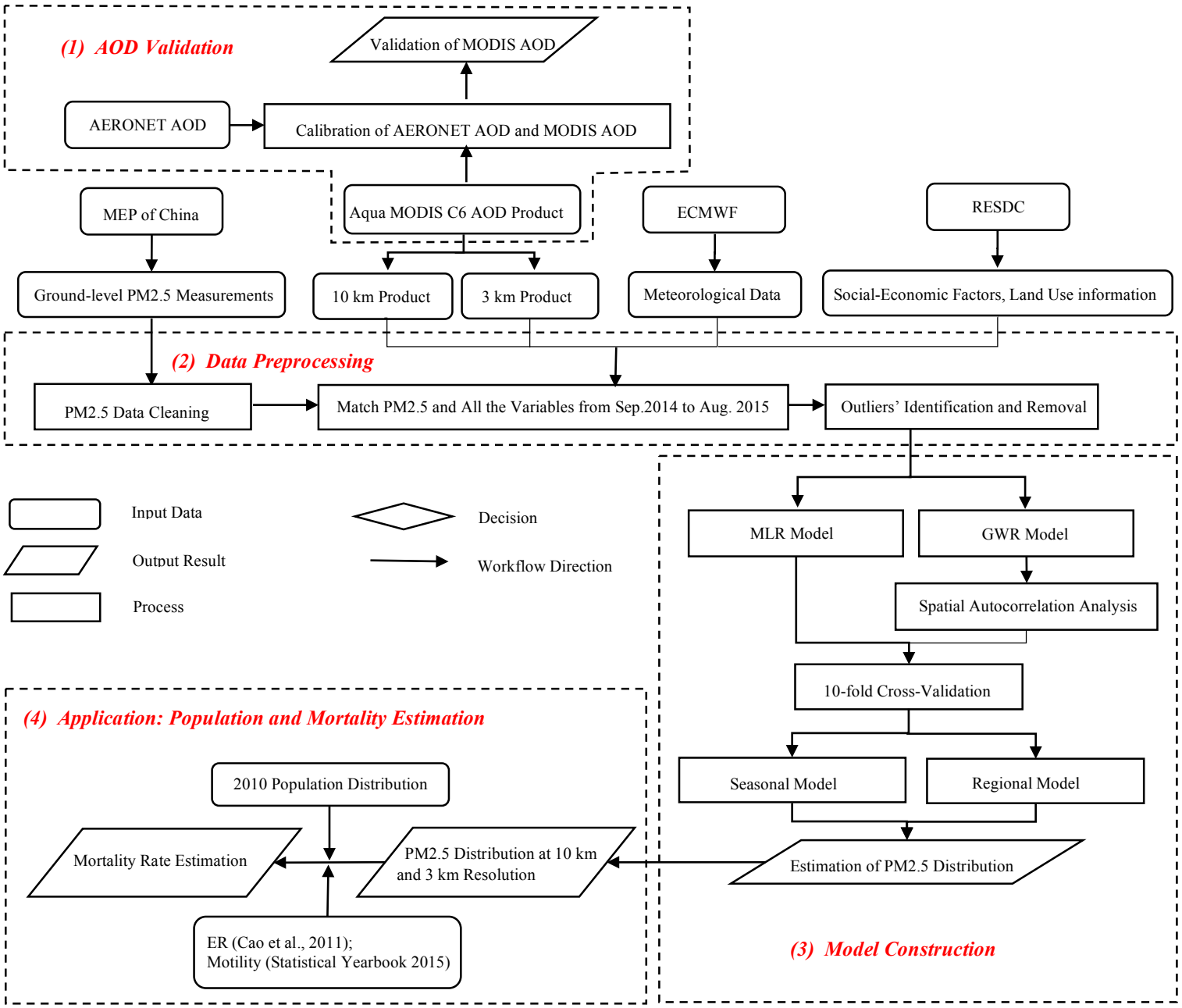

* AOD: Aerosol Optical Depth.
AERONET: **AE**rosol **RO**botic NETwork (http://aeronet.gsfc.nasa.gov/)
MEP of China: Ministry of Environmental Protection of the People's Republic China
ECMWF: The European Centre for Medium-Range Weather Forecasts (http://www.ecmwf.int/)
MLR: Multiple Linear Regression
GWR: Geographically Weighted Regression Model
RESDC: Data Center for Resources and Environmental Sciences, Chinese Academy of Sciences

Figure 4.1 Workflow of the methodology

4.2 MODIS AOD Validation with AERONET AOD

The AOD acquired from the AERONET Beijing site and Xianghe site were at 1640, 1020, 870, 675, 440,380 and 340nm wavelength. However, the MODIS AOD was at 550nm wavelength, so the ground-level AOD was interpolated at 550nm according to the following Ångström formula (Ångström. 1964):

$$\tau_\alpha(\lambda) = \beta\lambda^{-\alpha} \tag{4-1}$$

where $\tau_\alpha(\lambda)$ is the AOD at the wavelength λ, β is the Ångström turbidity and α presents the Ångström exponent. The Ångström exponent and Ångström turbidity can be computed respectively by Eq. (4-2) and Eq. (4-3):

$$\alpha = -\frac{\ln[\tau_\alpha(\lambda_1)/\tau_\alpha(\lambda_2)]}{\ln(\lambda_1/\lambda_2)} \tag{4-2}$$

$$\beta = \frac{\tau_\alpha(\lambda_1)}{\lambda_1^{-\alpha}} = \frac{\tau_\alpha(\lambda_2)}{\lambda_2^{-\alpha}} \tag{4-3}$$

where the AOD at 550 nm wavelength was interpolated with the AOD at 675nm (λ_1) and the AOD at 440 nm (λ_2) in this research.

As introduced in Chapter 3, the AERONET AOD data and the MODIS AOD data had different temporal and spatial resolutions. The Aqua satellite passes the BTH region around 13:30-14:00. So the AERONET AOD from 13:30 to 14:00 were averaged at Beijing and Xianghe sites and collocated with 10 km and 3 km MODIS AOD every day. However, satellite-derived AOD could not cover Xianghe and Beijing site everyday due to the cloud cover and other reasons. Furthermore, Xianghe site and Beijing site's AOD were not always valid from 13:30 to 14:00 PM during the study period. As a result, after the spatial and temporal matching, there were only 101 10 km AOD - AERONET collocations and 30 AOD - AERONET collocations in Beijing site. For Xianghe site, there were 96 and 40 collocations, respectively, for the 10 km AOD-AERONET and the 3 km AOD-AERONET. The results and analyses are presented in Chapter 5.

4.3 Data Preprocessing

Firstly, all the raster data sets' geographical coordinates are unified as *China_Lambert_Conformal_Conic*. Then the meteorological datasets acquired from the ECMWF were resampled to 3 km resolution and 10 km resolution for the 3 km MODIS AOD and 10 km MODIS AOD respectively by using bilinear interpolation. For the GDP, population and DEM data, their resolutions are less than 3 km. So these data sets were also aggregated to 3 km and 10 km resolution. This aggregation process was conducted by ArcGIS 10.3.1. and the aggregation techniques for GDP and population were "SUM" and that for DEM data was "MEAN". For the percent of urban area data, it had already been calculated on 3 km and 10 km as introduced in Chapter 2. For the PM2.5 concentrations acquired from MEP of China, the raw data was stored in text file.

So text files were converted to features classes. Then, for those PM2.5 sites located in the same pixel of the MODIS AOD, their PM2.5 concentrations were averaged. This step was conducted for both the 10 km and 3 km AOD data.

Every day's PM2.5 data at each site was matched with all the variables at the same time within the same pixel. Those PM2.5 concentrations with no AOD data matched are considered invalid data. Then there were 1497 lines of valid records for 3 km MODIS AOD model and 3132 lines of valid records for 10 km MODIS AOD models. For the MODIS data, only the AOD data with a quality (QA) flag 3 was used in this study so those lines with "QA_flag" <3 were removed. Then other variables and PM2.5's outliers were removed by Box-plot, which can be conducted in SPSS software.

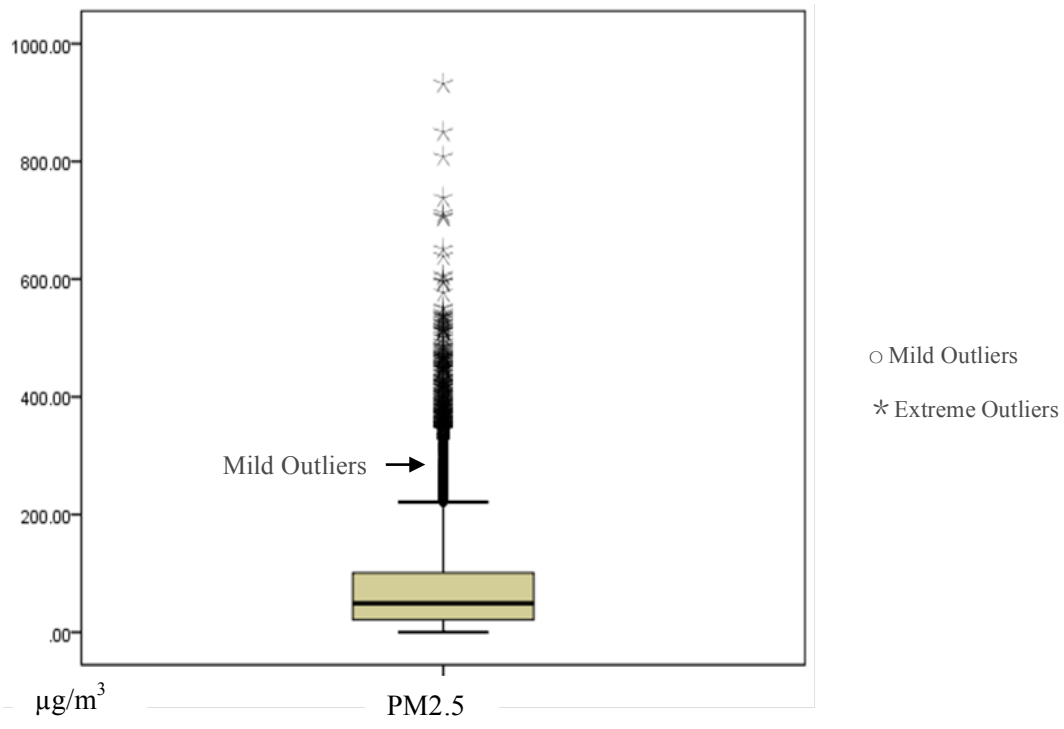

Figure 4.2 Box-Plot of the whole year's PM2.5 in the 10 km AOD model

Figure 4.2 shows the Box-plot of the PM2.5 concentrations inputted in 10 km model. "○" denotes mild outliers while "✶" demonstrates extreme outliers. In this Box-plot, the dots with PM2.5> Q3+1.5IQR and PM2.5< Q1-1.5IQR are considered as outliers. Q3 is the upper quartile and Q1 is the lower quartile; IQR is the interquartile range. Extreme outliers are those PM2.5 concentrations with values greater than Q3+3IQR or less than Q1-3IQR while mild outliers are those between Q3+3IQR to Q3+1.5IQR and those between Q1-3IQR to Q1-1.5IQR. In this study, both extreme and mild outliers were removed. This step

was also conducted for all the meteorological variables. After the outliers' removal, there were 1431 lines of records for the 3 km AOD MODIS model and 2851 lines for 10 km AOD model.

4.4 Model Construction.

4.4.1 Multiple Linear Regression Model

In this project, meteorological parameters and land use information were both taken into the MLR model. The MLR model in this study can be expressed by Eq. (4-4):

$$PM_{2.5} = \alpha_1 + \alpha_{AOD} \cdot AOD + \alpha_{Tem} \cdot Tem + \alpha_{RH} \cdot RH + \alpha_{BLH8:00} \cdot BLH08 + \alpha_{BLH20:00} \cdot BLH20 + \alpha_{Uwind} \cdot Uwind + \alpha_{Vwind} \cdot Vwind + \alpha_{SP} \cdot SP + \alpha_{POP} \cdot Pop + \alpha_{GDP} \cdot GDP + \alpha_{PofU} \cdot PofU + \alpha_{DEM} \cdot DEM \quad (4\text{-}4)$$

where $PM_{2.5}$ is the estimated PM2.5; α_1 is the intercept of this equation; α_{AOD}, α_{Tem} .... are the coefficients of corresponding factors; AOD is the MODIS AOD value; Tem and RH are the temperature and relative humidity values; $BLH08$ and $BLH20$ are the boundary layer height at 8:00 and 20:00; $Uwind$ and $Vwind$ are the Uwind speed and Vwind speed; SP is the surface pressure; Pop is the population concentration while $PofU$ is the percent of urban area, and DEM is the elevation value.

In this study, the SPSS software was used to build the MLR model. This model was firstly built for the whole study period (between September 2014 and August 2015) for both 10 km and 3 km product. Then, to determine whether the models are over-fitted, 10-fold cross validations were conducted. The whole dataset was split into ten folds and each of them had approximately 10% of the total data points. Then one fold was used for validation while the rest nine folds were used for training and this process was repeated for every fold.

Further, seasonal models were constructed to compare 3 km and 10 km AOD products' performances in different seasons. In this study, fall was from September 1, 2014 to November 30, 2015; winter was from December 1, 2014 to February 28, 2015; spring was from March 1, 2015 to May 31, 2015 and summer was from June 1, 2014 to August 31, 2015. After the seasonal models, regional models were built for all the cities to assess the models in smaller spatial scales.

4.4.2 Geographically Weighted Regression Model

The GWR model generates a continuous surface of parameters by considering parameters' spatial variations instead of assuming globally constant coefficient. The traditional GWR model on a daily basis can be expressed as Eq. (4-5)

$$PM_{2.5(i,j,d)} = \alpha_{1(i,j,d)} + \alpha_{AOD(i,j,d)} \cdot AOD_{(i,j,d)} + \alpha_{Tem(i,j,d)} \cdot TEM_{(i,j,d)} + \alpha_{RH(i,j,d)} \cdot RH_{(i,j,d)} + \alpha_{BLH8:00(i,j,d)} \cdot BLH08_{(i,j,d)} + \alpha_{BLH20:00(i,j,d)} \cdot BLH20_{(i,j,d)} + \alpha_{Uwind(i,j,d)} \cdot Uwind_{(i,j,d)} +$$

$\alpha_{Vwind(i,j,d)} \cdot Vwind_{(i,j,d)} + \alpha_{SP(i,j,d)} \cdot SP_{(i,j,d)} + \alpha_{POP(i,j)} \cdot Pop_{(i,j)} + \alpha_{GDP(i,j)} \cdot GDP_{(i,j)} + \alpha_{PofU(i,j)} \cdot PofU_{(i,j)} + \alpha_{DEM(i,j)} \cdot DEM_{(i,j)}$ (4-5)

where $PM_{2.5(i,j,d)}$ is ground-level PM2.5 at location (*i, j*) on day *d*; $\alpha_{1(i,j,d)}$ is the intercept of this equation, $\alpha_{AOD(i,j,d)}$, $\alpha_{Tem(i,j,d)}$ and ... are the slopes of corresponding variables. ; $AOD_{(i,j,d)}$ is the MODIS AOD value at location (*i, j*) on day *d*; $TEM_{(i,j,d)}$ is the temperature at location (i,j) on day *d* ; $RH_{(i,j,d)}$ is the relative humidity at location (*i, j*) on day *d*; $BLH08_{(i,j,d)}$ is the boundary layer height at 8:00 and $BLH20_{(i,j,d)}$ is the boundary layer height at 20:00 at location (*i, j*) on day *d* ; $Uwind_{(i,j,d)}$ is Uwind speed and $Vwind_{(i,j,d)}$ is Vwind speed at location (*i, j*) on day *d* ; $SP_{(i,j,d)}$ is the surface pressure at location (*i, j*) on day *d*; $Pop_{(i,j)}$ is the population at location (*i, j*); $GDP_{(i,j)}$ is the GDP at location (*i, j*); $PofU_{(i,j)}$ is the percent of Urban area at location (*i, j*); $DEM_{(i,j)}$ is the elevation at location (*i, j*). Population, GDP, the percent of urban area do not have daily variation so they are constant at the same location during the study period.

To generate this daily GWR model, there have to be at least 12 sites' data available in one day because there are 12 independent variables, otherwise Eq. (4-5) cannot be built or solved. However, 79 sites' data are not all valid every day because the AOD data does not cover the whole study area every day. For the 3 km MODIS AOD – PM2.5 pairs, 137 days' data during the study period are valid while 68.88% (93 days) of these days have less than 12 sites' data available within a day. For the 10 km MODIS AOD-PM2.5 pairs, 181 days have valid data for model construction however, only 55.80% (101 days) of them have more than 12 pairs within one day. Thus, if the GWR model is only built for those days with more than 12 sites' AOD available, a considerable amount of information of the rest days would be useless. To avoid the loss and the waste those days' information, in this project, the GWR model is built on an annual averaged basis and a seasonal averaged basis instead of a daily basis to generate a local R^2 for each PM2.5 monitoring station.

In this study, the GWR model was calculated using GWR4 software, which is a Microsoft Windows-based application software developed and programmed by Professor Tomoki Nakaya from Ritsumeikan University in Japan. In this study, the Gaussian GWR model was chosen as the model type because it is suitable for modelling numerical responses while other two model types, the Poisson and Logistic GWR model, are suitable for modelling count or binary responses (Nakaya, 2014). The adaptive kernel type was chosen due to the uneven distribution of the PM2.5 monitoring sites. Furthermore, the "Golden Section Search" was used to automatically determine the best bandwidth size while "AIC" (Akaike Information Criterion) was used for bandwidth selection. In general, AIC can be used to determine the model which is closest to reality and the best model should have the lowest AIC value (Fotheringham et al., 2003; Hu et al., 2012).At the same time, AIC can be used to assess whether the GWR model could generate

a better result than global regression model. Therefore, a global regression model was also built with the same datasets: global regression model generates globally constant coefficient. More introduction of AIC can be found elsewhere (Bozdogan et al., 1987).

Then, the models' residual was conducted with a spatial autocorrelation analysis. In this study, the spatial autocorrelation was analyzed by calculating Moran's I values in ArcGIS 10.3.1. The detailed introduction of Moran's I values can be found elsewhere (Hu et al., 2013). Generally, Moran's I value ranges from -1 to +1 (Cliff et al., 1981). When Moran's I value is greater than zero, it is indicated the existence of positive spatial autocorrelations while the negative value of Moran's denotes the negative autocorrelation. If Moran's I value is near zero, it means there is no spatial autocorrelation (Hu et al., 2013). The ideal GWR models should have residuals with no significant spatial autocorrelation (Wang et al., 2005; Zhao et al., 2010). In another word, the Moran's I value should be near zero (Hu et al., 2013).

After the spatial autocorrelation analysis, a 10-fold Cross Validation (CV) was conducted to verify whether the GWR model was over-fitted or not.

Then seasonal models were also built to identify different seasons' variation. For the GWR model, the analysis based on regional models was not conducted because when the spatial scale became smaller, the in-situ monitoring stations' number was not enough to build the GWR model.

4.5 Application: Estimation of the Mortality Rate Attributed to the PM2.5 Exceeded National Standard.

After determining every cell's population and corresponding PM2.5 exposure, the non-accidental mortality rate attributed to PM2.5 which exceeded could be derived. ER, RR and AF were involved in this section (Please refer to Chapter 2 for the definitions and explanations of ER, RR and AF). Based on the relationships between ER and RR, and that between AF and RR, AF can be derived by ER and their relationship is described by Eq. (4-6):

$$\mathrm{AF} = (\mathrm{ER} / (\mathrm{ER} + 100) \tag{4-6}$$

Based on Eq. (2-8), the mortality rate of every cell in this study can be determined by Eq. (4-7):

$$\Delta Total\ non-accidental\ Mortality_{pm2.5}(i,j) = pop\ (i,j) * Total\ non-accidental\ Mortality\ Baseline * AF_{PM2.5} * \Delta PM_{2.5}(i,j) \tag{4-7}$$

where $\Delta Total\ non-accidental\ Mortality_{pm2.5}(i,j)$ is the total non-accidental mortality rate at location (i,j) attributed to those PM2.5 concentrations higher than national yearly standard (15μg/m^3); $pop\ (i,j)$ is the population at location (i,j); total non-accidental mortality baseline was 0.647% as introduced in the Chapter 2; $AF_{PM2.5}$ is the attributed fraction of PM2.5 derived from Eq. (4-6);

$\Delta PM_{2.5}(i,j)$ is the difference between the estimated PM2.5 and the national yearly standard at location (i,j). This analysis was conducted by ArcGIS 10.3.1.

4.6 Chapter Summary

This chapter provides an overall and comprehensive introduction of the methodology used in this study. There are four modules involved in the methodology: AOD validation, data pre-processing, model construction and application. Firstly, AOD validation was to validate the MODIS AOD product with the ground-level AOD to assess the 10 km and 3 km AOD products' performance. Then data pre-processing module was to pre-process the satellite data, meteorological data, social-economic data and land use data for model construction. In the next step, the MLR and GWR models were both built to estimate PM2.5 concentrations and investigate its spatial distribution. At the last, the number of deaths attributed to long-term exposure of severe PM2.5 pollutions was also estimated with a spatial distribution.

Chapter 5. Results and Analysis

This chapter presents the discussion and the results. Section 5.1 describes the MODIS AOD validation results. Section 5.2 presents the MLR model's results. The GWR model's results are followed in Section 5.3. Section 5.4 discusses the remote sensing's application in mortality rate estimation. At the last, this chapter is summarized in Section 5.5.

5.1 MODIS AOD Validation

Firstly, the MODIS AOD at 3 km and 10 km resolution products were validated by the AERONET AOD measurements. As stated in Chapter 4, after temporal and spatial matching, there were 101 and 30 collocations, respectively, for the MODIS 10 km AOD-AERONET observations and the 3 km AOD-AERONET observations in Beijing site. In Xianghe site, the number of valid collocations for the 10 km AOD (96) was also higher than that of the 3 km AOD (40). All the satellite derived AOD and ground level observed AOD values fell in a reasonable range, 0.01 to 5, proposed by Xie et al. (2011). Figure 5.1 shows the time variations of the MODIS AOD values and the AERONET AOD measurements. As shown in Figures 5.1 (a) and (c), the 3 km AOD-AERONET collocations were concentrated in fall (between September 1 and November 30), spring (between March 1 and May 3) and summer (between June 1 and August 31), while there was only one pair of the AERONET AOD – MODIS 3 km AOD collocation in winter (between December 1and February 28). This invalid period might bring a bias when assessing the 10 km and 3 km AOD products' performance. As shown in Figures 5.1 (a), (b), (c) and (d), it can be drew: (1) both the 10 km and 3 km MODIS AOD products tended to overestimate AERONET observations; (2) for Xienghe site, this overestimate was more obvious in summer and for Beijing site, it was more obvious in summer and fall; (3) for both MODIS AOD products and AERONET observations, more fluctuation can be seen in summer in both sites.

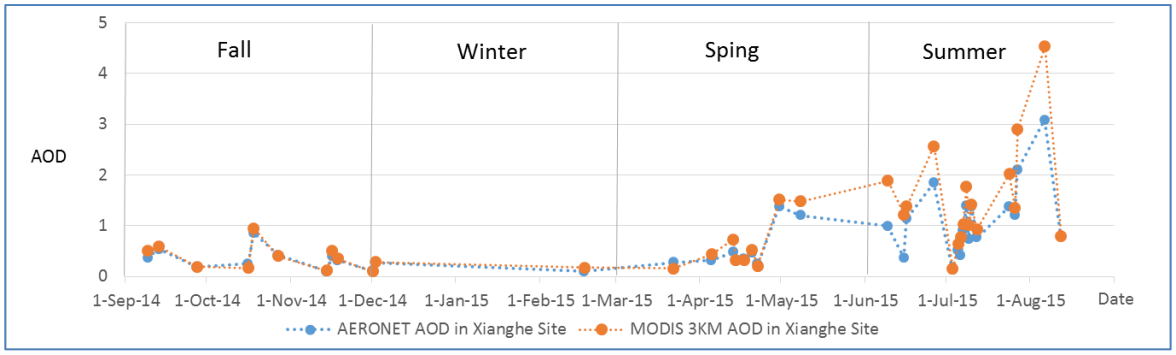

(a) AERONET AOD (Xianghe Site) – MODIS 3 km AOD

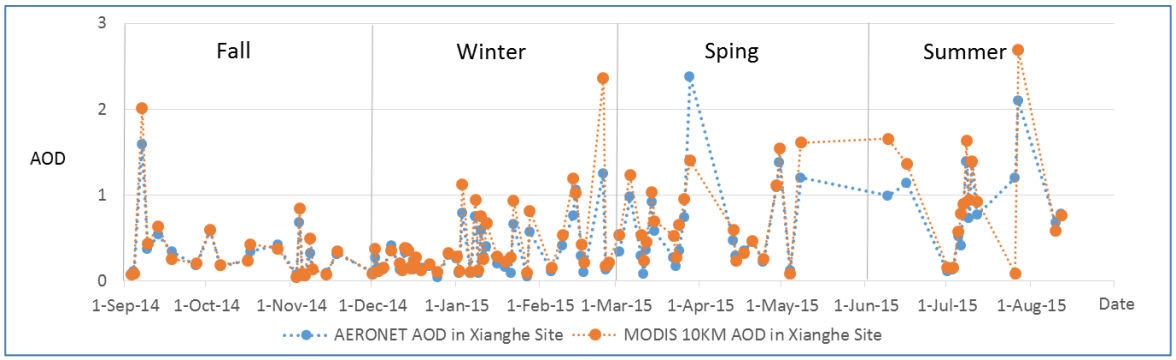

(b) AERONET AOD (Xianghe Site) – MODIS 10 km AOD

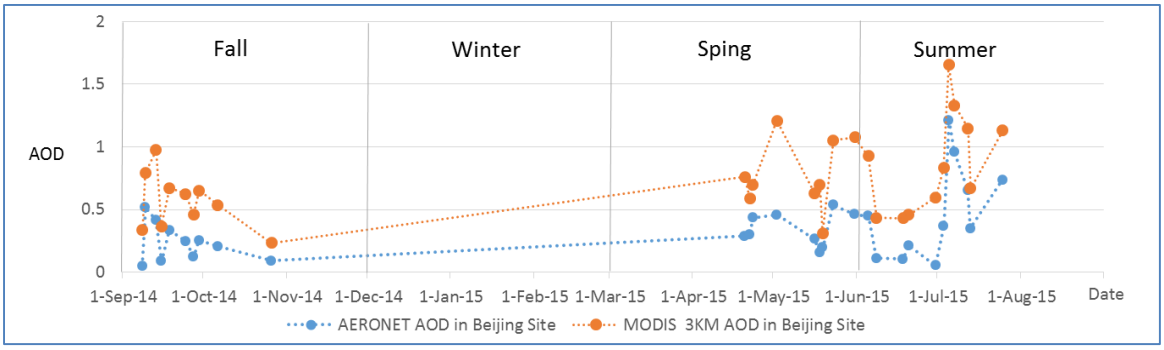

(c) AERONET AOD (Beijing Site) – MODIS 3 km AOD

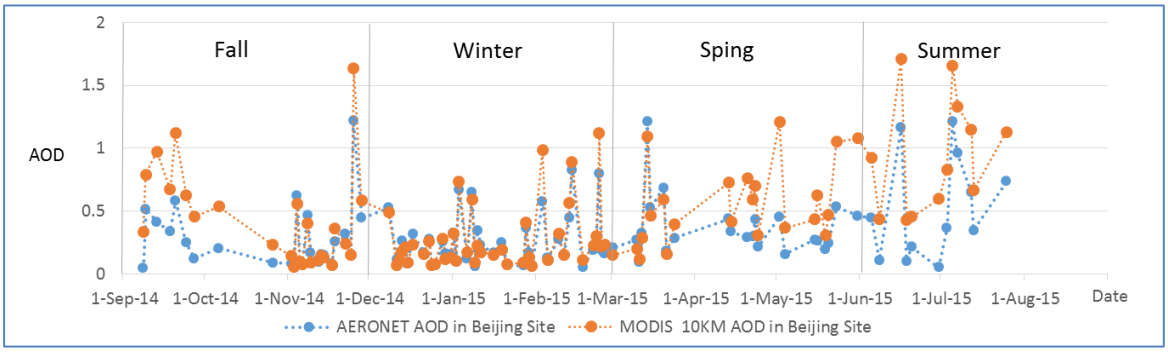

(d) AERONET AOD (Beijing Site) – MODIS 10 km AOD

Figure 5.1 Line charts for the 10 km MODIS AOD and the AERONET observations in Xianghe and Beijing sites

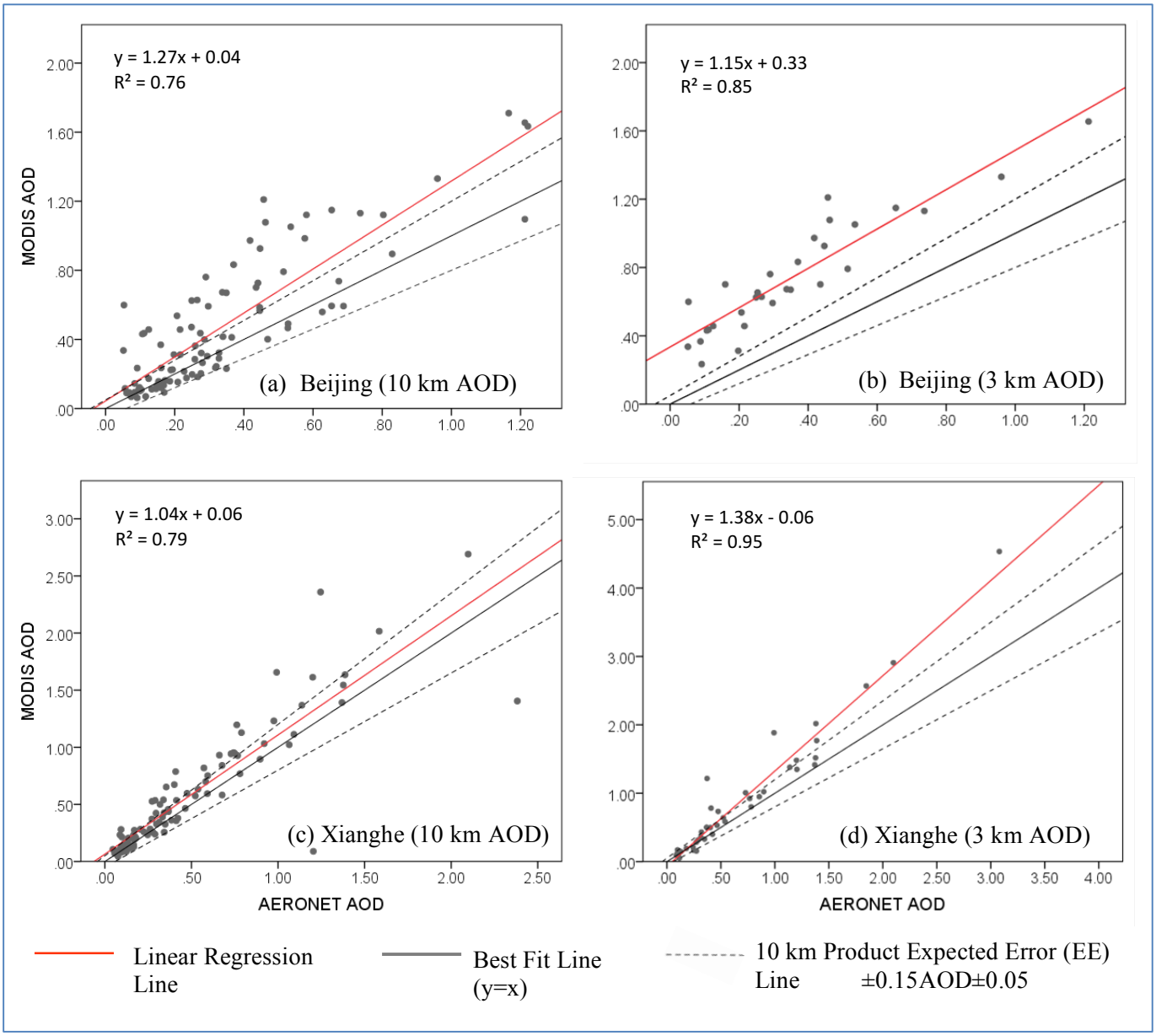

Figure 5.2 Scatter plots of the MODIS AOD retrievals against the AERONET observed AOD

Table 5.1 Statistics from the collocations shown in Figure 5.2. N= number of valid collocations. EE is ±0.15AOD±0.05 for all cases.

Station	Product Resolution	N	R^2	%below EE	%within EE	%above EE
Beijing	10 km	101	0.76	1.98	55.45	42.57
	3 km	30	0.85	0.00	0.00	100.00
Xianghe	10 km	96	0.79	2.08	64.58	33.33
	3 km	40	0.95	2.50	60.00	37.50

Figure 5.1 shows the scatter plots of collocations in two sites, in which red lines denote linear regression lines and black lines present the best fit lines (y=x). The black dash lines denote the expected error (EE) lines for the MODIS 10 km AOD product over land, $\Delta\tau = \pm 0.05 \pm 0.15\tau$, defined by NASA (Chu et al., 1998). The statistical information shown in Figure 5.2 is concluded in Table 5.1

From Figure 5.2 and Table 5.1, it can be found that for Beijing site, 55.45% MODIS 10 km-AERONET AOD collocations fall within EE lines and 42.57% collocations fall above EE lines, while all the MODIS 3 km-AERONET AOD collocations are above EE lines. This means for Beijing site, AOD was overestimated by 3 km product, while the 10 km AOD product was closer to the true value. However, R^2 of 10 km (0.76) is 9% lower than that of the 3 km AOD product (0.85), which means the 3 km AOD product was better correlated with the true value. This trend can also be found in Xianghe site's case: R^2 of 10 km and 3 km is 0.79 and 0.99, respectively. The 10 km AOD-AERONET AOD collocations were more distributed between EE lines (64.58%) while only 60% 3 km AOD-AERONET AOD collocations distribute between EE lines. For both cases, the percentage of collocations above EE lines is higher in 3 km than in 10 km product, which indicates 3 km product tended to overestimate ground-level AOD.

As a summary, the MODIS 10 km AOD-AERONET AOD and the MODIS 3 km AOD-AERONET AOD comparison in Beijing and Xianghe sites were investigated, in which 10 km product provided more collocated pairs with AERONET observations than 3 km product with AERONET observation. Meanwhile, both 10 km and 3 km MODIS AOD products were well correlated with AERONET AOD. According to the above analysis, the 3 km AOD product showed higher bias, while the 10 km AOD product showed more uncertainties. Because of the higher bias, the MODIS Atmosphere Team revised 3 km land product's EE to $\Delta\tau = \pm 0.05 \pm 0.2\text{AOD}$ (Leigh et al., 2014)

5.2 Multiple Linear Regression

This section includes the analysis on the annual MLR model, seasonal MLR models and the regional MLR models.

5.2.1 Annual Model Results

This subsection explained the annual MLR models from three aspects: the description of the statistical results, the 10-fold cross validation (CV) and an air pollution event during April 23, 2015 and April 28, 2015, described by daily PM2.5 concentrations.

5.2.1.1 Statistical Description

The annual MLR models were built by both the 10 km and 3 km AOD products with meteorological factors and land use information. The mean value of each parameter are shown in Table 5.2.

From Table 5.2, it can be learnt that for the dataset extracted by ground-level monitoring stations from the valid 3 km AOD and corresponding other parameters, the annual average PM2.5 was 42.14 (μg/m^3), 10 μg/m^3 lower than that in the dataset extracted from the valid 10 km AOD. The average AOD value was 0.77 in the 3 km AOD dataset while that in the 10 km AOD was lower (0.51). The relative humidity was 33.56% in the 3 km AOD dataset and 27.68% in the 10 km AOD dataset. The temperature was 299.76K in the 3 km AOD dataset and 288.79 in the 10 km AOD dataset. The surface pressures in both datasets were similar, around 98.50 Kpa. The average Uwind speed was higher in the 10 km AOD dataset (1.38m/s) than in the 3 km AOD dataset (0.95 m/s). For the Vwind speed, it was 0.65m/s in the 3 km AOD dataset while in the 10 km AOD dataset, the wind speed was 0.11m/s from the negative direction. In terms of the BLH in the 3 km AOD dataset, the average value acquired at 8:00 and 20:00 were 1.61 km and 0.11 km, respectively, and those in the 10 km AOD dataset were 1.32 km and 0.15 km. The average elevation in the 3 km AOD dataset was 81.57 m, which was 10 m lower than that in the 10 km AOD dataset. For the percent of the urban area, it was 67.67% in the 3 km AOD dataset and 42.01% in the 10 km AOD dataset. This is because most of the ground-level monitoring stations are located in urban areas, so the area closer to the monitoring stations was more likely to be an urban area. Thus, with the increase of the grid size, more non-urban areas were likely to be contained in the same grid. So the percent of urban area tended to be decreased with the increase of the grid size. Because the different grids' sizes, GDP and population within a pixel were remarkably different in two dataset. The averaged GDP was RMB 120,000 yuan in the 3 km AOD dataset and RMB 890,000 yuan in the 10 km AOD dataset. For the averaged population within a grid, it was 60,000 people in the 3 km AOD dataset and 530,000 people in the 10 km AOD dataset.

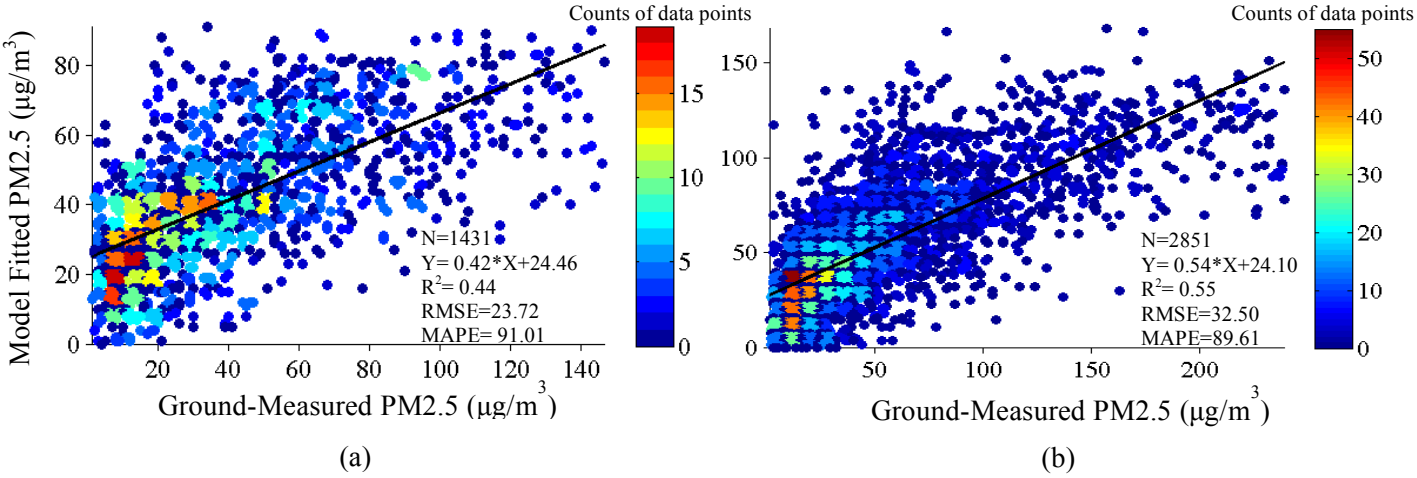

Figure 5.3 Scatter plots for the MLR Model's results between the ground-measured PM2.5 and the predicted PM2.5 concentrations from (a) the 3 km AOD model, and (b) the 10 km AOD model

Table 5.2 3 km AOD and 10 km AOD annual MLR models' results for all independent variables.

Factors	3 km AOD MLR Model				10 km AOD MLR Model			
	Mean	Coefficient	Sig.	VIF	Mean	Coefficient	Sig.	VIF
PM2.5 (μg/m^3)	42.14				52.27			
Constant		-22.51	0.74			195.45	0.00	
AOD	0.77	3.59	0.00	1.67	0.51	82.27	0.00	1.4
Relative Humidity (%)	33.56	-59.84	0.00	2.19	27.68	-108.89	0.00	1.6
Temperature (K)	299.76	0.93	0.00	1.94	288.79	Not Significant		
Surface Pressure(KPa)	98.11	-2.01	0.00	4.16	98.86	-1.07	0.00	4.13
Uwind Speed (m/s)	0.95	Not Significant			1.38	2.34	0.00	1.32
Vwind Speed (m/s)	0.65	0.13	0.00	1.46	-0.11	Not Significant		
Boundary Layer Height at 8:00 (km)	1.61	-122.26	0.00	2.14	1.32	-3.42	0.00	1.18
Boundary Layer Height at 20:00 (km)	0.11	188.53	0.00	1.04	0.15	-162.46	0.00	1.06
GDP (RMB 1000 Yuan)	119.22	0.03	0.00	10.8	887.27	0.002	0.00	1.07
Elevation (m)	81.57	-0.30	0.00	4.28	91.96	-0.26	0.00	4.27
Population (1000 People)	62.81	0.04	0.00	1.12	534.43	Not Significant		
Percent of Urban Area (%)	61.67	Not Significant			42.01	Not Significant		

Mean: the averaged value of each independent variable;

Coefficient: the coefficient of each independent variable in specific regression model;

Sig.: significance level. Sig.=0.00 indicate the variable is statistically significant at the 0.00 level.

VIF: variance inflation factor

Confidence levels of the MLR models have been assessed by using F tests for each parameter. The results of this study were significant with 95% confidence level ($\alpha = 0.05$). Figure 5.3 shows the scatter plots of MLR models' results between monitoring stations measurement and predicted PM2.5 concentrations generated from the 3 km AOD model (Figure 5.3.(a)) and the 10 km AOD model(Figure 5.3.(b)). There were 1431 data points in the 3 km AOD product and 2851 data points in the 10 km AOD model in total. In these two scatter plots, the red colour means the high density of data points. It can be noticed that in the 3 km AOD MLR model, ground measured PM2.5 concentrations ranged from 0 to 140 (μg/m^3) and the predicted PM2.5 ranged from 0 to 90 (μg/m^3). These ranges for the 10 km AOD MLR model were relatively broader: the ground measured PM2.5 was from 0 to 240 (μg/m^3) and the predicted PM2.5 was from 0 to 170 (μg/m^3). The coefficient of determination (R^2) for the 3 km AOD MLR model

was 0.44 and that of the 10 km AOD MLR model was 0.55: the 10 km AOD MLR model could explain 55% of the variability, while the 3 km AOD MLR model could only explain 44% of the variability. The slops of 3 km and of the 10 km AOD MLR model were 0.42 and 0.54, respectively, while their intercepts were similar around 24. This means both of the models tended to overestimate the ground-level PM2.5 concentrations when PM2.5 was lower than 42-52 ($\mu g/m^3$) while when PM2.5 concentration was higher than this level, two models tended to underestimate the real values. Specifically, this overestimation and underestimation were more severe in 3 km AOD MLR model. The root-mean-square deviations (RMSE) of two model indicate the average magnitude of the forecast errors was 23.72 in the 3 km AOD MLR model and was 32.50 in the 10 km AOD MLR Model: the 10 km AOD MLR model predicts PM2.5 with more errors though it has better coefficient of determination. This was mainly because the range of the predicted PM2.5 was 0-90 ($\mu g/m^3$) in the 3 km AOD MLR model and was 0-170 ($\mu g/m^3$) in the 10 km AOD MLR model: the boarder range might bring higher predicted error even the 10 km AOD MLR model had a higher R^2. The Mean Absolute Percent Error (MAPE) refers to the percentage of the over-forecasted or under-forecasted part. The 3 km AOD MLR-predicted PM2.5 had a higher MAPE (91.09%) than that of PM2.5 predicted by the 10 km AOD product.

The coefficient, significance level and variance inflation factor (VIF) of each variable in two annual MLR modes are shown in Table 5.2. For the MLR model derived from the 3 km AOD product, Uwind speed and the percent of urban area were not significant while in MLR model derived from the 10 km AOD, temperature, Vwind speed, population and the percent of urban area were all not significant. The VIF of all the significant parameters in two models all ranged from 0 to 10, which means there was no significant multicollinearity between independent variables (Okazaki et al., 2014). In terms of the coefficient, AOD, Uwind and Vwind speed, GDP and population in both models showed positive values of coefficient which means with the increase of these parameters, PM2.5 increased. Meanwhile, the coefficient of relative humidity, surface pressure, BLH at 8:00 and elevation were all negative values, which demonstrated that PM2.5 increased with the decrease of these parameters.

5.2.1.2 10-Fold Cross Validation

To assess whether the models were over-fitted, a 10-fold CV was conducted after the annual MLR model construction. CV's scatter plots are shown in Figure 5.4. The predicted PM2.5 in CV of two models had similar ranges with those of annual MLR models: the predicted PM2.5 of the 3 km AOD Model's CV was from 0 to 90 ($\mu g/m^3$) and that of the 10 km AOD model's CV ranged from 0 to 160 ($\mu g/m^3$). R^2 of the 3 km AOD MLR CV was 0.40, lower than that of the 3 km AOD MLR model. Similarly, in the 10 km AOD MLR model, CV's R^2 (0.53) was a little bit lower than that of the MLR model. This means both MLR models were slightly over-fitted. In 10-fold CV, RMSE of the 3 km AOD MLR model (24.52) was still

lower than RMSE of the 10 km AOD MLR model (39.12). However, for MAPE, it was 91.73% in CV of the 3 km AOD MLR model, lower than that of the 10 km AOD MLR CV (92.40%), which was opposite with the MAPE's pattern in predicted models as shown in Figure 5.3.

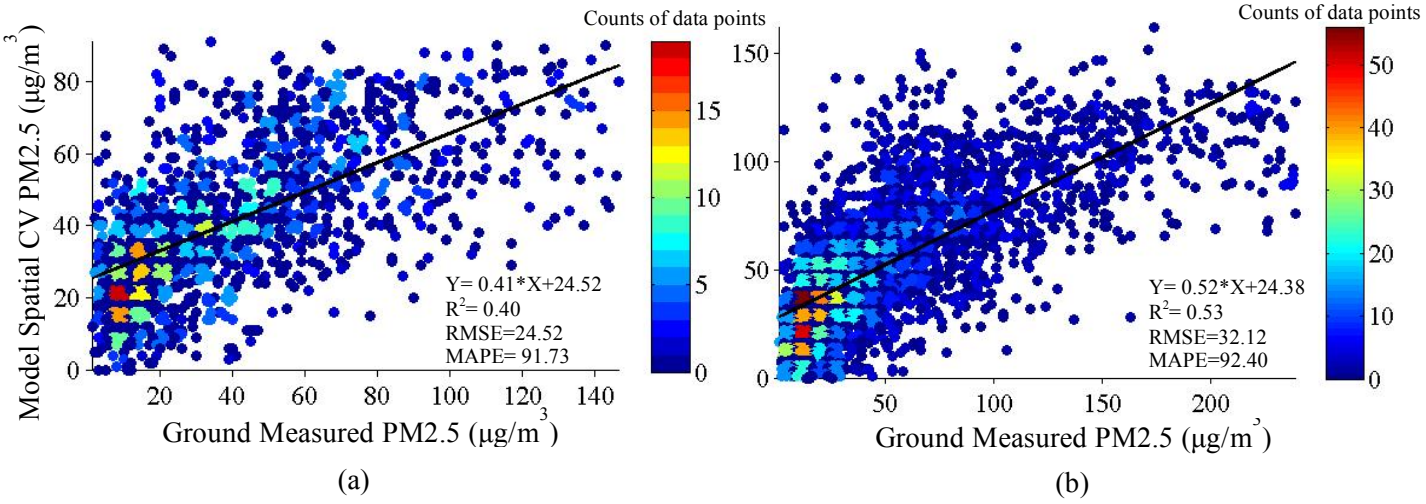

Figure 5.4 Scatter plots for 10 – fold CV of the MLR model from (a) the 3 km AOD model, and (b) the 10 km AOD model

5.2.1.3 An Air Pollution Event

Based on the annual MLR model, every day's PM2.5 concentration map in the BTH region was generated. To present the daily PM2.5 concentrations, in this sub subsection, an air pollution event between April 23, 2015 and April 28, 2015 is presented and described. Figure 5.5 shows the PM2.5 distributions generated by the 3 km AOD MLR model during this event period and Figure 5.6 presents the PM2.5 distributions derived from 10 km MLR model during the same period. In Figure 5.5, the predicted PM2.5 in six figures ranges from 0 to 120 (μg/m^3): red colour denotes high PM2.5 concentration and blue colour denotes low concentrations. On April 23, 2015 (Figure 5.3(a)), the highest PM2.5 concentrations derived from the 3 km AOD MLR model were around 90 μg/m^3 and distributed in Cangzhou, Hengshui and the eastern part of Baoding in Hebei Province. Beijing, Shijiangzhuang and Chengde in Hebei Province had relatively lower PM2.5 concentrations. Because of the lack of valid AOD data, PM2.5 concentrations of other cities are unknown, such as Handan, Zhangjiakou in Hebei Province and Tianjin. In April 24, PM2.5 concentrations in Baoding, Tianjin, Beijing, and Baoding Hebei Province were all increased around 60 -90 μg/m^3. In the next day (Figure 5.3 (c)), PM2.5 concentrations in the eastern BTH region kept increasing, especially in Tianjin, while the PM2.5 in Zhangjiakou, western Baoding and western Shijiazhuang Hebei Province were dissipated to some extent. On April 26 (Figure 5.5 (d)), Beijing, Tianjin, Qinhuangdao, Langfang, Cangzhou, Hengshui, the north of Chengde and the north of Shijiazhuang in Hebei Province were all

covered with PM2.5 concentration higher than 90 μg/m^3 and the PM2.5 in some part in Beijing, Langfang and Tianjin reached the highest value, 120 μg/m^3. Those areas along the western border of the BTH region had relatively less PM2.5 pollution. April 26 can be regarded as the mostly polluted day during this air pollution event. After 24 hours, from the limited amount of pixels in Tianjin, Tangshan, Cangzhou and Langfang in Hebei Province, it can be found the PM2.5 concentrations were dissipated in a large extent. However, due to the lack of valid PM2.5 estimation in Beijing, Zhangjiakou and Chengde in Hebei Province, it is hard to learn the PM2.5's change in those areas. In the last day, as shown in Figure 5.5 (f), most of the valid pixels roughly illustrated a clear air in the BTH region.

However, compared with the 10 km AOD MLR model derived PM2.5 in this period, the 3 km AOD MLR model tended to overestimate the PM2.5 concentrations in the BTH region. Figure 5.6 shows the process of air pollution's accumulation and dissipation in this event derived from the 10 km AOD MLR model. The predicted PM2.5 in six figures ranged from 0 to 80 (μg/m^3): red colour also denotes high PM2.5 concentration and blue colour denotes low values. Another difference is, compared with the 3 km AOD MLR model, the 10 km AOD MLR model provided greater coverage. For example, in April 25, the PM2.5 concentrations in northern part of Chengde in Hebei Province was unknown in the map of the 3 km AOD model (Figure 5.6 (c)), while in the map mapped by the 10 km AOD model (Figure 5.6 (c)), PM2.5 in the northern Chengde in Hebei Province was estimated around 30 (μg/m^3) with a greater coverage. However, with a higher resolution, 3 km AOD MLR model could show model variations on the ground. This is also explained in Section 5.3.1 in detail.

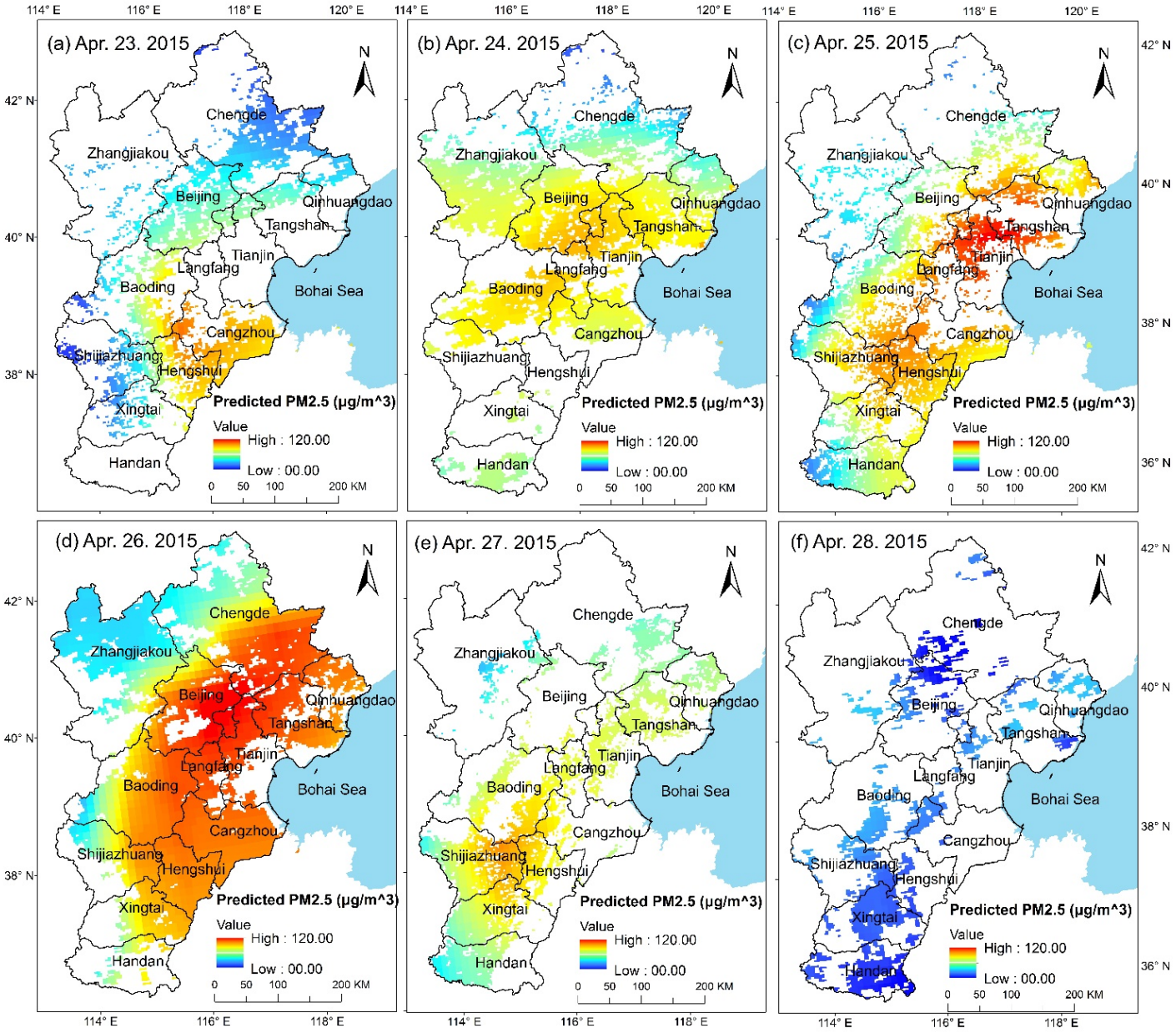

Figure 5.5 3 km AOD model-predicted PM2.5 concentrations from April 23 to 28, 2015

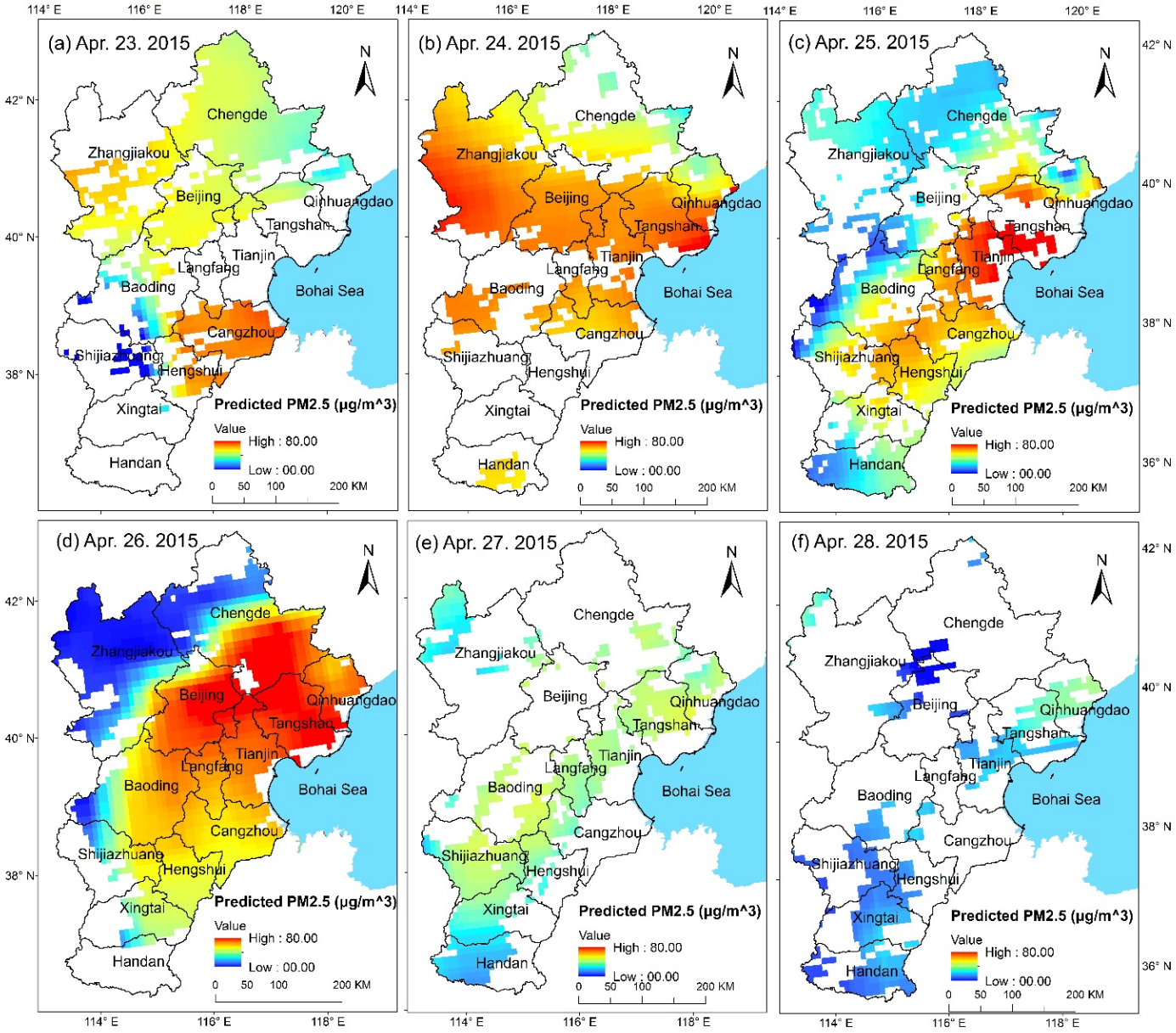

Figure 5.6 10 km AOD model-predicted PM2.5 concentrations from April 23 to 28, 2015

5.2.2 Seasonal Model

After the annual MLR model construction, seasonal models were also built to determine MLR models' performance in different seasons.

The statistical results of two models in four seasons are shown in Table 5.3. The counts of the training samples in fall and spring were higher in the 10 km AOD MLR models than in the 3 km AOD MLR models. On the contrary, the count of the training samples in summer was higher in the 3 km AOD

MLR model (641) than in the 10 km AOD MLR model (472). The count of the training samples in winter was only 27 in the 3 km AOD MLR model, which was the smallest count between four seasons. In contrast, winter's training samples' count (1127) was the greatest one between four seasons in the 10 km MOD MLR model and it has 1100 samples more than that of the 3 km MLR model, which was an extreme difference. So the different structure of the samples' counts in four seasons might be one of the reasons which introduced basis in the annual MLR models, and it might also result in different performance of two models in four seasons.

Table 5.3 Statistical results from seasonal MUL models

	3 km AOD model				10 km model			
Season	N	R^2	RMSE ($\mu g/m^3$)	MAPE (%)	N	R^2	RMSE ($\mu g/m^3$)	MAPE (%)
Fall	322	0.42	20.38	99.99	420	0.49	23.97	98.69
Winter	27	0.78	6.78	35.84	1127	0.7	32.02	80.43
Spring	467	0.46	24.58	81.56	832	0.6	27.91	67.52
Summer	614	0.48	22.82	71.92	472	0.51	23.72	63.32
Mean	357.5	0.54	18.64	72.3275	712.75	0.58	26.905	77.49

N: Number of the training samples.

R^2: Coefficient of determination

RMSE ($\mu g/m^3$): Root-Mean-Square Error

MAPE (%): Mean Absolute Percent Error

For the 3 km AOD MLR model, compared with the annual model, R^2 was slightly improved to 0.46 in the spring model and to 0.48 in the summer model. For the winter model. R^2 was significantly improved to 0.78 and RMSE and MAPE were also decreased in a large extent compared with the annual model. However, the model has worse performance in fall ($R^2 = 0.42$). Meanwhile, for the 10 km AOD MLR model, R^2 was also highly improved in the winter model ($R^2 = 0.7$) and the fall model also has the lowest R^2 in four seasons.

By comparing both the 3 km and 10 km AOD seasonal MLR models, it can be found that except winter, R^2 of the seasonal MLR models with the 3 km AOD were still lower than with the 10 km AOD model during three other seasons. The average R^2 of four seasons' 3 km AOD MLR model was 0.54, 0.10 higher than annual model; average R^2 from seasonal model was only improved 0.03.

It can be concluded that winter model performed better than the other three seasons' model for both the 3 km and 10 km AOD models and MLR models had the worst performance in fall with both AOD product. Please refer to Appendix II for each parameter's mean value, coefficient and significance.

5.2.3 Regional Model

As introduced in Section 5.2.1, the counts of the training samples were different in four seasons and this difference might bring basis. Similarly, counts of the valid training samples were also different between cities. Figure 5.7 shows the valid training samples' total counts of each city from the 3 km AOD model and the 10 km AOD model. The difference between the counts were not only a result of the AOD coverage, but also because each city has different numbers of in-situ monitoring stations. Please refer to Appendix I for the information in each city's in-situ stations.

From Figure 5.7, it can be found for the 3 km AOD model, the count of each city's training samples was from 36 to 272 and for the 10 km AOD model, and their counts were higher, from 94 to 1650. As a whole, the central BTH region, including Beijing, Baoding, Tianjin, Shijiazhuang, and Tangshan in Hebei Province, tended to have more training samples, on the contrast, northern and southern parts of the BTH region tended to have less training samples, such as Zhangjiakou Xingtai and Handan in Hebei Province. No matter for the 3 km or 10 km AOD model, Beijing has the highest counts of sample. This spatial structure of sample's counts may affect the whole area derived-model's performance in different cities.

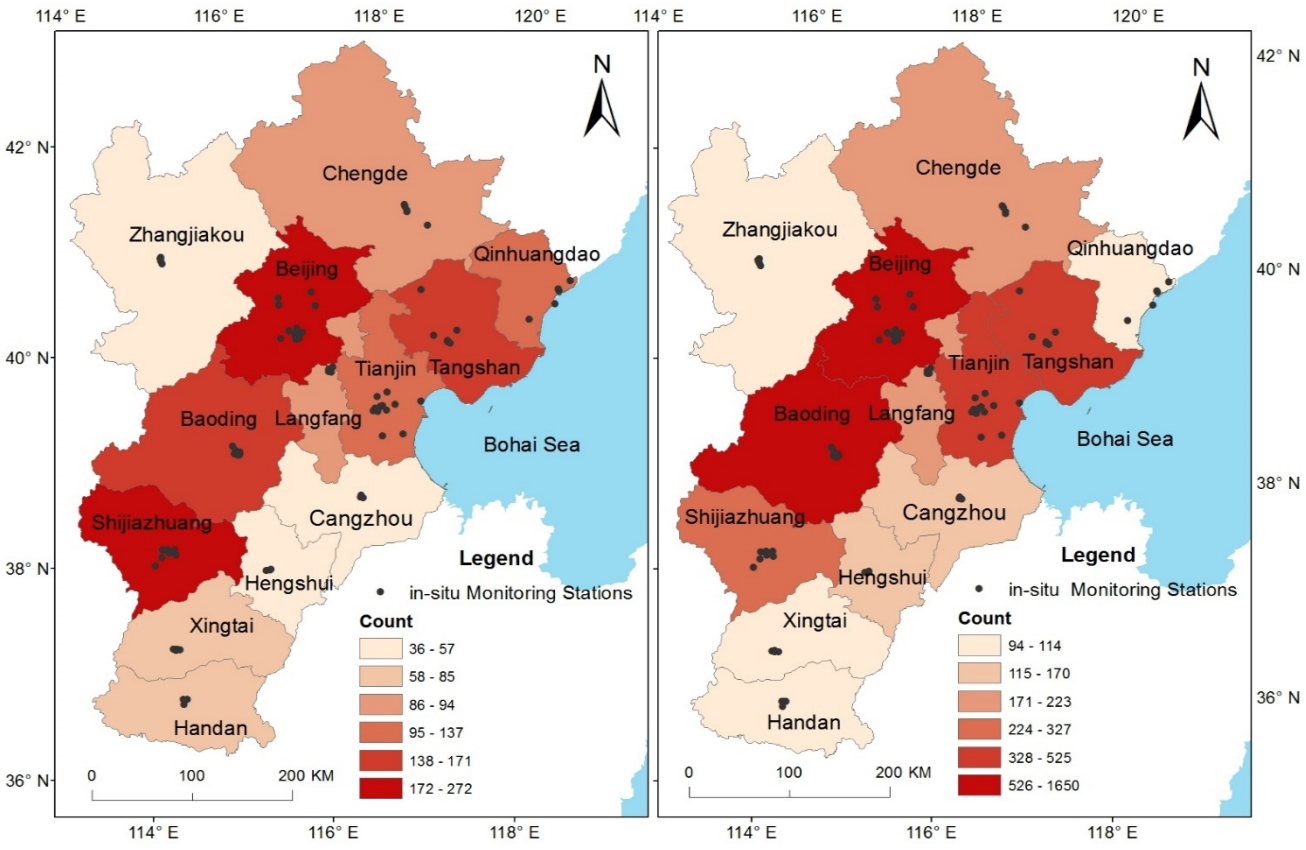

Figure 5.7 Training samples' count of each city from (a) the 3 km AOD model and (b) the 10 km AOD model

The statistical results of each city's model are shown in Table 5.4 and Figure 5.8 presents the regional MLR's R^2 in a box plot. It can be found for regional models with the 3 km AOD, all the cities' R^2 was lower than 0.44 (R^2 of the model based on whole study area) except Hengshui ($R^2 = 0.47$). Moreover, the MLR model could not even be built with Cangzhou and Handan's dataset because the independent variables were not significant and could not explain any variations. This indicates building the models with smaller spatial scales could not help 3 km AOD MLR models to improve the model performance and the relevant research should be based on a larger spatial scale when using the 3 km AOD product. Also, it also suggests more in-situ stations should be built to increase the training samples' counts and the performance of models.

Table 5.4 Regional MUL models' results

Cities	3 km AOD				10 km AOD			
	N	R^2	RMSE ($\mu g/m^3$)	MAPE (%)	N	R^2	RMSE ($\mu g/m^3$)	MAPE (%)
Baoding	155	0.10	28.82	45.61	165	0.51	37.52	99.12
Beijing	272	0.16	27.63	54.06	620	0.63	27.38	79.45
Cangzhou	37	Model cannot be built			168	0.64	25.42	93.48
Chengde	87	0.11	24.02	99.99	200	0.59	14.59	78.19
Handan	59	Model cannot be built			98	0.40	38.58	55.23
Hengshui	55	0.47	10.20	56.86	115	0.68	24.96	53.51
Langfang	91	0.06	23.86	118.62	180	0.65	32.44	83.31
Qinhuangdao	96	0.23	16.38	82.86	94	0.46	17.01	70.73
Shijiazhuang	184	0.18	23.93	83.18	248	0.46	32.52	78.89
Tangshan	141	0.27	25.78	86.65	350	0.56	34.42	89.81
Tianjin	133	0.32	23.40	66.44	404	0.70	31.60	64.04
Xingtai	84	0.09	12.48	88.13	94	0.53	34.12	72.88
Zhangjiakou	36	0.30	20.84	87.35	113	0.56	16.30	66.83
Mean	110	0.21	21.58	79.07	219.15	0.57	28.22	75.81

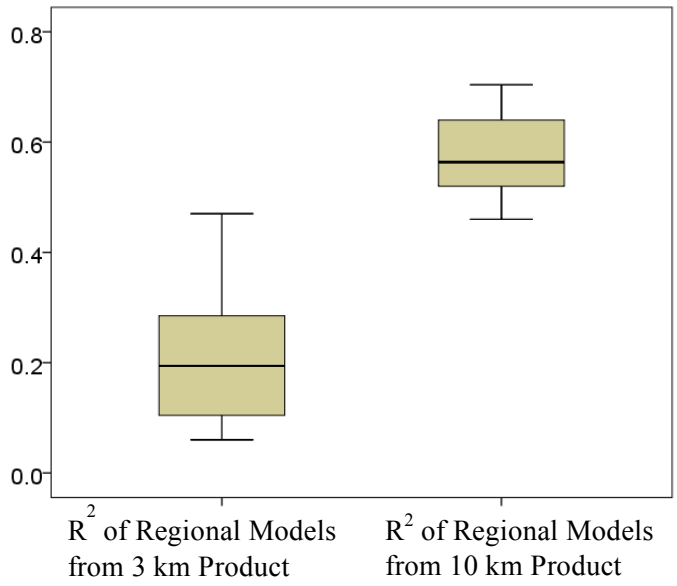

Figure 5.8 Box-Plot of the regional MLR models' R^2

On the contrast, with a smaller spatial scale, the 10 km AOD regional models' R^2 of most cities increased from 0.55 (R^2 of the model based on whole study area) except Baoding, Handan, Qinhuangdao, Shijiazhuang and Xingtai in the Hebei Province. R^2 of all the cities were ranged from 0.46 to 0.7 and the average R^2 of each city was 0.57, which indicated the smaller spatial scale helped the 10 km AOD MLR model to improve the estimation performance and also helped to study the spatial variation within a region.

5.3 Geographically Weighted Regression Model

In this section, the GWR model was explained from two aspects: an annual model and seasonal models.

5.3.1 Annual Model

The statistical results of the GWR model, including AIC, local R^2, RMSE, MAPE and Moran's I value, are shown in Table 5.5. As introduced in Chapter 4, a 10-fold CV was also conducted and the same statistical results of CV are also shown in Table 5.5. At the same time, to assess whether the GWR model could improve estimation accuracy, the global regression's results are also listed in the same table.

Table 5.5 Statistical results of the GWR model, 10-fold CV for the GWR model and the corresponding MLR model from the 3 km and 10 km AOD products.

Model Type		N	AIC	Local R^2	RMSE ($\mu g/m^3$)	MAPE (%)	Moran's I
3 km AOD	GWR Model	79	539.40	0.82-0.96	5.83	0	0.08
	10-Fold CV for GWR	79		0.81-0.96	8.69	9.37	0.03
	Global Regression Model	79	552.65	0.90	7.24	8.12	
10 km AOD	GWR Model	79	533.62	0.83-0.95	5.61	6.63	-0.03
	10-Fold CV for GWR	79		0.82-0.96	10.02	10.95	0.16
	Global Regression Model	79	548.19	0.91	7.17	10.47	

In this study, the GWR model was based on the annual average data of each monitoring station, so the number of training samples for the GWR model, CV and global regression was all of 79. When determining whether the models' residual had spatial autocorrelation, it should be noticed in Table 5.5 that no matter for the GWR model or the global regression model with the 3 km or 10 km product, Moran's I were all near zero. As mentioned in Chapter4, negative value of Moran's I denote a negative autocorrelation while positive values means the existence of positive spatial autocorrelation. In this situation, the ideal GWR model's Moran' I value should be near zero, otherwise, other spatial models, such as spatial lag,

should be used instead of the GWR model. Therefore, GWR models built in this study were qualified for further analysis.

In terms of AIC, the 3 km AOD GWR model's AIC was 539.40, lower than AIC of the 3 km AOD global regression model (552.65). For 10 km GWR model, AIC was 533.62, which was also lower than the 10 km AOD global regression model's AIC (548.19). As mentioned in Chapter 4, a lower AIC indicates an increase of the estimation results. Therefore, in this study, no matter the 3 km or 10 km AOD GWR model, GWR model performed better in predicting PM2.5 concentrations than global regressions did. Meanwhile, AIC of the 3 km AOD GWR model was slightly higher than AIC of the 10 km AOD GWR model, which indicates when using the GWR model, the 10 km AOD model still has a higher accuracy than 3 km AOD models.

From Table 5.5, it can be learnt local R^2 of the 3 km AOD GWR model was from 0.82 to 0.96 and its CV's local R^2 had a similar range: 0.81 to 0.96. For the 3 km AOD product, the GWR model had a local R^2 ranged from 0.83-0.96 and its CV's local R^2 was also similar. To decide whether GWR models were overestimated or not, Figure 5.9 shows the box-plot of GWR models and CVs' local R^2. From this table, it can be found for the 3 km AOD model, although the median local R^2 of CV was slightly higher than that of the GWR model, first quartile and third quartile of local R^2 of the GWR model and CV were similar. Thus it can be concluded the 3 km AOD GWR model was not over-fitted. On the contrast, for the 10 km AOD model, it can be found from Figure 5.9 that although the GWR model and CV had similar ranged, 0.83 was an outlier of the GWR model's local R^2 and the GWR model's actual local R^2 range should be from 0.86 to 0.95. Therefore, it can be carefully concluded that, the 10 km AOD GWR model was slightly over-fitted but this over-fitting was at an acceptable level.

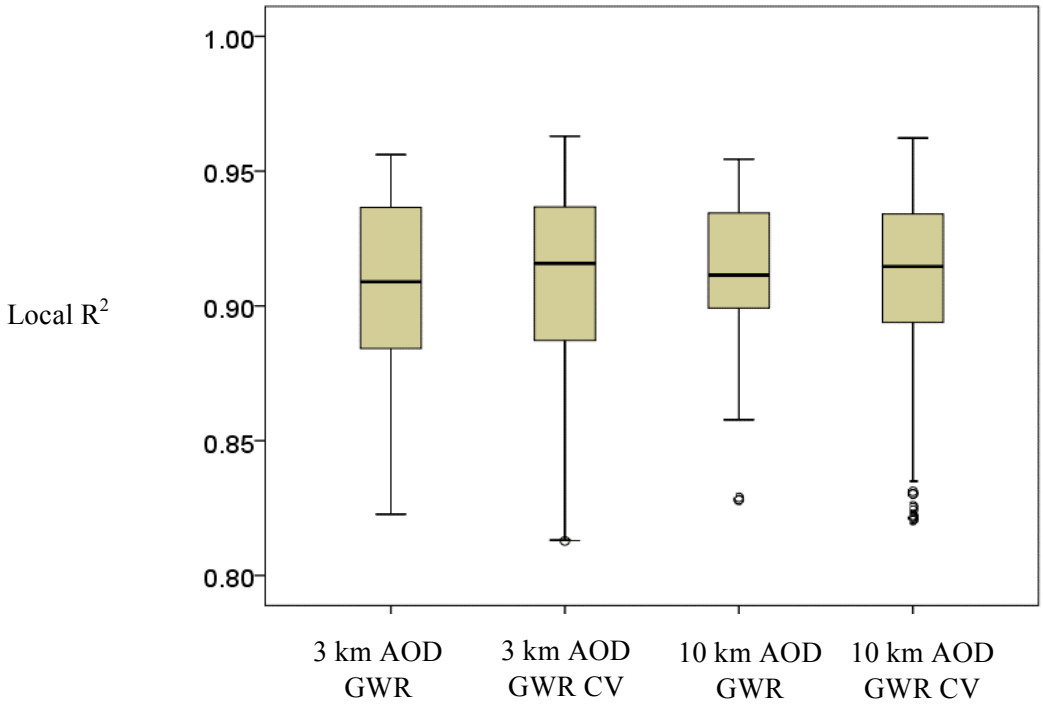

Figure 5.9 Local R^2 of GWR models and corresponding CVs from two AOD products

Comparing the 3 km AOD GWR model's RMSE and MAPE (Table 5.5) with those of global regression, it can be found the GWR model brought with more accuracy. Meanwhile, the 10 km AOD GWR model also has a higher accuracy than its global regression.

Then based on the 3 km and 10 km AOD WGR model, the estimations of annual average PM2.5 distribution were mapped in Figure 5.10. As a whole, the 3 km AOD GWR model (Figure5.10 (a)) and the 10 km AOD model (Figure 5.10 (b)) present similar spatial distributions of PM2.5 concentrations. In these two figures, red colour denotes high PM2.5 while blue colour indicates relatively clean air. The estimated PM2.5 concentrations were ranged from 0 to 110 ($\mu g/m^3$).

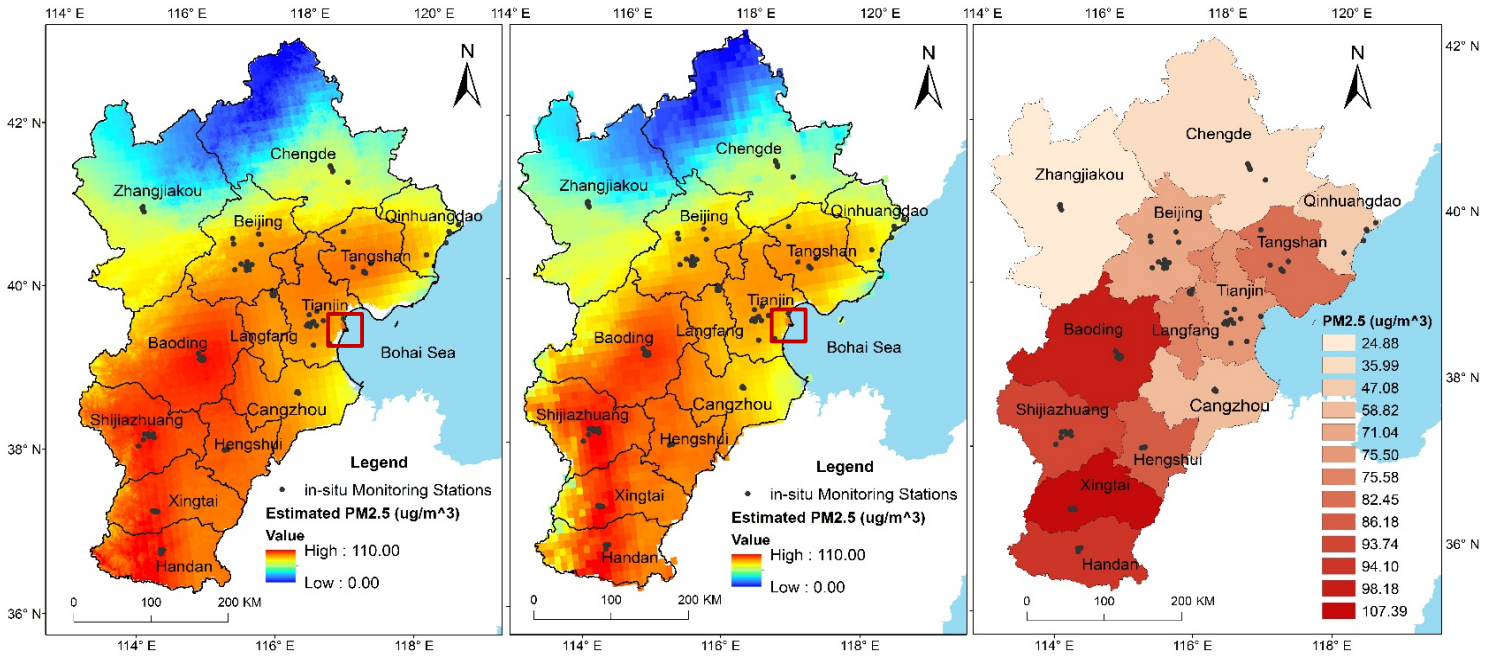

(a) (b) (c)

Figure 5.10 Estimated PM2.5 generated by the annual GWR model from (a) the 3 km AOD product, (b) the 10 km AOD and (c) the average PM2.5 of each city from their ground-level monitoring stations

Figure 5.10 (c) shows the each city's average PM2.5 concentrations from their ground-level monitoring stations during the research period and this figure is as same as Figure 3.4. As shown in Figure 5.10 (a) and (b), the mountainous area and the plateau region (Chengde and Zhangjiakou) had low concentrations of PM2.5 (10 to 45 μg/m^3). Beijing, Tianjin, Qinhuangdao, Tangshan, Langfang and Cangzhou in Hebei Province had median levels of PM2.5 pollutions: 20-85 (μg/m^3). It should be noticed that Tianjin harbour, marked with a red square in Figures (a) and (b), had a much higher value of PM2.5 (85.36 μg/m^3) than other areas in Tianjin (around 70-75 μg/m^3). This also proved that the transportation was an important source of PM2.5. The rest cities, Baoding, Shijiazhuang, Xingtai, Handan, and Hengshui in Hebei Province were polluted with the highest level of PM2.5 (80-110 μg/m^3) in the BTH region. This distribution agreed with the ground level monitoring data.

Figure 5.10 (c) is generated only by the monitoring stations clustered in urban area. However, ground-level monitoring stations measurement actually could only represent a limited area around the station. That is to say, the rest of the area's PM2.5 was not able to be taken into consideration when calculating the average value of this city and when mapping Figure 5.10 (c). Additionally, Figure 5.10 (c) could not present the variation of PM2.5 concentrations in those areas without ground-level monitoring stations. Speaking of the variation, the 3 km AOD GWR model was able to present more variations than

the 10 km AOD GWR model did. Figure 5.11presents the PM2.5 concentrations in Beijing estimated by the 3 km AOD GWR model (see Figure 5.11 (a)) and the 10 km AOD GWR model (see Figure 5.11 (b)). Though Figure 5.11estimated PM2.5 in Beijing with similar distribution and level from 20 to 85μg/m^3, the 3 km AOD generated map can present more variations no matter within the urban area or along the administrative boundary. However, due to the combination and influence of meteorological dataset with lower spatial resolution (0.125°×0.125°), the grids' patterns of meteorological dataset can be easily identified in the PM2.5 concentrations' map generated by the 3 km AOD GWR model (see Figure 5.11(a)).

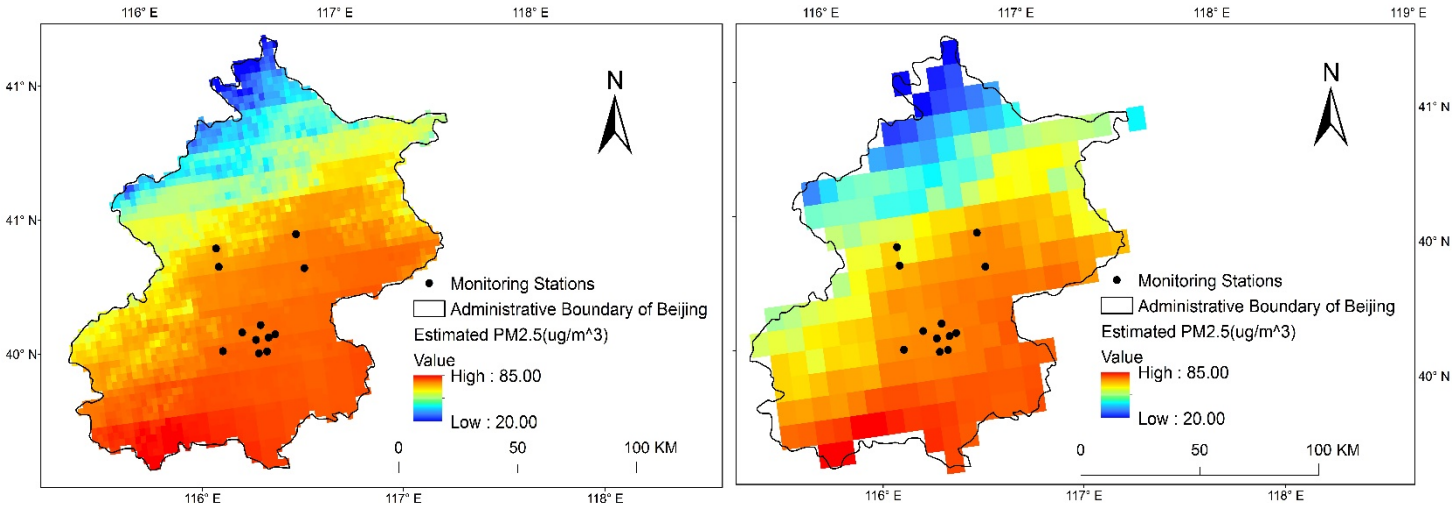

(a) (b)

Figure 5.11 Estimated PM2.5 generated by the GWR model from (a) the 3 km AOD product and (b) the 10 km AOD product in Beijing

5.3.2 Seasonal Model

After the annual model, seasonal model was also generated to learn each season's characteristics in PM2.5 pollution and to assess the GWR model's performance in four seasons. As mentioned in Section 5.2.2, in this study, winter season was in lack of the 3 km AOD training samples, and once the number of the training sample was too low, the GWR model's construction would be failed (the reason has been explained in Chapter 4). As a consequence, winter model of the 3 km AOD GWR model was failed to be built. The statistical results of other seasons are shown in Table 5.6. For all the other seasons in the 3 km and 10 km AOD GWR models, the numbers of training samples were all 79. At the same time, Moran's I of models were all near zero.

Table 5.6 Statistical results of seasonal GWR models from the 3 km and 10 km AOD products

Model Type		N	Local R^2	RMSE (μg/m^3)	MAPE (%)	Moran's I
3 km AOD GWR Model	Fall	79	0.64-0.96	9.19	8.49	0.06
	Winter	Model construction was failed due to the limited number of training samples (see Section 4.4.2)				
	Spring	79	0.74-0.92	9.29	7.08	-0.2
	Summer	79	0.61-0.84	8.65	7.25	0.02
10 km AOD GWR Model	Fall	79	0.69-0.95	8.1	8.73	0.09
	Winter	79	0.83-0.96	8.82	7.32	-0.04
	Spring	79	0.75-0.93	7.26	5.06	-0.22
	Summer	79	0.62-0.85	9.27	6.92	0

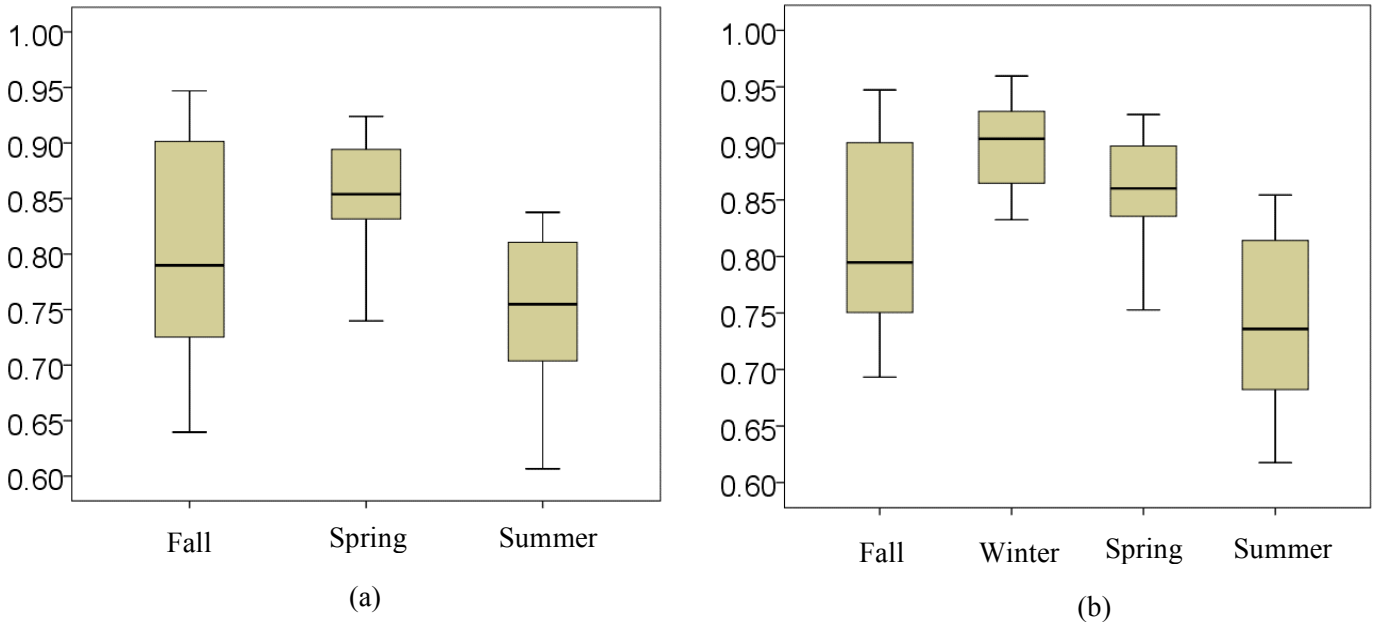

Figure 5.12 Local R^2 of seasonal GWR models from (a) the 3 km AOD product and (b) the 10 km AOD product.

Figure 5.12 shows box-plots of all the models' local R^2. From Table 5.6 and Figure 5.12, it can be found for the 3 km AOD seasonal GWR model, the spring model had a relatively higher and clustered range of local R^2 (0.74-0.92). Compared with other two seasons' models, the summer model had a lower range of local R^2 (0.61-0.84). This indicate the spring model has the best performance while the GWR model in the winter did not perform as good as in the other two seasons. For winter, this sequence was the winter model

(0.83<local R^2<0.96), the spring model (0.75<local R^2<0.93), the fall model (0.69<local R^2<0.95) and the summer model (0.62<local R^2<0.85). Comparing the local R^2 in the same season of two AOD products' models, it can also be drew that 3 km and 10 km AOD had similar performance in the same season.

Following the seasonal GWR model, PM2.5 concentration's distribution were mapped and shown in Figures 5.13 (fall and winter) and 5.14 (spring and summer). To make it easier to learn PM2.5's change trend during the study period, the same colour bar was used in all estimated maps, ranged from 0 to 130μg/m^3. Moreover, the ground-level monitoring stations' averaged PM2.5 concentration of each city was also mapped for each season. When studying the seasonal trend of PM2.5 concentrations from GWR model -generated results, it could be concluded that, fall and winter had the more severe PM2.5 pollution while spring and summer were polluted less in general. Among these seasons, PM2.5 pollution was most severe in winter (see Figure 5.13(d)). In addition, the high values of PM2.5 (around 110-130 μg/m^3) were distributed in Baoding, Shijiazhuang, Xingtai, Hengshui and Handan in Hebei Province. By comparing the PM2.5's spatial distribution generated by two AOD products in the same season, it should be noticed that, in general, they have similar estimations in fall (see Figures 5.13 (a) and (b)), spring (see Figures 5.14 (a) and (b)) and summer (see Figures 5.1 (d) and (e)). These estimation agreed with the distribution generated by ground-level monitoring stations' measurements. However, some difference between the predictions from two AOD products' model can be observed. For example, when we take the 10 km AOD GWR model as the basis to discuss, the 3 km AOD GWR model tended to underestimate the western and eastern part of Handan in fall (see Figures 5.13 (a) and (b)); the 3 km AOD GWR model also tended to slightly underestimate PM2.5 in Baoding and Handan in Hebei Province; however, it estimated slightly higher PM2.5 in Zhangjiakou and Beijing in summer than the 10 km AOD GWR model did.

However, these bias between two products' estimated results can hardly be validated because there was no monitoring station in those areas. In addition, the circumstance in the past cannot be retrieved even the monitoring stations could be built in the future. However, building more ground-level monitoring stations will contribute to adding more "control points" and to increasing the estimation accuracy in the whole region.

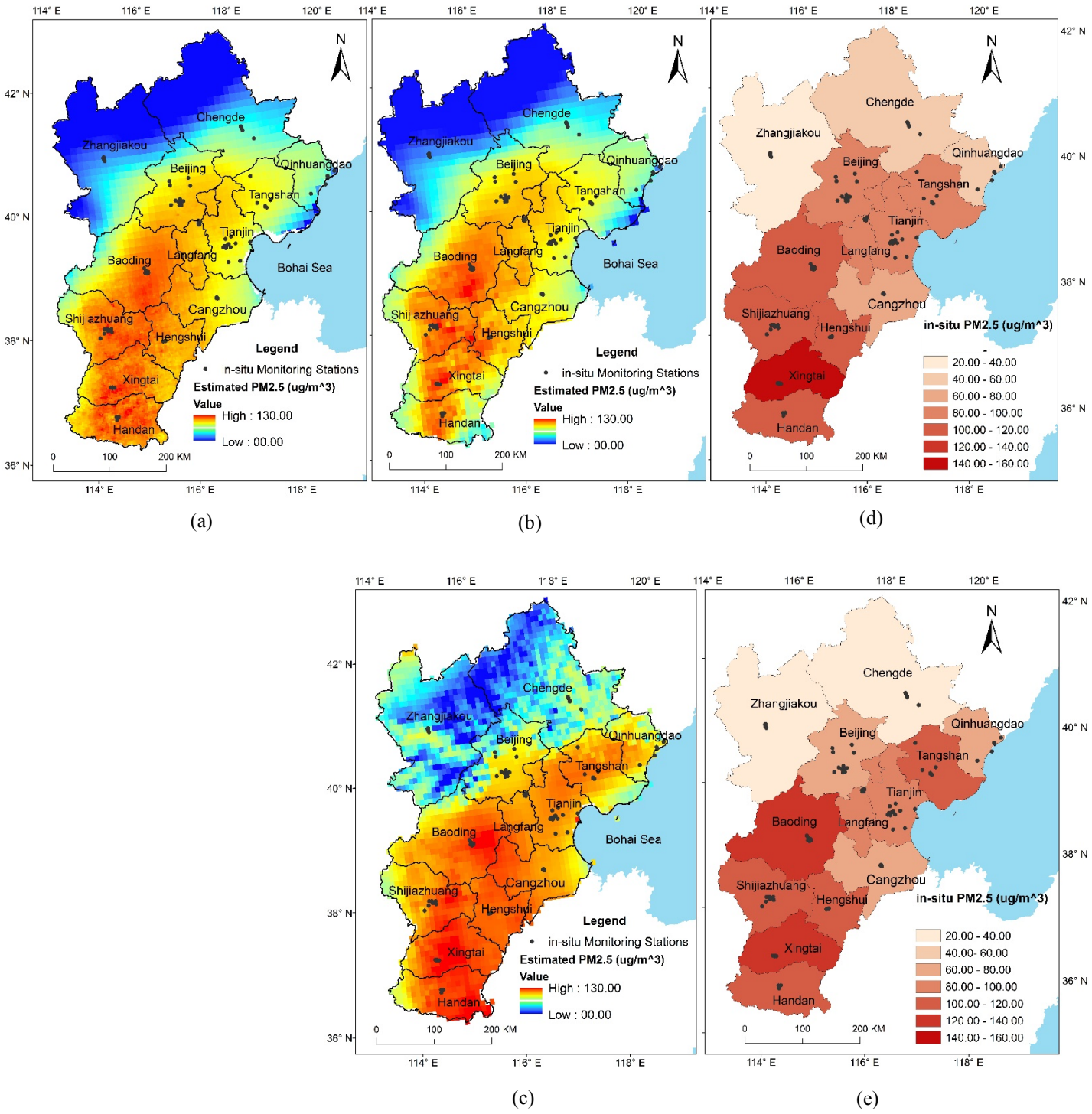

Figure 5.13 Estimated PM2.5 generated by the seasonal GWR model from (a) the 3 km AOD product in fall , (b)the 10 km AOD product in fall, (c) the 10 km AOD product in winter, (d) the average PM2.5 of each city in fall, and (e) in winter from their ground-level monitoring stations

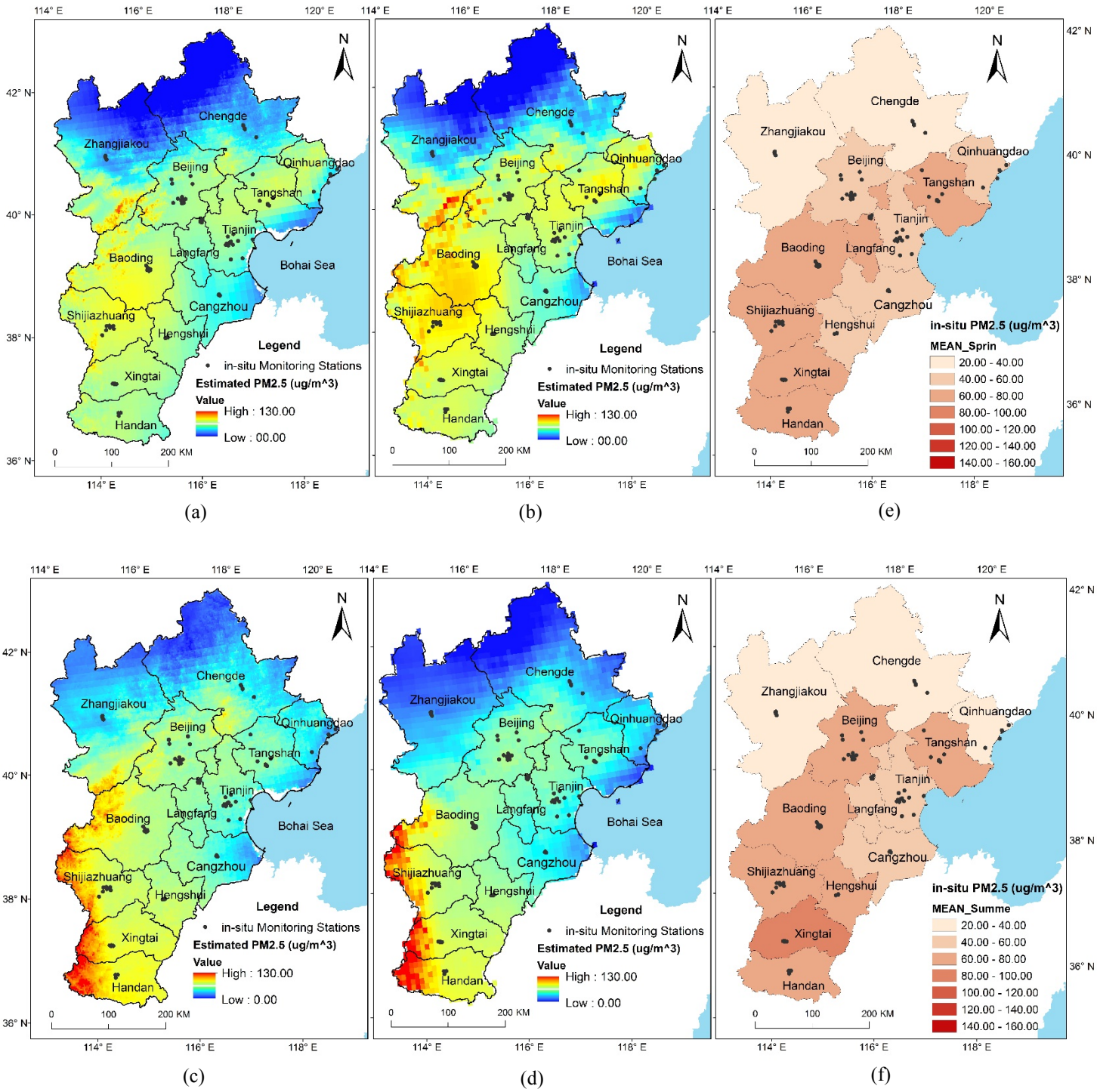

Figure 5.14 Estimated PM2.5 generated by the seasonal GWR model from (a) the 3 km AOD product in spring, and (b) in summer, (c) the 10 km AOD product in spring, and (d) in summer, (e) the averaged PM2.5 of each city in spring, and (f) in summer from their ground-level monitoring stations.

5.4 Application: The Number of Deaths' Estimation

Based on the annual GWR model generated in Section 5.3.1 and the method to estimate the number of deaths (Section 4.5), the number of the non-accidental deaths attributed to the PM2.5 concentration exceeding national standard (15 μg/m^3) during the study period were produced. Figure 5.15 shows the estimation results of the number of the non-accidental deaths: Figure 5.15 (a) demonstrates the number of deaths within a pixel generated by the GWR model based on the 3 km AOD and Figure 5.15 (b) shows that of the 10 km AOD GWR model. Because the grids' sizes were different, the highest number of deaths in Figure 5.15 (b) was higher than that of Figure 5.15 (a). Then the sum of each city's total deaths attributed to the exceeded PM2.5 was also calculated and this result from the 3 km AOD GWR model is shown in Figure 5.15 (c). Because that from 10 km AOD GWR model delivers the same information with Figure 5.15 (c) so it is not presented in this thesis.

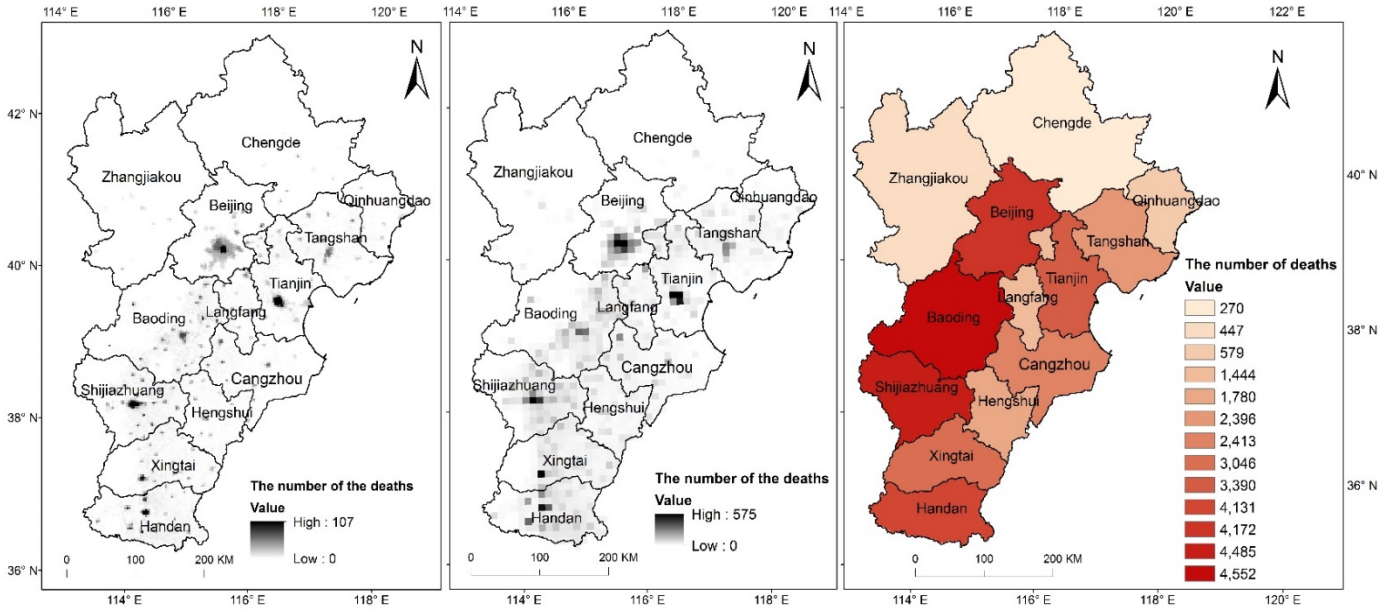

(a) (b) (c)

Figure 5.15 Number of the non-accidental deaths estimated by the GWR model based on (a) the 3 km AOD product, (b) the 10 km AOD product, and (c) the sum of the total deaths' number in each city generated by Figure 5.15(a).

(*number of the deaths: the deaths number shown in this figure denotes the non-accidental deaths attributed to long-term exposure to the PM2.5 exceeding Chinese national standard)

The total non-accidental deaths attributed to the excessive PM2.5 was 33104 estimated by the 3 km AOD GWR model' result (see Figure 5.15(a)) and was 33, 357 estimated by the 10 km AOD GWR model's

result (see Figure 5.15 (b)). There were three obvious hot spots of deaths in Beijing, Tianjin and Shijiazhuang, which might be owing to the high density of their population. However, when it comes to the sum of a city's whole deaths attributed to PM2.5 exceeding 15 μg/m^3, Baoding had the largest number of deaths (4, 452). Additionally, the number of deaths in Shijiazhuang, Beijing and Handan all exceeded 4000. Chengde and Zhangjiakou, with the lowest annual average PM2.5 concentrations, had the lowest deaths' number (270 and 447, respectively) in the BTH region.

Traditional statistical documents only provide the mortality rate or the population of a region or city. In this study, with the help of remote sensing, it can be learned where, statistically, the mortality risks increased the most. Thus, this section gives an example of how to apply remote sensing techniques in other fields, such as public health.

5.6 Chapter Summary

This chapter shows the major results obtained based on the methodology. Firstly, the MODIS AOD products were validated with the AERONET AOD and the results showed both the 3 km and 10 km AOD products tended to overestimate the AERONET AOD. At the same time, the 3 km AOD showed higher bias while 10 km product showed more uncertainties. Secondly, no matte for annual or seasonal MLR models, the 10 km AOD MLR model showed higher accuracy than the 3 km AOD MLR model. Then, an air pollution event in April 2015 was also described by using daily PM2.5 concentrations derived from the MLR model. Thirdly, seasonal MLR models could help both the 3 km AOD and 10 km AOD to improve the estimation accuracy, but regional models could only help the 10 km AOD model to increase the estimation accuracy. For the seasonal models, the MLR models performed better in winter than in three other seasons. Fourthly, the GWR model performed better in predicting PM2.5 concentrations than global regressions did. In addition, when using the GWR model, the 10 km AOD models still had a slightly higher accuracy than 3 km AOD models. However, 3 km AOD models could present more local variations. For seasonal GWR models, 3 km and 10 km AOD GWR models had a similar performance in the same season. At the last, the number of deaths attributed to those PM2.5 concentrations which exceeded Chinese national standard was estimated. The results showed the total deaths reached 33,100 in the BTH region during study period and this number was highest in Baoding (4452). At the same time, three hot-spots of deaths could be observed in Beijing, Tianjin and Shijiazhuang.

Chapter 6. Conclusions and Recommendations

This chapter presents key findings responding to research objectives of this study, the limitation and contribution of this research, and the suggestions for future studies.

6.1 Key Findings Responding to Research Objectives

This study aims to estimate PM2.5 concentrations in the BTH region using MODIS AOD products, meteorological datasets and land use information based on MLR and GWR models. The key findings responding to each specific objective are summarized below.

6.1.1 Objective 1: MODIS 3 km and 10 km AOD Products' Validation

3 km AOD product was released in 2014 as a part of MODIS Collection 6 product. Until now, 3km AOD product has not been widely used in the BTH region. One of this study's achievements is the validation of the 3 km AOD product in the BTH region.

By comparing the 3 km MODIS AOD with AERONET AOD and 10 km MODIS AOD with AERONET AOD, both the 3 km and 10 km AOD products had a good correlation with AERONET AOD and this correlation was observed better in the 3 km AOD validation; both the 3 km AOD and 10 km AOD products tended to overestimate ground-measured AOD and this overestimation was more severe in the 3 km AOD validation. As a whole, 3km AOD product shows higher bias but better correlation with the true values while the 10 km AOD showed more uncertainties in predicting ground-level AOD.

6.1.2 Objective 2: MODIS 3 km and 10 km AOD Products' Assessment in PM2.5 Estimation

PM2.5 concentrations was estimated by the MODIS 3 km and 10 km AOD products along with meteorological datasets and land use surrogates. All cities' annual averaged PM2.5 exceeded Chinese national standards. In addition, different seasons and cities present varied characteristics.

By comparing the MODIS 3km and 10 km AOD products, it was found the 10 km AOD had a much better accuracy in PM2.5 estimation. Meanwhile, the 10 km AOD-derived PM2.5 estimation's spatial coverage was greater than that of the 3 km AOD – derived PM2.5 estimation. This is not only because of its spatial resolution, but also owing to different algorithms of two products. On the contrast, the 3 km AOD product performed better in presenting spatial variations, which may help governments to identify the emission sources.

6.1.3 Objective 3: Multiple Linear Regression and Geographically Weighted Model's Performance

In this study, the MLR model was used to generate the daily distributions, which enables it to study the temporal trend of PM2.5's change. However, due to the lack of non-retrieved days' AOD, the MLR model-estimated PM2.5's accuracy still has space to be improved. MLR model is actually one of the global regression with global coefficients.

The GWR model, estimating local coefficients and local R^2, was able to improve the estimation accuracy than the corresponding global regression model. However, in this study, the GWR model was not able to generate daily concentrations due to the lack of collocations between satellite AOD and ground-level PM2.5. Thus, this study also suggests more ground-level monitoring stations ("control points") should be built in the future.

6.1.4 Objective 4: Mortality Estimation

Academic research should not only be investigating data products and models: it should also explore corresponding application. This study applies the models constructed using remote sensing datasets and statistical regression in public health field. It was estimated that during the study period in BHT region, more than 30, 000 people died due to the long-term exposure to PM2.5 concentrations exceeding Chinese national standard. Additionally, from this study, it can also be learnt where statistically, the mortality risks increased the most.

6.2 Limitations of this Thesis

Though this study achieved each objectives and made responding contributions, limitation and uncertainties should be concerned

At the first, the vertical structure and components of aerosol was not considered and this would affect PM2.5's estimation accuracy. This is because AOD presents the whole atmospheric aerosol distribution, while ground-level PM2.5 are measured near the Earth's surface.

Secondly, this study only utilized Aqua MODIS AOD product for time matching with meteorological data, but Terra MODIS AOD product was not explored. However, if the Terra MODIS AOD was also used, the non-retrieved day's AOD might be reduced and the PM2.5 might be estimated with a higher accuracy and a greater coverage. Another consequence of only using Aqua MODIS AOD product is the PM2.5 estimation in this study was actually just based on the PM2.5 at 14:00, not the whole day.

Thirdly, the lack of the AOD data in non-retrieved days and regions bring biases in AOD validation and PM2.5 estimation. Similar biases also existed when estimating PM2.5 in the whole BTH region because the ground level stations are limited in number and distributed unevenly.

In addition, for the GWR model, the estimation was on an annual or seasonal averaged basis. Daily estimation failed when using the GWR model due to the lack of ground-level stations.

At the last, meteorological parameters and land use surrogates were just described and simulated by statistical methods in this study. How each parameter affects PM2.5's accumulation and dispersion was not studied deeply. These parameters actually have remarkable potentials in PM2.5 studies. For example, by combing wind speed and direction, the pollutants' sources may be predicted.

6.3 Recommendations for Future Studies

According to limitations, some research directions are proposed as followed:

Firstly, aerosol's vertical structure and components should be explored by more remote sensing techniques, such as Lidar.

Secondly, by integrating other remote sensing's datasets, such as Terra MODIS AOD product and Landsat 8 data, the non-retrieved days or pixels should be reduced.

Then, more spatial regression models should be explored in this field, such as Spatial Lag, for spatial relationship's research.

Moreover, the research scale should be enlarged to a national or global level, so that the pollutants' sources and transfer's trend can be identified.

Last but not the least, more ground-level monitoring stations should be constructed. This point seems to conflict the intention of using remote sensing method: with more stations to monitor ground PM2.5, remote sensing results may be useless or unimportant. But this advice does not mean the more stations, the better. Actually, with the current monitoring stations, PM2.5 estimation using remote sensing can already generate an acceptable result. However, these stations are mostly located in urban areas, leaving rural area unobserved. So if more ground-level monitoring stations should be built with a scientific distribution (or a better pattern) and kept in a reasonable number, the estimation accuracy would be improved, not only in urban area, but also in other areas.

References

Ackerman, S.A., 1997. Remote sensing aerosols using satellite infrared observations. Journal of Geophysical Research: Atmospheres, 102(D14), pp.17069-17079.

AERONET, 2016a. AERONER Site. http://aeronet.gsfc.nasa.gov/cgi-bin/type_piece_of_map_opera_v2_new?long1=-180&long2=180&lat1=-90&lat2=90&multiplier=2&what_map=4&nachal=1&formatter=0&level=3&place_code=10&place_limit=0. Accessed 20 March, 2016.

AERONET, 2016b. CIMEL Sunphotometer. http://aeronet.gsfc.nasa.gov/new_web/system_descriptions.html. Accessed 20 March, 2016.

AirNow Network, 2016. Organizations. https://www.airnow.gov/index.cfm?action=airnow.international).2016. Accessed 20 March, 2016.

Anenberg, S.C., West, J.J., Fiore, A.M., Jaffe, D.A., Prather, M.J., Bergmann, D., Cuvelier, K., Dentener, F.J., Duncan, B.N., Gauss, M. and Hess, P., 2009. Intercontinental impacts of ozone pollution on human mortality. Environmental Science & Technology, 43(17), pp.6482-6487.

Ångström, A., 1964. The parameters of atmospheric turbidity. Tellus, 16(1), pp. 64-75.

Baccarelli, A., 2009. Breathe Deeply into Your Genes! Genetic Variants and Air Pollution Effects. American Journal of Respiratory and Critical Care Medicine, 179(6), pp.431-432.

B.C. Air Quality., n.d. New Provincial Ambient Air Quality Criteria for PM2.5. http://www.bcairquality.ca/regulatory/pm25-objective.html. Accessed 20 March 2016.

Bell, M.L., Davis, D.L. and Fletcher, T., 2004. A retrospective assessment of mortality from the London smog episode of 1952: the role of influenza and pollution. Environmental Health Perspectives, 112(1), pp.6.

Bell, M.L., Son, J.Y., Peng, R.D., Wang, Y. and Dominici, F., 2015. Brief Report: Ambient PM2. 5 and Risk of Hospital Admissions: Do Risks Differ for Men and Women? Epidemiology, 26(4), pp.575-579.

Beloconi, A., Kamarianakis, Y. and Chrysoulakis, N., 2016. Estimating urban PM10 and PM2.5 concentration, based on synergistic MERIS/AATSR aerosol observations, land cover and morphology data. Remote Sensing of Environment, 172, pp.148-164.

Benas, N., Beloconi, A. and Chrysoulakis, N., 2013. Estimation of urban PM10 concentration, based on MODIS and MERIS/AATSR synergistic observations. Atmospheric Environment, 79, pp. 448-454.

Benas, N., Chrysoulakis, N. and Giannakopoulou, G., 2013. Validation of MERIS/AATSR synergy algorithm for aerosol retrieval against globally distributed AERONET observations and comparison with MODIS aerosol product. Atmospheric Research, 132, pp.102-113.

Bevan, S.L., North, P.R., Los, S.O. and Grey, W.M., 2012. A global dataset of atmospheric aerosol optical depth and surface reflectance from AATSR. Remote Sensing of Environment, 116, pp.199-210.

Bilal, M., Nichol, J.E., Bleiweiss, M.P. and Dubois, D., 2013. A Simplified high resolution MODIS Aerosol Retrieval Algorithm (SARA) for use over mixed surfaces. Remote Sensing of Environment, 136, pp.135-145.

Bilal, M., Nichol, J.E. and Chan, P.W., 2014. Validation and accuracy assessment of a Simplified Aerosol Retrieval Algorithm (SARA) over Beijing under low and high aerosol loadings and dust storms. Remote Sensing of Environment, 153, pp.50-60.

Bibi, H., Alam, K., Chishtie, F., Bibi, S., Shahid, I. and Blaschke, T., 2015. Intercomparison of MODIS, MISR, OMI, and CALIPSO aerosol optical depth retrievals for four locations on the Indo-Gangetic plains and validation against AERONET data. Atmospheric Environment, 111, pp.113-126.

Bozdogan, H., 1987. Model selection and Akaike's information criterion (AIC): The general theory and its analytical extensions. Psychometrika, 52(3), pp.345-370.

Burnett, R.T., Pope III, C.A., Ezzati, M., Olives, C., Lim, S.S., Mehta, S., Shin, H.H., Singh, G., Hubbell, B., Brauer, M. and Anderson, H.R., 2014. An integrated risk function for estimating the global burden of disease attributable to ambient fine particulate matter exposure. Environmental Health Perspectives, 122(4), pp.397.

Cao, J., Chow, J.C., Lee, F.S. and Watson, J.G., 2013. Evolution of PM2. 5 measurements and standards in the US and future perspectives for China. Aerosol Air Quality Research, 13(4), pp.1197-1211.

Cao, J., Xu, H., Xu, Q., Chen, B. and Kan, H., 2012. Fine particulate matter constituents and cardiopulmonary mortality in a heavily polluted Chinese city. Environmental Health Perspectives, 120(3), pp.373.

Cao, J., Yang, C., Li, J., Chen, R., Chen, B., Gu, D. and Kan, H., 2011. Association between long-term exposure to outdoor air pollution and mortality in China: a cohort study. Journal of Hazardous Materials, 186(2), pp.1594-1600.

CCME., 2011. Ambient Air Monitoring Protocol for PM2.5 and Ozone Canada-wide Standards for Particulate Matter and Ozone. http://www.ccme.ca/files/Resources/air/pm_ozone/pm_oz_cws_monitoring_protocol_pn1456_e.pdf. Accessed 20 March, 2016.

CCME., n.d. Canadian Ambient Air Quality Standards (CAAQS). http://www.ccme.ca/en/current_priorities/air/caaqs.html. Accessed 20 March 2016.

Chameides, W.L., Yu, H., Liu, S.C., Bergin, M., Zhou, X., Mearns, L., Wang, G., Kiang, C.S., Saylor, R.D., Luo, C. and Huang, Y., 1999. Case study of the effects of atmospheric aerosols and regional haze on agriculture: An opportunity to enhance crop yields in China through emission controls. Proceedings of the National Academy of Sciences, 96(24), pp. 13626-13633.

Change, I.C., 2001. IPCC third assessment report. Cambridge and New York: Cambridge University Press. Volumes I (The Scientific Basis), II (Impacts, Adaptation, and Vulnerability) and III (Mitigation).

Chen, D., Wang, Y., McElroy, M.B., He, K., Yantosca, R.M. and Sager, P.L., 2009. Regional CO pollution and export in China simulated by the high-resolution nested-grid GEOS-Chem model. Atmospheric Chemistry and Physics, 9(11), pp. 3825-3839.

Chen, J., Qiu, S., Shang, J., Wilfrid, O.M., Liu, X., Tian, H. and Boman, J., 2014. Impact of relative humidity and water soluble constituents of PM2. 5 on visibility impairment in Beijing, China. Aerosol Air Quality Research, 14, pp. 260-268.

China Meteorological Administration., 2015. Basic Introduction of Each Province. http://www.cma.gov.cn/. Accessed 20 March 2016.

China Statistical Yearbook., 2015. Statistic Data. http://www.stats.gov.cn/tjsj/ndsj/2015/indexeh.htm. Accessed 20 March 2016.

Chin, M., Ginoux, P., Kinne, S., Torres, O., Holben, B.N., Duncan, B.N., Martin, R.V., Logan, J.A., Higurashi, A. and Nakajima, T., 2002. Tropospheric aerosol optical thickness from the GOCART model and comparisons with satellite and Sun photometer measurements. Journal of the Atmospheric Sciences, 59(3), pp.461-483.

Choi, Y., Ghim, Y.S. and Holben, B.N., 2016. Identification of columnar aerosol types under high aerosol optical depth conditions for a single AERONET site in Korea. Journal of Geophysical Research: Atmospheres, 121, pp. 1264-1277.

Chow, J.C., 1995. Measurement methods to determine compliance with ambient air quality standards for suspended particles. Journal of the Air & Waste Management Association, 45(5), pp.320-382.

Chu, D.A., Kaufman, Y.J., Remer, L.A. and Holben, B.N., 1998. Remote sensing of smoke from MODIS airborne simulator during the SCAR-B experiment. Journal of Geophysical Research: Atmospheres, 103(D24), pp.31979-31987.

Chu, D. A., Kaufman, Y. J., Zibordi, G., Chern, J. D., Mao, J., Li, C., & Holben, B. N.,2003. Global monitoring of air pollution over land from the Earth Observing System-Terra Moderate Resolution Imaging Spectroradiometer (MODIS). Journal of Geophysical Research: Atmospheres, 108(D21).

Chu, D.A., Tsai, T.C., Chen, J.P., Chang, S.C., Jeng, Y.J., Chiang, W.L. and Lin, N.H., 2013. Interpreting aerosol lidar profiles to better estimate surface PM 2.5 for columnar AOD measurements. Atmospheric Environment, 79, pp.172-187.

Chudnovsky, A.A., Koutrakis, P., Kloog, I., Melly, S., Nordio, F., Lyapustin, A., Wang, Y. and Schwartz, J., 2014. Fine particulate matter predictions using high resolution Aerosol Optical Depth (AOD) retrievals. Atmospheric Environment, 89, pp.189-198.

Chung, Y.S., Kim, H.S., Dulam, J. and Harris, J., 2003. On heavy dustfall observed with explosive sandstorms in Chongwon-Chongju, Korea in 2002. Atmospheric Environment, 37(24), pp.3425-3433.

Cliff, A.D. and Ord, J.K., 1981. Spatial processes: models & applications, Vol. 44. London: Pion.

CMCC, 2014. Canada-wind standards for particulate matter and ozone (2012 final report). http://www.ccme.ca/files/Resources/air/pm_ozone/PN_1526_2012_CWS_for_PM_and_Ozone_Final_Report.pdf. Accessed 20 March 2016.

Corsini, E., Budello, S., Marabini, L., Galbiati, V., Piazzalunga, A., Barbieri, P., Cozzutto, S., Marinovich, M., Pitea, D. and Galli, C.L., 2013. Comparison of wood smoke PM2. 5 obtained from the combustion of FIR and beech pellets on inflammation and DNA damage in A549 and THP-1 human cell lines. Archives of Toxicology, 87(12), pp.2187-2199.

Crouse, D.L., Peters, P.A., van Donkelaar, A., Goldberg, M.S., Villeneuve, P.J., Brion, O., Khan, S., Atari, D.O., Jerrett, M., Pope III, C.A. and Brauer, M., 2012. Risk of nonaccidental and cardiovascular mortality in relation to long-term exposure to low concentrations of fine particulate matter: a Canadian national-level cohort study. Environmental Health Perspectives, 120(5), pp.708.

Deng, J., Wang, T., Jiang, Z., Xie, M., Zhang, R., Huang, X. and Zhu, J., 2011. Characterization of visibility and its affecting factors over Nanjing, China. Atmospheric Research, 101(3), pp. 681-691.

Di Nicolantonio, W., Cacciari, A., Bolzacchini, F., Ferrero, L., Volta, M. and Pisoni, E., 2007. MODIS aerosol optical properties over North Italy for estimating surface-level PM2. 5. In Proceedings of Envisat Symposium, pp. 3-27.

Dominici, F., Peng, R.D., Bell, M.L., Pham, L., McDermott, A., Zeger, S.L. and Samet, J.M., 2006. Fine particulate air pollution and hospital admission for cardiovascular and respiratory diseases. The Journal of the American Medical Association, 295(10), pp.1127-1134.

Donner, L., 2016. Aerosols, Clouds, and Precipitation as Scale Interactions in the Climate System and Controls on Climate Change. Bulletin of the American Physical Society, 10.1103/BAPS.2016.MARCH.F12.5

Duan, F.K., He, K.B., Ma, Y.L., Yang, F.M., Yu, X.C., Cadle, S.H., Chan, T. and Mulawa, P.A., 2006. Concentration and chemical characteristics of PM 2.5 in Beijing, China: 2001–2002. Science of the Total Environment, 355(1), pp.264-275.

Durkee, P.A., Jensen, D.R., Hindman, E.E. and Haar, T.H., 1986. The relationship between marine aerosol particles and satellite-detected radiance. Journal of Geophysical Research: Atmospheres, 91(D3), pp. 4063-4072.

Eck, T.F., Holben, B.N., Dubovik, O., Smirnov, A., Goloub, P., Chen, H.B., Chatenet, B., Gomes, L., Zhang, X.Y., Tsay, S.C. and Ji, Q., 2005. Columnar aerosol optical properties at AERONET sites in central eastern Asia and aerosol transport to the tropical mid-Pacific. Journal of Geophysical Research: Atmospheres, 110(D6), pp. 1-18.

Eck, T.F., Holben, B.N., Sinyuk, A., Pinker, R.T., Goloub, P., Chen, H., Chatenet, B., Li, Z., Singh, R.P., Tripathi, S.N. and Reid, J.S., 2010. Climatological aspects of the optical properties of fine/coarse mode aerosol mixtures. Journal of Geophysical Research: Atmospheres, 115(D19), pp. 1-15

Emili, E., Popp, C., Petitta, M., Riffler, M., Wunderle, S. and Zebisch, M., 2010. PM 10 remote sensing from geostationary SEVIRI and polar-orbiting MODIS sensors over the complex terrain of the European Alpine region. Remote Sensing of Environment, 114(11), pp.2485-2499.

Engel-Cox, J.A., Holloman, C.H., Coutant, B.W. and Hoff, R.M., 2004. Qualitative and quantitative evaluation of MODIS satellite sensor data for regional and urban scale air quality. Atmospheric Environment, 38(16), pp. 2495-2509.

EPA., 2013. National Ambient Air Quality Standards (NAAQS) (78 FR 3086). http://kjs.mep.gov.cn/hjbhbz/bzwb/dqhjbh/dqhjzlbz/201203/t20120302_224165.htm Accessed 20 March 2016.

EPA., n.d. PM 2.5 Objectives and History. http://archive.epa.gov/pesticides/region4/sesd/pm25/web/html/p2.html#3. Accessed 20 March 2016.

Forouzanfar, M.H., Alexander, L., Anderson, H.R., Bachman, V.F., Biryukov, S., Brauer, M., Burnett, R., Casey, D., Coates, M.M., Cohen, A. and Delwiche, K., 2015. Global, regional, and national comparative risk assessment of 79 behavioural, environmental and occupational, and metabolic risks or clusters of risks in 188 countries, 1990–2013: a systematic analysis for the Global Burden of Disease Study 2013. The Lancet, 386(10010), pp. 2287-2323.

Fotheringham, A.S., Brunsdon, C. and Charlton, M., 2003. Geographically weighted regression: the analysis of spatially varying relationships. John Wiley & Sons, pp. 158.

Franklin, M., Koutrakis, P. and Schwartz, J., 2008. The role of particle composition on the association between PM2. 5 and mortality. Epidemiology (Cambridge, Mass.), 19(5), pp. 680.

Franklin, M., Zeka, A. and Schwartz, J., 2007. Association between PM2. 5 and all-cause and specific-cause mortality in 27 US communities. Journal of Exposure Science and Environmental Epidemiology, 17(3), pp. 279-287.

Fry, J.S., Lee, P.N., Forey, B.A. and Coombs, K.J., 2013. How rapidly does the excess risk of lung cancer decline following quitting smoking? A quantitative review using the negative exponential model. Regulatory Toxicology and Pharmacology, 67(1), pp.13-26.

Gamble, J.F., 1998. PM2. 5 and mortality in long-term prospective cohort studies: cause-effect or statistical associations. Environmental Health Perspectives, 106(9), pp.535.

Gao, M., Guttikunda, S.K., Carmichael, G.R., Wang, Y., Liu, Z., Stanier, C.O., Saide, P.E. and Yu, M., 2015. Health impacts and economic losses assessment of the 2013 severe haze event in Beijing area. Science of the Total Environment, 511, pp.553-561.

George, J.P., Harenduprakash, L. and Mohan, M., 2008, February. Multi year changes of Aerosol Optical Depth in the monsoon region of the Indian Ocean since 1986 as seen in the AVHRR and TOMS data. In Annales Geophysicae, 26 (1), pp. 7-11.

Ginoux, P., Chin, M., Tegen, I., Prospero, J.M., Holben, B., Dubovik, O. and Lin, S.J., 2001. Sources and distributions of dust aerosols simulated with the GOCART model. Journal of Geophysical Research: Atmospheres, 106(D17), pp. 20255-20273.

Ginoux, P., Prospero, J.M., Gill, T.E., Hsu, N.C. and Zhao, M., 2012. Global-scale attribution of anthropogenic and natural dust sources and their emission rates based on MODIS Deep Blue aerosol products. Reviews of Geophysics, 50(3), pp.23-40.

Guo, J.P., Wu, Y.R., Zhang, X.Y. and Li, X.W., 2013. Estimation of PM2. 5 over eastern China from MODIS aerosol optical depth using the back propagation neural network. Environmental Science, 34(3), pp.817-825.

Guo,Yuling., Li-hua, X., Fang, W. and Jing, H., 2009, May. The progress and prospect of remote sensing for aerosol optical depth. Urban Remote Sensing Event, 2009, pp. 1-6.

Gupta, P., Christopher, S.A., Wang, J., Gehrig, R., Lee, Y.C. and Kumar, N., 2006. Satellite remote sensing of particulate matter and air quality assessment over global cities. Atmospheric Environment, 40(30), pp.5880-5892.

Gupta, P. and Christopher, S.A., 2009a. Particulate matter air quality assessment using integrated surface, satellite, and meteorological products: Multiple regression approach. Journal of Geophysical Research: Atmospheres, 114(D14).

Gupta, P. and Christopher, S.A., 2009b. Particulate matter air quality assessment using integrated surface, satellite, and meteorological products: 2. A neural network approach. Journal of Geophysical Research: Atmospheres, 114(D20).

Hadjimitsis, D.G., 2009. Aerosol optical thickness (AOT) retrieval over land using satellite image-based algorithm. Air Quality, Atmosphere & Health, 2(2), pp. 89-97.

Holben, B.N., Eck, T.F., Slutsker, I., Tanre, D., Buis, J.P., Setzer, A., Vermote, E., Reagan, J.A., Kaufman, Y.J., Nakajima, T. and Lavenu, F., 1998. AERONET—A federated instrument network and data archive for aerosol characterization. Remote Sensing of Environment, 66(1), pp. 1-16.

Holben, B.N., Tanre, D., Smirnov, A., Eck, T.F., Slutsker, I., Abuhassan, N., Newcomb, W.W., Schafer, J.S., Chatenet, B., Lavenu, F. and Kaufman, Y.J., 2001. An emerging ground-based aerosol climatology: Aerosol optical depth from AERONET. Journal of Geophysical Research: Atmospheres, 106(D11), pp. 12067-12097.

Hsu, N.C., Tsay, S.C., King, M.D. and Herman, J.R., 2004. Aerosol properties over bright-reflecting source regions. IEEE Transactions on Geoscience and Remote Sensing, 42(3), pp. 557-569.

Hu, X., Waller, L.A., Al-Hamdan, M.Z., Crosson, W.L., Estes, M.G., Estes, S.M., Quattrochi, D.A., Sarnat, J.A. and Liu, Y., 2013. Estimating ground-level PM 2.5 concentrations in the southeastern US using geographically weighted regression. Environmental Research, 121, pp.1-10.

Hu, X.M., Ma, Z., Lin, W., Zhang, H., Hu, J., Wang, Y., Xu, X., Fuentes, J.D. and Xue, M., 2014. Impact of the Loess Plateau on the atmospheric boundary layer structure and air quality in the North China Plain: A case study. Science of The Total Environment, 499, pp.228-237.

Hu, Z., 2009. Spatial analysis of MODIS aerosol optical depth, PM 2.5, and chronic coronary heart disease. International Journal of Health Geographics, 8(1), pp. 11-20.

Huang, W., Cao, J., Tao, Y., Dai, L., Lu, S.E., Hou, B., Wang, Z. and Zhu, T., 2012. Seasonal variation of chemical species associated with short-term mortality effects of PM2. 5 in Xi'an, a central city in China. American Journal of Epidemiology, pp. 342.

Irwig, L., Irwig, J., Trevena, L. and Sweet, M., 2008. Relative risk, relative and absolute risk reduction, number needed to treat and confidence intervals, pp.138.

Jones, B.E., VanDerslice, J., Jephson, A., Dean, N.C. and Pirozzi, C.S., 2015. Short-Term Effects of Particulate Air Pollution Exposure On Incidence And Severity Of Pneumonia. Am J Respir Crit Care Med, 191, pp. 5250.

Just, A.C., Wright, R.O., Schwartz, J., Coull, B.A., Baccarelli, A.A., Tellez-Rojo, M.M., Moody, E., Wang, Y., Lyapustin, A. and Kloog, I., 2015. Using high-resolution satellite aerosol optical depth to estimate daily PM2. 5 geographical distribution in Mexico City. Environmental Science & Technology, 49(14), pp.8576-8584.

Kahn, R.A., Gaitley, B.J., Martonchik, J.V., Diner, D.J., Crean, K.A. and Holben, B., 2005. Multiangle Imaging Spectroradiometer (MISR) global aerosol optical depth validation based on 2 years of coincident Aerosol Robotic Network (AERONET) observations. Journal of Geophysical Research: Atmospheres, 110(D10).

Kan, H., Chen, R. and Tong, S., 2012. Ambient air pollution, climate change, and population health in China. Environment International, 42, pp.10-19.

Kaufman, Y.J. and Sendra, C., 1988. Algorithm for automatic atmospheric corrections to visible and near-IR satellite imagery. International Journal of Remote Sensing, 9(8), pp.1357-1381.

Keuken, M.P., Moerman, M., Voogt, M., Blom, M., Weijers, E.P., Röckmann, T. and Dusek, U., 2013. Source contributions to PM 2.5 and PM 10 at an urban background and a street location. Atmospheric Environment, 71, pp.26-35.

Kioumourtzoglou, M.A., Schwartz, J.D., Weisskopf, M.G., Melly, S.J., Wang, Y., Dominici, F. and Zanobetti, A., 2016. Long-term PM2. 5 exposure and neurological hospital admissions in the Northeastern United States. Environmental Health Perspectives, 124(1), pp.23.

Kloog, I., Nordio, F., Coull, B.A. and Schwartz, J., 2012. Incorporating local land use regression and satellite aerosol optical depth in a hybrid model of spatiotemporal PM2. 5 exposures in the Mid-Atlantic states. Environmental Science & Technology, 46(21), pp.11913-11921.

Koelemeijer, R.B.A., Homan, C.D. and Matthijsen, J., 2006. Comparison of spatial and temporal variations of aerosol optical thickness and particulate matter over Europe. Atmospheric Environment, 40(27), pp.5304-5315.

Kumar, N., Chu, A. and Foster, A., 2007. An empirical relationship between PM 2.5 and aerosol optical depth in Delhi Metropolitan. Atmospheric Environment, 41(21), pp.4492-4503.

Laden, F., Neas, L.M., Dockery, D.W. and Schwartz, J., 2000. Association of fine particulate matter from different sources with daily mortality in six US cities. Environmental Health Perspectives, 108(10), pp.941.

Lang, J.L., Cheng, S.Y., Li, J.B., Chen, D.S., Zhou, Y., Wei, X., Han, L.H. and Wang, H.Y., 2013. A monitoring and modeling study to investigate regional transport and characteristics of PM2. 5 pollution. Aerosol Air Quality Research, 13(3), pp. 943-956.

Lee, H., Honda, Y., Hashizume, M., Guo, Y.L., Wu, C.F., Kan, H., Jung, K., Lim, Y.H., Yi, S. and Kim, H., 2015. Short-term exposure to fine and coarse particles and mortality: A multicity time-series study in East Asia. Environmental Pollution, 207, pp. 43-51.

Lee, H.J., Coull, B.A., Bell, M.L. and Koutrakis, P., 2012. Use of satellite-based aerosol optical depth and spatial clustering to predict ambient PM 2.5 concentrations. Environmental Research, 118, pp. 8-15.

Lei, Y., Wei, R., Wang, S., Wang, Y., Du, L. and Shen, H., 2015. Factor Analysis of Mass Concentration Characterization of PM2. 5 and its Impact Factors in a Suburban Roadside: Taking a National Road of Zhengzhou, China as an Example. Nature Environment and Pollution Technology, 14(2), pp. 409.

Leigh, M., Robert, L., Shana, M., Lorraine R., 2014. MODIS Atmosphere Team Webinar Series #5: Overview of the 3 km aerosol product in Collection 6. http://modis-atmos.gsfc.nasa.gov/products_C006update.html. Accessed 20 March 2016.

Leroy, M., Deuze, J.L., Bréon, F.M., Hautecoeur, O., Herman, M., Buriez, J.C., Tanré, D., Bouffies, S., Chazette, P. and Roujean, J.L., 1997. Retrieval of atmospheric properties and surface bidirectional reflectances over land from POLDER/ADEOS. Journal of Geophysical Research: Atmospheres, 102(D14), pp. 17023-17037.

Levin, Z. and Cotton, W.R. eds., 2008. Aerosol pollution impact on precipitation: a scientific review. Springer Science & Business Media, pp. 55.

Li, B. and Hou, L., 2015. Discuss on Satellite-Based Particulate Matter Monitoring Technique. The ISPRS Archives, 40(7), pp. 219.

Li, C., Hsu, N.C. and Tsay, S.C., 2011. A study on the potential applications of satellite data in air quality monitoring and forecasting. Atmospheric Environment, 45(22), pp. 3663-3675.

Li, C., Lau, A.K.H., Mao, J. and Chu, D.A., 2005. Retrieval, validation, and application of the 1-km aerosol optical depth from MODIS measurements over Hong Kong. IEEE Transactions on Geoscience and Remote Sensing, 43(11), pp. 2650-2658.

Li, Y., Xue, Y., de Leeuw, G., Li, C., Yang, L., Hou, T. and Marir, F., 2013. Retrieval of aerosol optical depth and surface reflectance over land from NOAA AVHRR data. Remote Sensing of Environment, 133, pp.1-20.

Li, Q. and Wang, J., 2015. Aerosol Retrieval Using Remote Sensing Data over Jing-Jin-Ji Area with SARA Algorithm. Scientific Journal of Earth Science, 5(3).

Lim, S.S., Vos, T., Flaxman, A.D., Danaei, G., Shibuya, K., Adair-Rohani, H., AlMazroa, M.A., Amann, M., Anderson, H.R., Andrews, K.G. and Aryee, M., 2013. A comparative risk assessment of burden of disease and injury attributable to 67 risk factors and risk factor clusters in 21 regions, 1990–2010: a systematic analysis for the Global Burden of Disease Study 2010. The Lancet, 380(9859), pp.2224-2260.

Lin, C., Li, Y., Yuan, Z., Lau, A.K., Li, C. and Fung, J.C., 2015. Using satellite remote sensing data to estimate the high-resolution distribution of ground-level PM 2.5. Remote Sensing of Environment, 156, pp.117-128.

Lin, G., Fu, J., Jiang, D., Hu, W., Dong, D., Huang, Y. and Zhao, M., 2013. Spatio-temporal variation of PM2. 5 concentrations and their relationship with geographic and socioeconomic factors in China. International Journal of Environmental Research and Public Health, 11(1), pp.173-186.

Liu, Y., He, K., Li, S., Wang, Z., Christiani, D.C. and Koutrakis, P., 2012. A statistical model to evaluate the effectiveness of PM 2.5 emissions control during the Beijing 2008 Olympic Games. Environment International, 44, pp.100-105.

Liu, Y.J., Zhang, T.T., Liu, Q.Y., Zhang, R.J., Sun, Z.Q. and Zhang, M.G., 2014. Seasonal variation of physical and chemical properties in TSP, PM10 and PM2. 5 at a roadside site in Beijing and their influence on atmospheric visibility. Aerosol Air Quality Research, 14(3), pp.954-969.

Liu, Y., Paciorek, C.J. and Koutrakis, P., 2009. Estimating Regional Spatial and Temporal Variability of PM^ sub 2.5^ Concentrations Using Satellite Data, Meteorology, and Land Use Information. Environmental Health Perspectives, 117(6), pp.886.

Liu, Y., Park, R.J., Jacob, D.J., Li, Q., Kilaru, V. and Sarnat, J.A., 2004. Mapping annual mean ground-level PM2. 5 concentrations using Multiangle Imaging Spectroradiometer aerosol optical thickness over the contiguous United States. Journal of Geophysical Research: Atmospheres, 109(D22).

Liu, Y., Sarnat, J.A., Kilaru, V., Jacob, D.J. and Koutrakis, P., 2005. Estimating ground-level PM2. 5 in the eastern United States using satellite remote sensing. Environmental Science & Technology, 39(9), pp.3269-3278.

Liu, Y., Wang, Z., Wang, J., Ferrare, R.A., Newsom, R.K. and Welton, E.J., 2011. The effect of aerosol vertical profiles on satellite-estimated surface particle sulfate concentrations. Remote Sensing of Environment, 115(2), pp.508-513.

Lu, F., Xu, D., Cheng, Y., Dong, S., Guo, C., Jiang, X. and Zheng, X., 2015. Systematic review and meta-analysis of the adverse health effects of ambient PM 2.5 and PM 10 pollution in the Chinese population. Environmental Research, 136, pp.196-204.

Lyapustin, A., Wang, Y., Laszlo, I., Kahn, R., Korkin, S., Remer, L., Levy, R. and Reid, J.S., 2011. Multiangle implementation of atmospheric correction (MAIAC): 2. Aerosol algorithm. Journal of Geophysical Research: Atmospheres, 116(D3).

Ma, W., Wang, L., Lin, H., Liu, T., Zhang, Y., Rutherford, S., Luo, Y., Zeng, W., Zhang, Y., Wang, X. and Gu, X., 2015. The temperature–mortality relationship in China: An analysis from 66 Chinese communities. Environmental research, 137, pp.72-77.

Ma, Z., Hu, X., Huang, L., Bi, J. and Liu, Y., 2014. Estimating ground-level PM2. 5 in China using satellite remote sensing. Environmental Science & Technology, 48(13), pp.7436-7444.

MAP., 2012. Ambient Air Quality Standards. http://hbj.new.cqcs.gov.cn/upfiles/2013-3/2013327153015207.pdf. Accessed 20 March 2016.

Marcazzan, G.M., Vaccaro, S., Valli, G. and Vecchi, R., 2001. Characterisation of PM10 and PM2. 5 particulate matter in the ambient air of Milan (Italy). Atmospheric Environment, 35(27), pp. 4639-4650.

Matus, K., Nam, K.M., Selin, N.E., Lamsal, L.N., Reilly, J.M. and Paltsev, S., 2012. Health damages from air pollution in China. Global Environmental Change, 22(1), pp. 55-66.

McArthur, L.J., Halliwell, D.H., Niebergall, O.J., O'Neill, N.T., Slusser, J.R. and Wehrli, C., 2003. Field comparison of network Sun photometers. Journal of Geophysical Research: Atmospheres, 108(D19).

Mei, L., Xue, Y., Kokhanovsky, A.A., von Hoyningen-Huene, W., de Leeuw, G. and Burrows, J.P., 2013. Retrieval of aerosol optical depth over land surfaces from AVHRR data. Atmospheric Measurement Techniques Discussions, 6(1), pp.2227-2251.

Mélin, F., Clerici, M., Zibordi, G., Holben, B.N. and Smirnov, A., 2010. Validation of SeaWiFS and MODIS aerosol products with globally distributed AERONET data. Remote Sensing of Environment, 114(2), pp.230-250.

Meng, X., Fu, Q., Ma, Z., Chen, L., Zou, B., Zhang, Y., Xue, W., Wang, J., Wang, D., Kan, H. and Liu, Y., 2016. Estimating ground-level PM 10 in a Chinese city by combining satellite data, meteorological information and a land use regression model. Environmental Pollution, 208, pp.177-184.

MEPCN., 2011. Determination of atmospheric articles PM10 and PM2.5 in ambient air by gravimetric method (HJ 618-2011). http://kjs.mep.gov.cn/hjbhbz/bzwb/dqhjbh/jcgfffbz/201109/t20110914_217272.htm. Accessed 20 March 2016.

Miao, Y., Liu, S., Zheng, Y., Wang, S., Liu, Z., & Zhang, B., 2015. Numerical study of the effects of Planetary Boundary Layer structure on the pollutant dispersion within built-up areas. Journal of Environmental Sciences, 32, pp.168-179.

MOE., 2005. Transboundary air pollution in Ontario, Ontario Ministry of the Environment, http://www.ene.gov.on.ca/stdprodconsume/groups/lr/@ene/@resources/documents/resource/std01_079137. Pdf. Accessed 6 September 2015.

Munchak, L.A., Levy, R.C. and Mattoo, S., 2014. Comparison of C5 and C6 Aqua-MODIS dark target aerosol validation, http://ntrs.nasa.gov/search.jsp?R=20140012665, Accessed 6 September 2015.

Nakaya, T., 2014. GWR User Manual. https://geodacenter.asu.edu/drupal_files/gwr/GWR4manual.pdf. Accessed 20 March 2016.

NASA., n,d.a. AERONET OVERVIW. http://aeronet.gsfc.nasa.gov/new_web/system_descriptions.html. Accessed 20 March 2016.

NASA., n.d.b. MISR Introduction. https://www-misr.jpl.nasa.gov/index.cfmhttps://www-misr.jpl.nasa.gov/index.cfm. Accessed 20 March 2016.

NASA., n.d.c. Dark Target. http://darktarget.gsfc.nasa.gov/products/land-10. Accessed 20 March, 2016.

NASA, 2000. Aerosol Optical Depth: Global Maps. http://earthobservatory.nasa.gov/GlobalMaps/view.php?d1=MODAL2_M_AER_OD. Accessed 20 March 2016.

NASA., 2016. MODIS Specifications. http://modis.gsfc.nasa.gov/about/specifications.php. Accessed 20 March 2016.

Nawahda, A., Yamashita, K., Ohara, T., Kurokawa, J. and Yamaji, K., 2012. Evaluation of premature mortality caused by exposure to PM2. 5 and ozone in East Asia: 2000, 2005, 2020. Water, Air, & Soil Pollution, 223(6), pp.3445-3459.

NOAA., n.d. ESRL Global Monitoring Division - GRAD - Surface Radiation Budget Network (SURFRAD). http://www.esrl.noaa.gov/gmd/grad/surfrad/aod/. Accessed 20 March 2016.

North, P., Brockmann, C., Fischer, J., Gomez-Chova, L., Grey, W., Heckel, A., Moreno, J., Preusker, R. and Regner, P., 2008, September. MERIS/AATSR synergy algorithms for cloud screening, aerosol retrieval and atmospheric correction. In Proc. 2nd MERIS/AATSR User Workshop, ESRIN, Frascati pp. 22-26.

Ontrario MECC., n.d. Fine Particulate Matter. http://www.airqualityontario.com/science/pollutants/particulates.php. Accessed 20 March 2016.

Okazaki, S., Sakaguchi, M., Miwa, K., Furukado, S., Yamagami, H., Yagita, Y., Mochizuki, H. and Kitagawa, K., 2014. Association of interleukin-6 with the progression of carotid atherosclerosis a 9-year follow-up study. Stroke, 45(10), pp.2924-2929.

Paciorek, C.J. and Liu, Y., 2008a. Limitations of remotely-sensed aerosol as a spatial proxy for fine particulate matter. Harvard University Biostatistics Working Paper Series, Year 2008, pp. 89.

Paciorek, C.J., Liu, Y., Moreno-Macias, H. and Kondragunta, S., 2008b. Spatiotemporal associations between GOES aerosol optical depth retrievals and ground-level PM2. 5. Environmental Science & Technology, 42(15), pp.5800-5806.

Park, S.S., Kim, Y.J., Cho, S.Y. and Kim, S.J., 2007. Characterization of PM2. 5 aerosols dominated by local pollution and Asian dust observed at an urban site in Korea during aerosol characterization experiments (ACE)–Asia Project. Journal of the Air & Waste Management Association, 57(4), pp.434-443.

Pope 3rd, C.A., 2000. Epidemiology of fine particulate air pollution and human health: biologic mechanisms and who's at risk?. Environmental Health Perspectives, 108(Suppl 4), pp.713.

Pope III, C.A., Burnett, R.T., Thun, M.J., Calle, E.E., Krewski, D., Ito, K. and Thurston, G.D., 2002. Lung cancer, cardiopulmonary mortality, and long-term exposure to fine particulate air pollution. Jama, 287(9), pp.1132-1141.

Quaas, J., & Boucher, O, 2005. Constraining the first aerosol indirect radiative forcing in the LMDZ GCM using POLDER and MODIS satellite data. Geophysical Research Letters, 32(17).

Queensland Government., 2016. Tapered element oscillating microbalance. https://www.qld.gov.au/environment/pollution/monitoring/air-pollution/oscillating-microbalance/. Accessed 20 March, 2016.

Remer, L.A., Mattoo, S., Levy, R.C. and Munchak, L., 2013. MODIS 3km aerosol product: algorithm and global perspective. Atmospheric Measurement Techniques Discussions (AMTD), 6; pp. 69-112

Roberts, G., Mauger, G., Hadley, O. and Ramanathan, V., 2006. North American and Asian aerosols over the eastern Pacific Ocean and their role in regulating cloud condensation nuclei. Journal of Geophysical Research: Atmospheres, 111(D13).

Ryan, P.H. and LeMasters, G.K., 2007. A review of land-use regression models for characterizing intraurban air pollution exposure. Inhalation Toxicology, 19(sup1), pp. 127-133.

Saide, P.E., Carmichael, G.R., Spak, S.N., Gallardo, L., Osses, A.E., Mena-Carrasco, M.A. and Pagowski, M., 2011. Forecasting urban PM10 and PM2. 5 pollution episodes in very stable nocturnal conditions and complex terrain using WRF–Chem CO tracer model. Atmospheric Environment, 45(16), pp. 2769-2780.

San José, R., Pérez, J.L., Morant, J.L. and González, R.M., 2008. Elevated PM10 and PM2. 5 concentrations in Europe: a model experiment with MM5-CMAQ and WRF/CHEM. WIT Transactions on Ecology and the Environment, 116(1), pp. 3-12.

Sano, I., Mukai, S., Yamano, M., Takamura, T., Nakajima, T. and Holben, B., 2003. Calibration and validation of retrieved aerosol properties based on AERONET and SKYNET. Advances in Space Research, 32(11), pp. 2159-2164.

Sayer, A.M., Hsu, N.C., Bettenhausen, C. and Jeong, M.J., 2013. Validation and uncertainty estimates for MODIS Collection 6 “Deep Blue” aerosol data. Journal of Geophysical Research: Atmospheres, 118(14), pp. 7864-7872.

Schwartz, S.E., Arnold, F., Blanchet, J.P., Durkee, P.A., Hofmann, D.J., Hoppel, W.A., King, M.D., Lacis, A.A., Nakajima, T., Ogren, J.A. and Toon, O.B., 1995. Group report: Connections between aerosol properties and forcing of climate. Aerosol Forcing of Climate, pp. 251-280.

Shi, L., Zanobetti, A., Kloog, I., Coull, B.A., Koutrakis, P., Melly, S.J. and Schwartz, J.D., 2016. Low-concentration PM2. 5 and mortality: Estimating acute and chronic effects in a population-based study. Environmental Health Perspectives, 124(1), pp. 46.

Slutsker, I. and Kinne, S., 1999. Wavelength dependence of the optical depth of biomass burning, urban, and desert dust aerosols. J Geophysical Research, 104(3133331349), pp. 93-105.

SKYNET., 2016. SKYNET/skyradiometer site map. http://atmos2.cr.chiba-u.jp/skynet/. Accessed 20 March 2016.

Sokolik, I.N. and Toon, O.B., 1996. Direct radiative forcing by anthropogenic airborne mineral aerosols. Nature, 381(6584), pp. 681-683.

Sørensen, M., Autrup, H., Hertel, O., Wallin, H., Knudsen, L.E. and Loft, S., 2003. Personal exposure to PM2.5 and biomarkers of DNA damage. Cancer Epidemiology Biomarkers & Prevention, 12(3), pp. 191-196.

Steenland, K. and Armstrong, B., 2006. An overview of methods for calculating the burden of disease due to specific risk factors. Epidemiology, 17(5), pp. 512-519.

Sun, L., Sun, C., Liu, Q. and Zhong, B., 2010. Aerosol optical depth retrieval by HJ-1/CCD supported by MODIS surface reflectance data. Science China Earth Sciences, 53(1), pp. 74-80.

Sun, L., Wei, J., Bilal, M., Tian, X., Jia, C., Guo, Y. and Mi, X., 2015. Aerosol Optical Depth Retrieval over Bright Areas Using Landsat 8 OLI Images. Remote Sensing, 8(1), pp. 23.

Sun, Y., Zhuang, G., Wang, Y., Zhao, X., Li, J., Wang, Z. and An, Z., 2005. Chemical composition of dust storms in Beijing and implications for the mixing of mineral aerosol with pollution aerosol on the pathway. Journal of Geophysical Research: Atmospheres, 110(D24).

Retalis, A., Paronis, D. and Katsanos, D., 2015, October. Intercomparison between MODIS 3km aerosol optical depth product and ground PM10 measurements over Athens-Greece. In SPIE Remote Sensing, pp. 96400.

Tai, A.P., Mickley, L.J. and Jacob, D.J., 2010. Correlations between fine particulate matter (PM 2.5) and meteorological variables in the United States: Implications for the sensitivity of PM 2.5 to climate change. Atmospheric Environment, 44(32), pp. 3976-3984.

Tanré, D., Devaux, C., Herman, M., Santer, R. and Gac, J.Y., 1988. Radiative properties of desert aerosols by optical ground-based measurements at solar wavelengths. Journal of Geophysical Research: Atmospheres, 93(D11), pp. 14223-14231.

Tanré, D. and Legrand, M., 1991. On the satellite retrieval of Saharan dust optical thickness over land: Two different approaches. Journal of Geophysical Research: Atmospheres, 96(D3), pp. 5221-5227.

Tao, M., Chen, L., Wang, Z., Tao, J., Che, H., Wang, X. and Wang, Y., 2015. Comparison and evaluation of the MODIS Collection 6 aerosol data in China. Journal of Geophysical Research: Atmospheres, 120(14), pp. 6992-7005.

Tao, J., Zhang, M., Chen, L., Wang, Z., Su, L., Ge, C., Han, X. and Zou, M., 2013. A method to estimate concentrations of surface-level particulate matter using satellite-based aerosol optical thickness. Science China Earth Sciences, 56(8), pp. 1422-1433.

The Central People's Government of the People's Republic of China., 2016. Province Introduction. http://www.gov.cn/. Accessed 20 March 2016.

The World Bank., 2009. Air Pollution in Ulaanbaatar Initial Assessment of Current Situation and Effects of Abatement Measures. http://documents.worldbank.org/curated/en/2009/12/11817540/mongolia-air-pollution-ulaanbaatar-initial-assessment-current-situation-effects-abatement-measures. Accessed 20 March 2016.

Thomas, G.E., Carboni, E., Sayer, A.M., Poulsen, C.A., Siddans, R. and Grainger, R.G., 2009. Oxford-RAL Aerosol and Cloud (ORAC): Aerosol retrievals from satellite radiometers. Satellite Aerosol Remote Sensing Over Land, pp. 193-225.

Thurston, G.D., Ahn, J., Cromar, K.R., Shao, Y., Reynolds, H.R., Jerrett, M., Lim, C.C., Shanley, R., Park, Y. and Hayes, R.B., 2015. Ambient Particulate Matter Air Pollution Exposure and Mortality in the NIH-AARP Diet and Health Cohort. Environmental Health Perspectives. DOI: 10.1289/ehp.1509676

Tie, X., Madronich, S., Li, G., Ying, Z., Zhang, R., Garcia, A.R., Lee-Taylor, J. and Liu, Y., 2007. Characterizations of chemical oxidants in Mexico City: A regional chemical dynamical model (WRF-Chem) study. Atmospheric Environment, 41(9), pp. 1989-2008.

Torres, O., Bhartia, P.K., Herman, J.R., Sinyuk, A., Ginoux, P. and Holben, B., 2002. A long-term record of aerosol optical depth from TOMS observations and comparison to AERONET measurements. Journal of the Atmospheric Sciences, 59(3), pp. 398-413.

United Nations., 2015. Population Division. http://esa.un.org/unpd/wpp/. Accessed 20 March, 2016.

US EPA., 2006. Technical Guidance for Tribes on Air Monitoring Issues. http://www3.epa.gov/air/tribal/tam.html. Accessed 20 March 2016.

Vachon, F., Royer, A., Aube, M., Toubbe, B., O'Neill, N.T. and Teillet, P.M., 2004. Remote sensing of aerosols over North American land surfaces from POLDER and MODIS measurements. Atmospheric Environment, 38(21), pp. 3501-3515.

Van Donkelaar, A., Martin, R.V. and Park, R.J., 2006. Estimating ground-level PM2. 5 using aerosol optical depth determined from satellite remote sensing. Journal of Geophysical Research: Atmospheres, 111(D21).

Van Donkelaar, A., Martin, R.V., Brauer, M., Kahn, R., Levy, R., Verduzco, C. and Villeneuve, P.J., 2010. Global estimates of ambient fine particulate matter concentrations from satellite-based aerosol optical depth: development and application. Environmental Health Perspectives, 118(6), pp.847.

Van Donkelaar, A., Martin, R.V., Brauer, M. and Boys, B.L., 2015a. Use of satellite observations for long-term exposure assessment of global concentrations of fine particulate matter. Environmental Health Perspectives, 123(2), pp.135.

Van Donkelaar, A., Martin, R.V., Spurr, R.J. and Burnett, R.T., 2015b. High-resolution satellite-derived PM2. 5 from optimal estimation and geographically weighted regression over North America. Environmental Science & Technology, 49(17), pp. 10482-10491.

Vermote, E.F., Tanré, D., Deuzé, J.L., Herman, M. and Morcette, J.J., 1997. Second simulation of the satellite signal in the solar spectrum, 6S: An overview. EEE Transactions on Geoscience and Remote Sensing, I, 35(3), pp. 675-686.

Wang, J., Li, X., Zhang, W., Jiang, N., Zhang, R. and Tang, X., 2016. Secondary PM 2.5 in Zhengzhou, China: Chemical Species Based on Three Years of Observations. Aerosol and Air Quality Research, 16, pp.91-104.

Wang, J., Wang, S., Voorhees, A.S., Zhao, B., Jang, C., Jiang, J., Fu, J.S., Ding, D., Zhu, Y. and Hao, J., 2015a. Assessment of short-term PM 2.5-related mortality due to different emission sources in the Yangtze River Delta, China. Atmospheric Environment, 123, pp.440-448.

Wang, J., Zhu, C., & Zhu, Y., 2015b. Estimating the POLDER sensitivity to aerosol size using PARASOL observations. Remote Sensing Letters, 6(1), pp. 88-96.

Wang, Q., Ni, J. and Tenhunen, J., 2005. Application of a geographically-weighted regression analysis to estimate net primary production of Chinese forest ecosystems. Global Ecology and Biogeography, 14(4), pp. 379-393.

Watson, J.G., 2002. Visibility: Science and regulation. Journal of the Air & Waste Management Association, 52(6), pp. 628-713.

Wellenius, G.A., Bateson, T.F., Mittleman, M.A. and Schwartz, J., 2005. Particulate air pollution and the rate of hospitalization for congestive heart failure among medicare beneficiaries in Pittsburgh, Pennsylvania. American Journal of Epidemiology, 161(11), pp. 1030-1036.

WHO. Regional Office for Europe and World Health Organization, 2006. Air quality guidelines: global update 2005: particulate matter, ozone, nitrogen dioxide, and sulfur dioxide. World Health Organization, pp. 13-123.

WHO., 2015. WHO Expert Consultation: Available evidence for the future update of the WHO Global Air Quality Guidelines (AQGs). http://www.euro.who.int/__data/assets/pdf_file/0013/301720/Evidence-future-update-AQGs-mtg-report-Bonn-sept-oct-15.pdf. Accessed 20 March 2016.

WHO., n.d. Air pollution. http://www.who.int/sustainable-development/cities/health-risks/air-pollution/en/. Accessed 20 March 2016.

Wilson, W.E. and Suh, H.H., 1997. Fine particles and coarse particles: concentration relationships relevant to epidemiologic studies. Journal of the Air & Waste Management Association, 47(12), pp. 1238-1249.

Winkel, A., Rubio, J.L., Vonk, J. and Ogink, N.W., 2015. Equivalence testing of filter-based, beta-attenuation, TEOM, and light-scattering devices for measurement of PM 10 concentration in animal houses. Journal of Aerosol Science, 80, pp.1 1-26.

Wu, Y., Guo, J., Zhang, X., Tian, X., Zhang, J., Wang, Y., Duan, J. and Li, X., 2012. Synergy of satellite and ground based observations in estimation of particulate matter in eastern China. Science of the Total Environment, 433, pp.20-30.

Xia, S. and Huijie, Z., 2009. Retrieval algorithm for optical parameters of aerosol over land surface from POLDER data. Acta Optica Sinica, 29(7), pp. 1772-1777.

Xie, Y., Zhang, Y., Xiong, X., Qu, J.J. and Che, H., 2011. Validation of MODIS aerosol optical depth product over China using CARSNET measurements. Atmospheric Environment, 45(33), pp. 5970-5978.

Xie, Y., Wang, Y., Zhang, K., Dong, W., Lv, B. and Bai, Y., 2015. Daily estimation of ground-level PM2. 5 concentrations over Beijing using 3 km resolution MODIS AOD. Environmental Science & Technology, 49(20), pp. 12280-12288.

Yao, X., Chan, C.K., Fang, M., Cadle, S., Chan, T., Mulawa, P., He, K. and Ye, B., 2002. The water-soluble ionic composition of PM2. 5 in Shanghai and Beijing, China. Atmospheric Environment, 36(26), pp. 4223-4234.

You, W., Zang, Z., Zhang, L., Li, Y., Pan, X. and Wang, W., 2016. National-Scale Estimates of Ground-Level PM2. 5 Concentration in China Using Geographically Weighted Regression Based on 3 km Resolution MODIS AOD. Remote Sensing, 8(3), pp. 184.

You, W., Zang, Z., Zhang, L., Zhang, M., Pan, X. and Li, Y., 2016. A nonlinear model for estimating ground-level PM 10 concentration in Xi'an using MODIS aerosol optical depth retrieval. Atmospheric Research, 168, pp. 169-179.

Yu, S., Mathur, R., Schere, K., Kang, D., Pleim, J., Young, J., Tong, D., Pouliot, G., McKeen, S.A. and Rao, S.T., 2008. Evaluation of real-time PM2. 5 forecasts and process analysis for PM2.5 formation over the eastern United States using the Eta-CMAQ forecast model during the 2004 ICARTT study. Journal of Geophysical Research: Atmospheres, 113(D6).

Yu, Y., Lu, X., &Zhu, Y., 2015. Inversion of AOD Based on HJ-1 Satellite Data. The Administration and Technique of Environmental Monitoring, V4, pp. 30-34

Zanobetti, A., Austin, E., Bind, M.A.C. and Schwartz, J., 2015. Estimating Causal Effects of PM2.5 On Daily Deaths in Boston. Am J Respir Crit Care Med, 191, pp. 3198.

Zeger, S.L., Dominici, F., McDermott, A. and Samet, J.M., 2008. Mortality in the Medicare population and chronic exposure to fine particulate air pollution in urban centers (2000-2005). Environmental Health Perspectives, 116(12), pp. 1614.

Zhang, F., Liu, X., Zhou, L., Yu, Y., Wang, L., Lu, J., Wang, W. and Krafft, T., 2016. Spatiotemporal patterns of particulate matter (PM) and associations between PM and mortality in Shenzhen, China. BMC Public Health, 16(1).

Zhang, L., Shi, R., Liu, C. and Zhou, C., 2015, September. Retrieval of aerosol optical depth over Beijing using Landsat8/OLI data. In SPIE Optical Engineering+ Applications, pp.961011-961011.

Zhang, X., 2013. The Application of Satellite Remote Sensing in Time-series Study of Associations between PM2.5 and Pediatric Asthma/Wheeze Emergency Department Visits in Metropolitan Atlanta, Emory University.

Zhao, N., Yang, Y. and Zhou, X., 2010. Application of geographically weighted regression in estimating the effect of climate and site conditions on vegetation distribution in Haihe Catchment, China. Plant Ecology, 209(2), pp.349-359.

Zhou, C.Y., Liu, Q.H., Tang, Y., Wang, K., Sun, L. and He, Y.X., 2009. Comparison between MODIS aerosol product C004 and C005 and evaluation of their applicability in the north of China. Journal of Remote Sensing, 13(5), pp.854-862.

Appendix I

City	City's Averaged PM2.5 ($\mu g/m^3$)	Station	Station Code	Longitude	Latitude	Station's Averaged PM2.5($\mu g/m^3$)
Zhangjiakou	24.88	North Pump Room	1061A	114.89	40.81	20.02
		The People'S Park	1057A	114.90	40.83	24.56
		Shijihao Garden	1060A	114.90	40.77	25.18
		Agent Factory	1058A	114.89	40.79	26.02
		Wujing Ku	1059A	114.88	40.82	28.65
Chengde	35.99	The Bank Of China	1063A	117.95	40.99	32.94
		Li Palace	1066A	117.94	41.00	33.83
		Cultural Center	1065A	118.18	40.77	34.16
		The Railway	1062A	117.96	40.94	34.68
		Development Zone	1064A	117.96	40.93	44.32
Qinhuangdao	47.08	Diyiguan	1043A	119.77	40.02	40.49
		The Construction Of Building	1046A	119.19	39.72	43.85
		Beidaihe Environmental Protection Bureau	1042A	119.53	39.83	48.64
		The City Government	1045A	119.61	39.94	50.66
		Monitoring station	1044A	119.60	39.96	51.78
Cangzhou	58.82	The Municipal Environmental Protection Bureau	1073A	116.87	38.32	57.77
		Cangxian Construction Bureau	1071A	116.89	38.30	58.44
		Television Station	1072A	116.86	38.31	60.27
Beijing	71.04	Huairou Town	1009A	116.65	40.31	60.90
		Dingling	1002A	116.23	40.30	67.90
		Shunyi New Town	1008A	116.66	40.18	68.41
		Changping Town	1010A	116.23	40.23	69.07
		Temple Of Heaven	1004A	116.42	39.89	71.87
		Wanshouxigong	1001A	116.37	39.89	72.26
		Ancient City	1012A	116.20	39.91	72.36

		Dongsi	1003A	116.44	39.94	73.41
		Olympic Sports Center.	1011A	116.40	39.99	73.54
		Haidian Wanliu	1007A	116.31	39.97	73.58
		Guanyuan	1006A	116.37	39.94	74.24
		Agriculture Exhibition Hall	1005A	116.47	39.95	74.90
Tianjin	75.50	Dagu Road	1017A	117.26	39.14	67.97
		Han North Road	1026A	117.74	39.12	69.01
		Qingjian Road	1015A	117.19	39.12	69.40
		Yongming Road	1024A	117.47	38.84	70.28
		Yuejin Road	1021A	117.32	39.09	70.87
		Hangtian Road	1025A	117.43	39.13	71.56
		The Fourth Street	1023A	117.22	39.09	74.44
		Southport Road	1014A	117.36	39.26	74.49
		Forward Road	1018A	117.23	39.12	76.64
		Monitoring Center	1013A	117.17	39.10	80.69
		Nanjing Road	1016A	117.19	39.13	81.59
		Beichen Science And Technology Park	1019A	117.23	39.23	81.64
		Tuanbowa	1027A	117.22	38.85	84.16
		Tianshan Road	1020A	117.28	39.14	84.28
Langfang	75.58	Environmental Monitoring And Supervision Center	1069A	116.72	39.56	69.42
		North China Institute Of Technology	1070A	116.74	39.53	75.25
		Medicinal Materials Company	1067A	116.71	39.54	75.68
		Development Zone	1068A	116.76	39.57	81.97
Hengshui	86.18	North Motor Factory	1074A	115.69	37.75	83.32
		The City Monitoring Stations	1075A	115.64	37.74	87.47
		The Municipal Environmental Protection Bureau	1076A	115.69	37.74	87.77
Tangshan	82.45	Materiel Administration	1038A	117.97	40.18	79.00
		Ceramic Company	1039A	118.18	39.64	80.10
		No.12 Middle School	1040A	118.18	39.66	82.06
		Radar Station	1037A	118.02	39.73	82.67

		Supply and Marketing Agency	1036A	118.20	39.63	84.23
		Xiao Mountains	1041A	118.31	39.74	86.63
Shijiazhuang	93.74	Fenglong Mountain	1035A	114.36	37.91	80.17
		The Worker Hospital	1029A	114.53	38.05	85.99
		Xinangaojiao	1032A	114.45	37.99	87.98
		Century Park	1033A	114.54	38.02	92.85
		The People'S Hall	1034A	114.52	38.05	95.50
		High-Tech Zone	1030A	114.61	38.05	96.33
		Xibeishuiyuan	1031A	114.47	38.06	103.77
		Chemical School	1028A	114.61	38.00	107.35
Handan	94.10	Congtai Park	1050A	114.50	36.62	87.96
		Mining Institute	1049A	114.50	36.58	92.96
		Dongwushuichuli Factory	1048A	114.54	36.62	96.57
		Environmental Protection Agency	1047A	114.51	36.62	98.90
Baoding	98.18	Film Factory	1055A	115.46	38.88	91.19
		The Reception Center	1053A	115.47	38.91	93.97
		Huadian Area	1052A	115.52	38.89	96.95
		Swimming Center	1051A	115.49	38.86	97.43
		Surface Water Factory	1054A	115.45	38.96	99.83
		Monitoring station	1056A	115.52	38.87	109.72
Xingtai	107.39	Teacher College	1078A	114.46	37.11	99.31
		Road And Bridge Corporation	1079A	114.53	37.09	107.56
		The Municipal Environmental Protection Bureau	1080A	114.49	37.11	108.36
		Dahuo Spring	1077A	114.49	37.09	114.33

Appendix II

	Season / Factors	Fall			Winter			Spring			Summer		
		Mean	Coefficient	Sig.	Mean	Coefficient	Sig.	Mean	Coefficient	Sig.	Mean	Coefficient	Sig.
3KM Model	PM2.5 ($\mu g/m^3$)	29.56			23.33			44.711	-404.83		47.61		
	Constant		-324.35	0.00		39.73	0.00			0.00		-857.809	0.00
	AOD	0.52	4.04	0.00	0.16	Not Significant		0.7395	3.02	0.00	0.096483	3.18	0.00
	Relative Humidity (%)	35.75	-53.65	0.00	22.45	Not Significant		22.516	Not Significant		41.3049	Not Significant	
	Temperature (K)	294.81	1.28	0.00	278.02	Not Significant		298.01	1.51	0.00	304.63121	4.373965	0.00
	Surface Pressure(KPa)	98.8	Not Significant		99.30	Not Significant		98.375	Not Significant		97.48473	-4.52777	0.00
	Uwind Speed (m/s)	0.58	1.94	0.00	1.80	-4.29	0.00	2.1481	0.86	0.00	0.21586	Not Significant	
	Vwind Speed (m/s)	0.11			-1.28	2.52	0.00	0.9127	-0.09	0.04	0.83303	0.155408	0.01
	Boundary Layer Height at 8:00 (KM)	1.29	-190.42	0.00	1.12	Not Significant		1.9076	Not Significant		1.5746418	-0.1165	0.00
	Boundary Layer Height at 20:00 (KM)	0.11	312.03	0.00	0.16	Not Significant		0.1472	Not Significant		0.0956363	0.439414	0.00
	GDP (Thousand Yuan)	121.91	Not Significant		45.02	Not Significant		110.33	-0.03	0.01	127.84001	Not Significant	
	Elevation (m)	99.02	Not Significant		76.26	-0.06	0.00	70.51	Not Significant		81.07	-0.043	0.00
	Population (Thousand People)	50.62	Not Significant		9.11	Not Significant		68.202	-0.04	0.02	67.47025	Not Significant	
	The Percent of Urban Area (%)	54.21	-12.32	0.00	12.76	Not Significant		63.383	Not Significant		66	Not Significant	

	Season / Factors	Fall			Winter			Spring			Summer		
		Mean	Coefficient	Sig.	Mean	Coefficient	Sig.	Mean	Coefficient	Sig.	Mean	Coefficient	Sig.
10KM Model	PM2.5 (μg/m3)	32.6			59.01	-295.08		53.71			51.12		
	Constant		-4.19	0.00			0.00		360.62	0.00		-1153.84	0.00
	AOD	0.41	57.94	0.00	0.35	130.34	0.00	0.59	71.35	0.00	0.83	35.55	0.00
	Relative Humidity (%)	32.68	-72.88	0.00	25.19	-90.4	0.00	21.59	Not Significant		39.96	Not Significant	
	Temperature (K)	292	1.01	0.00	278.56	1.3	0.00	291.96	Not Significant		304.83	0.49	0.00
	Surface Pressure(KPa)	98.26	-2.18	0.01	99.74	Not Significant		98.97	-3.09	0.00	97.25	-0.31	0.00
	Uwind Speed (m/s)	1.22	1.62	0.01	1.53	3.64	0.00	1.96	2.14	0.00	0.18	-1.38	0.02
	Vwind Speed (m/s)	-0.63	Not Significant		-0.96	Not Significant		0.65	Not Significant		1.06	-1.59	0.02
	Boundary Layer Height at 8:00 (KM)	1.32	-280.98	0.00	0.91	-397.41	0.00	1.72	-223.11	0.00	1.61	-162.88	0.00
	Boundary Layer Height at 20:00 (KM)	0.24	Not Significant		0.14	Not Significant		0.13	Not Significant		0.1	Not Significant	
	GDP (Thousand Yuan)	894.49	Not Significant		906.94	-0.01	0.02	836.81	-0.01	0.05	922.91	Not Significant	
	Elevation (m)	140.04	-0.03	0.04	81.41	Not Significant		78.09	-0.06	0.00	98.82	Not Significant	
	Population (Thousand People)	383.84	-0.01	0.01	564.33	Not Significant		599.26	Not Significant		481.91	Not Significant	
	The Percent of Urban Area (%)	34.53	Not Significant		44.95	0.07	0.23	47.08	Not Significant		40.6	Not Significant	